

## Electrocatalysts for the generation of hydrogen, oxygen and synthesis gas



Foteini M. Sapountzi <sup>a,\*</sup>, Jose M. Gracia <sup>b</sup>, C.J. (Kees-Jan) Weststrate <sup>a</sup>,  
Hans O.A. Fredriksson <sup>a</sup>, J.W. (Hans) Niemantsverdriet <sup>a,b</sup>

<sup>a</sup> *SynCat@DIFFER, Syngaschem BV, P.O. Box 6336, 5600 HH Eindhoven, The Netherlands*

<sup>b</sup> *SynCat@Beijing, Synfuels China Technology Co. Ltd, 1 Leyuan 2 South Street, Section C, Yanqi Economic Development Area, Beijing 101407, China*

### ARTICLE INFO

#### Article history:

Received 2 March 2016

Accepted 12 September 2016

Available online 22 September 2016

#### Keywords:

Alkaline electrolysis  
Polymer electrolyte membrane (PEM)  
electrolysis  
Solid oxide electrolysis  
Co-electrolysis electrode materials

### ABSTRACT

Water electrolysis is the most promising method for efficient production of high purity hydrogen (and oxygen), while the required power input for the electrolysis process can be provided by renewable sources (e.g. solar or wind). The thus produced hydrogen can be used either directly as a fuel or as a reducing agent in chemical processes, such as in Fischer–Tropsch synthesis. Water splitting can be realized both at low temperatures (typically below 100 °C) and at high temperatures (steam water electrolysis at 500–1000 °C), while different ionic agents can be electrochemically transferred during the electrolysis process ( $\text{OH}^-$ ,  $\text{H}^+$ ,  $\text{O}_2^-$ ). Singular requirements apply in each of the electrolysis technologies (alkaline, polymer electrolyte membrane and solid oxide electrolysis) for ensuring high electrocatalytic activity and long-term stability. The aim of the present article is to provide a brief overview on the effect of the nature and structure of the catalyst–electrode materials on the electrolyzer's performance. Past findings and recent progress in the development of efficient anode and cathode materials appropriate for large-scale water electrolysis are presented. The current trends, limitations and perspectives for future developments are summarized for the diverse electrolysis technologies of water splitting, while the case of  $\text{CO}_2/\text{H}_2\text{O}$  co-electrolysis (for synthesis gas production) is also discussed.

© 2016 The Authors. Published by Elsevier Ltd. This is an open access article under the CC BY-NC-ND license (<http://creativecommons.org/licenses/by-nc-nd/4.0/>).

### Contents

1. Hydrogen: potential energy carrier, clean fuel, valuable chemical and essential ingredient of synthesis gas .....	2
2. Water electrolysis technologies .....	2
2.1. Requirements for electrocatalysts .....	5
3. Anodes for water electrolysis: electrocatalysts for the oxygen evolution reaction .....	5
3.1. Alkaline electrolyzers .....	5
3.1.1. Ni, Co, Fe, Mn oxides .....	5
3.1.2. Perovskites .....	7
3.1.3. Novel structures .....	10
3.2. PEM electrolyzers .....	12
3.2.1. Mixed oxides .....	12
3.2.2. Supports for OER catalysts .....	13
3.2.3. Alternative preparation methods and novel structures .....	14
3.3. Solid oxide electrolysis .....	15
3.3.1. SOE with $\text{O}_2^-$ conducting oxides .....	15
3.3.2. SOE with $\text{H}^+$ conducting oxides .....	16
4. Cathodes for water electrolysis: electrocatalysts for the hydrogen evolution reaction .....	16
4.1. Alkaline electrolysis .....	17
4.1.1. Ni, Co, Fe based electrocatalysts .....	17
4.1.2. Novel structures .....	20

\* Corresponding author. Syngaschem BV, P.O. Box 6336, 5600 HH Eindhoven, The Netherlands.

E-mail address: [foteini@syngaschem.com](mailto:foteini@syngaschem.com) (F.M. Sapountzi).

4.2.	PEM electrolyzers .....	20
4.2.1.	Pt based electrocatalysts .....	20
4.2.2.	Sulphides, phosphides, carbides and nitrides .....	21
4.2.3.	Other materials .....	22
4.3.	Solid oxide electrolyzers (SOEs) .....	23
4.3.1.	SOE with O <sup>2-</sup> conducting oxides .....	23
4.3.2.	SOE with H <sup>+</sup> conducting oxides .....	24
5.	High temperature CO <sub>2</sub> /H <sub>2</sub> O co-electrolysis .....	25
5.1.	Operation and mechanisms .....	25
5.2.	Materials for co-electrolysis .....	25
6.	Outlook and summary .....	26
6.1.	Alkaline electrolysis .....	27
6.2.	PEM electrolysis .....	27
6.3.	Solid oxide electrolysis (SOE) .....	27
	Acknowledgement .....	28
	References .....	28

## 1. Hydrogen: potential energy carrier, clean fuel, valuable chemical and essential ingredient of synthesis gas

The increase in world's energy consumption during the last decades is a result both of the global rise in population and of the changes in the standards of living [1]. Indicatively, the average global power demand is predicted to be approximately 30 and 46 TW in 2050 and 2100 respectively [2]. Nowadays fossil fuels (i.e. coal, oil, natural gas) constitute the primary source that covers global energy needs. The continuously increasing energy demands, the limiting reserves of fossil fuels together with the environmental and societal problems created by the fossil fuel dependence (e.g. global warming, acid rain, local air quality deterioration) render an urgent need for the development of new energy strategies with limited greenhouse gas emissions. These will rely both on renewable energy sources (which are more abundant and cleaner compared to fossil fuels) and on chemical processes for synthetic fuel production (e.g. Fischer-Tropsch synthesis) [1–6].

A fundamental problem related with the use of solar and wind energies is their inability to operate independently from demand, since their unscheduled intermittent supply often mismatches the grid power demands. Thus, the development and application of systems for the efficient storage of excess electricity is entailed [7,8]. Electrocatalytic technologies can play a crucial role for the indirect storage of surplus renewable energy via the conversion of electricity to chemical energy [8]. Among them, water electrolysis is a promising alternative compared to electricity storage using batteries [9]. During water electrolysis, renewable energy can be used as the electricity source to split water into hydrogen and oxygen. The thus produced green hydrogen can be either stored and used in the chemical industry or used for electricity generation (through fuel cells or internal combustion engines) with zero post-combustion pollutants [6].

The use of hydrogen as an energy carrier has a number of advantages. Hydrogen (a) is relatively abundant in nature (in water) [1] and can be produced using either renewable or non-renewable sources [10], (b) can be used as a fuel in both fuel cells and internal combustion engines (the latter however suffers from concomitant NO<sub>x</sub> production) [8], (c) has high gravimetric energy density i.e. up to three times larger than liquid hydrocarbon-based fuels [4,11] (however worth to note is its low volumetric energy density which caused safety issues with its pressurized storage), (d) has small environmental footprint, since the only product of its oxidation is water [6,8]. Its use in the transport sector has been successfully introduced and Hua et al. recently reviewed the status of hydrogen-fueled buses in Europe, USA and Canada [12].

However, using hydrogen as a fuel requires appropriate infrastructures and huge investments. A more feasible scenario for tackling the energy problem concerns the employment of water

electrolysis for the production of synthetic fuels that can be used in the current infrastructures. Renewable energy sources will provide the electrons required for the splitting of water. In a parallel process, CO<sub>2</sub> will be captured from large point sources and be recycled with the utilization of the renewably produced hydrogen (reverse water-gas-shift reaction) for the production of synthetic fuels (Fischer-Tropsch synthesis) [13]. Additionally, hydrogen can be also used as a reducing agent of several other catalytic processes in the petroleum and chemical industry, e.g. for the refining and upgrading of crude oil and for ammonia synthesis respectively [1].

In 2015, the worldwide hydrogen production is around 50 Mt per year [1,8,10,13–16] and is covered by fossil fuels (steam reforming of natural gas, coal gasification, partial oxidation of hydrocarbons) [1,8,10,15,16]; however, this includes the concomitant production of CO<sub>2</sub>. Within the vision for a sustainable future, several methods, other than water electrolysis, for renewable hydrogen production have been developed, such as biomass gasification, thermochemical water splitting and photoelectrochemical water splitting [10,15]. Among them, water electrolysis is the only mature technology that is currently commercially available [15].

Hydrogen production via electrolysis using renewable energy sources amounts to only 4% of today's hydrogen production, mainly due to economic factors (i.e. lack of widely available renewable energy systems of low cost, high capital cost, high energy input required) [10]. This picture is going to change in the near future and increase in the use of renewable energy sources is expected, since the European Energy Directive has set the target for covering 14% of the energy needs by renewable energy sources by 2020. Hydrogen production by water electrolysis using renewable energy sources is expected to play a key role in the scenario of a green energy economy [8]. Clear advantages of this method is the high efficiency and the high purity of the produced hydrogen, which is of great importance for its subsequent conversion to electricity using low temperature polymer electrolyte fuel cells [17]. Furthermore, high purity oxygen is a valuable by-product of water electrolysis. Its utilization both in medical care and in chemical industry (blast furnaces, electric furnaces and glass melting, gasification) could lead to substantial decrease in the nominal cost of water electrolysis [18].

## 2. Water electrolysis technologies

Depending on the kind of electrolyte and thus the type of ionic agent (OH<sup>-</sup>, H<sup>+</sup>, O<sup>2-</sup>), and the operation temperature, water electrolyzers are classified into three main categories: alkaline [19], polymer-electrolyte membrane (PEM) [20,21] and solid oxide electrolyzers (SOE) [22–24]. The operating principles of the three main types of electrolysis technologies are presented in Fig. 1.

Solid oxide electrolyzers (SOEs) operate typically at temperatures above 500 °C, with water in the form of steam. The SOE

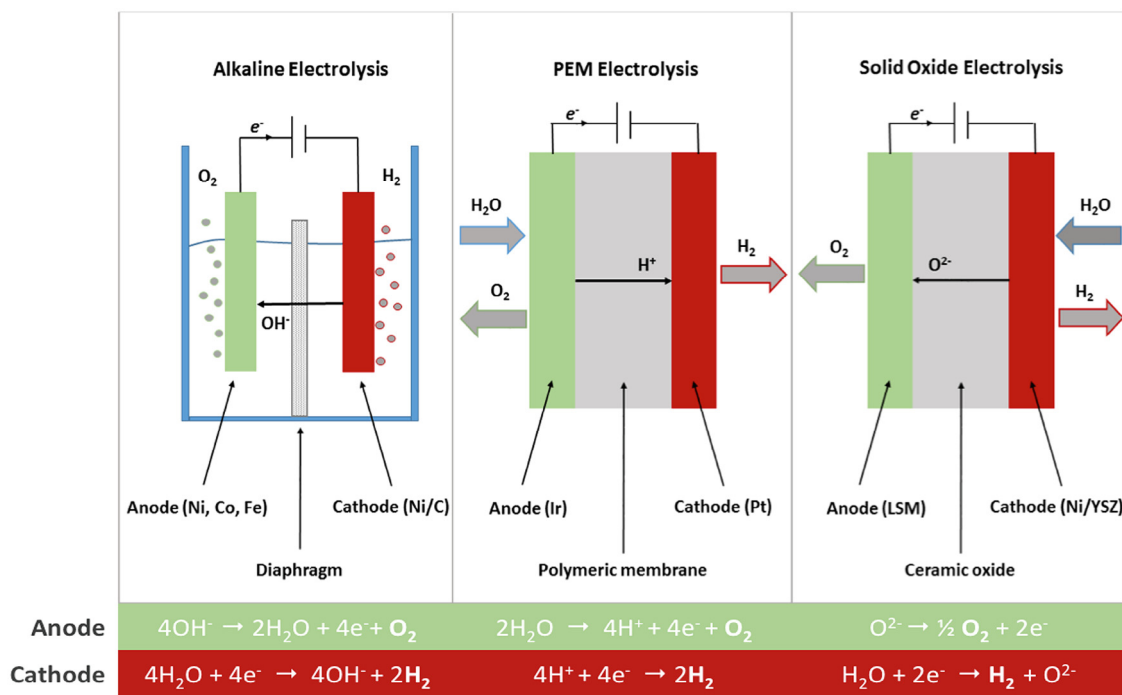


**Fig. 1.** Operation principles of alkaline, PEM (proton-exchange membrane) and solid oxide water electrolysis. The overall reaction is  $\text{H}_2\text{O} \rightarrow \text{H}_2 + \frac{1}{2}\text{O}_2$ . Oxygen evolution occurs at the anode, hydrogen evolves at the cathode. The case of solid oxide electrolysis shown is that of an  $\text{O}^{2-}$ -conducting electrolyte, with a nickel/yttria-stabilized zirconia cathode and a lanthanum strontium manganite (LSM) anode.

technology traditionally utilizes  $\text{O}^{2-}$  conductors (mainly yttria stabilized zirconia (YSZ)). However, in the last years, several ceramic proton conductors have emerged and found application in solid oxide fuel cells. The use of ceramic proton conductors in steam electrolysis has gained much attention since these materials show higher ionic conductivity and better efficiency compared to that of oxygen-ion conductors at the intermediate temperature range (500–700 °C). Moreover, they exhibit better chemical compatibility with Ni, which is the most used hydrogen electrode for SOEs. We refer to Traversa and coworkers [25] for a recent review on proton-conducting SOE.

Alkaline and PEM electrolyzers operate at the low temperature range (typically below 100 °C) where water is liquid. Recent progress on the development of polymeric membranes with protonic conductivity operative at temperatures up to 200 °C has been carried out in the field of fuel cell technology [26–28], which can extend the temperatures for PEM electrolysis as well.

In alkaline electrolyzers, the anode and cathode electrodes are immersed in a liquid alkaline electrolyte, most commonly potassium hydroxide. A diaphragm permeable for  $\text{OH}^-$  between the two electrodes serves to separate the product gases. In solid oxide and PEM electrolyzers the solid electrolytes, ceramic and polymers, respectively, fulfill the role of gas separator.

Each of the types of electrolysis has its own pros and cons (summarized in Table 1), but all three technologies are appealing and promising for sustainable energy application. Alkaline electrolysis is well established as the most applied commercial technology, with suppliers such as De Nora SAP, Norsk Hydro, Electrolyzer Corp, Teledyne Energy Systems and General Electric [19]. Main advantages of alkaline electrolysis are low cost owing to the use of non-noble electrodes and long-term stability. On the contrary, the acidic environment in PEM electrolyzers hinders the kinetics of the redox reactions and necessitates the use of expensive noble metal catalysts and materials for the bipolar plates. This, together with the high cost of polymeric membranes, is the main limitation for the commercialization of PEM electrolysis in the near term.

Thermodynamic analysis by Todd et al. indicates that water electrolysis under high pressure has lower energy requirements [29]. Alkaline electrolyzers can in principle operate at higher pressures, although at higher degradation rates [30]. However, the use of a liquid electrolyte does not allow operation at differential pressures, in order to avoid gas and electrolyte permeation through the diaphragm. On the other hand, operation under different pressures at the two sides of the electrolyzer would facilitate hydrogen storage, since hydrogen will be produced at high pressure and the need for additional compressing systems will be eliminated, while on the other hand water could be supplied (and oxygen will be produced) at near atmospheric pressure [31].

The solid form of the electrolyte in SOEs and PEMs enables a more compact design and operation at differential pressures is feasible and favorable. Moreover, the solid nature of the electrolyte makes SOEs and PEMs more dynamic systems with faster response upon application of a variable power load compared to liquid alkaline electrolyzers where diffusion rates can be slow.

Regarding ohmic losses, ionic conduction in the liquid electrolyte of alkaline electrolyzers is slow and the presence of the diaphragm can also further hinder  $\text{OH}^-$  transport, thus low current densities are generally observed in this technology. Ohmic losses are smaller both in SOEs, due to better ion conduction at the high operating temperature, and in PEM electrolyzers, due to the wide availability of polymeric membranes with high protonic conductivity.

The diaphragm in alkaline electrolysis largely prevents ionic conduction, but it can also be the source of reduced efficiency due to the unwanted permeation of gases. Apart from inhibiting the overall performance, it causes several safety issues. Gas crossover can occur also in the polymeric membrane in PEM electrolyzers, but to a lesser extent. In this case, the membrane thickness can minimize permeation of the gases. Even though ceramic electrolytes suppress gas permeation, safety issues also arise in the SOE. Satisfactory sealing between the anodic and cathodic chambers is difficult to achieve for long term at high operation temperatures and the risk of a sudden cracking is not negligible.

**Table 1**

The typical characteristics of the main electrolysis technologies.

Operation principles	Low Temperature Electrolysis			High Temperature Electrolysis		
	Alkaline ( $\text{OH}^-$ ) electrolysis		$\text{Proton Exchange} (\text{H}^+)$ electrolysis	Oxygen ion ( $\text{O}^{2-}$ ) electrolysis		
	Liquid	Polymer Electrolyte Membrane	$\text{H}^+ - \text{PEM}$	$\text{H}^+ - \text{SOE}$	$\text{O}^{2-} - \text{SOE}$	Co-electrolysis
Charge carrier	$\text{OH}^-$	$\text{OH}^-$	$\text{H}^+$	$\text{H}^+$	$\text{O}^{2-}$	$\text{O}^{2-}$
Temperature	20–80°C	20–200°C	20–200°C	500–1000°C	500–1000°C	750–900°C
Electrolyte	liquid	solid (polymeric)	solid (polymeric)	solid (ceramic)	solid (ceramic)	solid (ceramic)
Anodic Reaction (OER)	$4\text{OH}^- \rightarrow 2\text{H}_2\text{O} + \text{O}_2 + 4\text{e}^-$	$4\text{OH}^- \rightarrow 2\text{H}_2\text{O} + \text{O}_2 + 4\text{e}^-$	$2\text{H}_2\text{O} \rightarrow 4\text{H}^+ + \text{O}_2 + 4\text{e}^-$	$2\text{H}_2\text{O} \rightarrow 4\text{H}^+ + 4\text{e}^- + \text{O}_2$	$\text{O}^{2-} \rightarrow \frac{1}{2}\text{O}_2 + 2\text{e}^-$	$\text{O}^{2-} \rightarrow \frac{1}{2}\text{O}_2 + 2\text{e}^-$
Anodes	Ni > Co > Fe (oxides) Perovskites: $\text{Ba}_{0.5}\text{Sr}_{0.5}\text{Co}_{0.8}\text{Fe}_{0.2}\text{O}_{3-\delta}$ , $\text{LaCoO}_3$	Ni-based	$\text{IrO}_2, \text{RuO}_2, \text{Ir}_{x}\text{Ru}_{1-x}\text{O}_2$ Supports: $\text{TiO}_2, \text{ITO}, \text{TiC}$	Perovskites with protonic-electronic conductivity	$\text{La}_{x}\text{Sr}_{1-x}\text{MnO}_3 + \text{Y-Stabilized ZrO}_2$ (LSM-YSZ)	$\text{La}_{x}\text{Sr}_{1-x}\text{MnO}_3 + \text{Y-Stabilized ZrO}_2$ (LSM-YSZ)
Cathodic Reaction (HER)	$2\text{H}_2\text{O} + 4\text{e}^- \rightarrow 4\text{OH}^- + 2\text{H}_2$	$2\text{H}_2\text{O} + 4\text{e}^- \rightarrow 4\text{OH}^- + 2\text{H}_2$	$4\text{H}^+ + 4\text{e}^- \rightarrow 2\text{H}_2$	$4\text{H}^+ + 4\text{e}^- \rightarrow 2\text{H}_2$	$\text{H}_2\text{O} + 2\text{e}^- \rightarrow \text{H}_2 + \text{O}^{2-}$	$\text{H}_2\text{O} + 2\text{e}^- \rightarrow \text{H}_2 + \text{O}^{2-}$ $\text{CO}_2 + 2\text{e}^- \rightarrow \text{CO} + \text{O}^{2-}$
Cathodes	Ni alloys	Ni, Ni-Fe, $\text{NiFe}_2\text{O}_4$	Pt/C $\text{MoS}_2$	Ni-cermets	Ni-YSZ Subst. $\text{LaCrO}_3$	Ni-YSZ perovskites
Efficiency	59–70%		65–82%	up to 100%	up to 100%	-
Applicability	commercial	laboratory scale	near-term commercialization	laboratory scale	demonstration	laboratory scale
Advantages	low capital cost, relatively stable, mature technology	combination of alkaline and $\text{H}^+$ -PEM electrolysis	compact design, fast response/start-up, high-purity $\text{H}_2$	enhanced kinetics, thermodynamics: lower energy demands, low capital cost	+ direct production of syngas	
Disadvantages	corrosive electrolyte, gas permeation, slow dynamics	low $\text{OH}^-$ conductivity in polymeric membranes	high cost polymeric membranes; acidic: noble metals	mechanically unstable electrodes (cracking), safety issues: improper sealing		
Challenges	Improve durability/reliability; and Oxygen Evolution	Improve electrolyte	Reduce noble-metal utilization	microstructural changes in the electrodes: delamination, blocking of TPBs, passivation	C deposition, microstructural change electrodes	

On the other hand, the high operating temperature of SOEs is the main characteristic that makes this technology advantageous compared to low temperature electrolysis. The thermodynamics of water electrolysis is shown in Fig. 2, adapted from Ebbesen et al. [32]. The total energy demand of the process,  $\Delta H$ , increases only slightly with increasing temperature, while the  $T\Delta S$  contribution

becomes increasingly more significant, and thus the electric energy input necessary to sustain the electrolysis,  $\Delta G$ , is considerably lower at high temperatures, thereby decreasing the cost of the produced hydrogen. For an average current density of  $7000 \text{ A/m}^2$  and an inlet steam temperature of  $800^\circ\text{C}$ , SOE stacks are predicted to operate at  $1.3 \text{ V}$  and have electrical energy consumption of  $3 \text{ kWh}$  per normal  $\text{m}^3$  of  $\text{H}_2$ , while  $4.5 \text{ kWh}$  is required for commercial alkaline electrolyzers. However, heating energy circulation and losses are not taken into account in these calculations [18,33]. In this sense, the net efficiency of SOEs is 40–60% (taking into account heating energy demands), which is lower than that of low temperature electrolyzers (59–70% and 65–82% for alkaline and PEM electrolyzers respectively, based on the hydrogen yield). However, this picture can change if the required heat is generated renewably (by heat from the sun or a nuclear power plant). Alternatively, in the case of integrated systems the required heat can be supplied from the waste heat of exothermic processes. SOEs in both cases can operate with near to 100% efficiency.

Another interesting feature of SOEs (in the case of  $\text{O}^{2-}$  conducting electrolytes), which is also related to their high temperature operation, is that this technology offers the possibility to co-electrolyze  $\text{H}_2\text{O}/\text{CO}_2$  mixtures for the production of syngas (composed of CO and  $\text{H}_2$ ) [34–37]. Syngas can be further converted to methanol or to higher hydrocarbons via the Fischer–Tropsch synthesis [13,14,38]. In such way, co-electrolysis can contribute to storage of the renewable electricity and reduction of  $\text{CO}_2$  emission.  $\text{CO}_2/\text{H}_2\text{O}$  co-electrolysis represents demonstrated technology and can be a

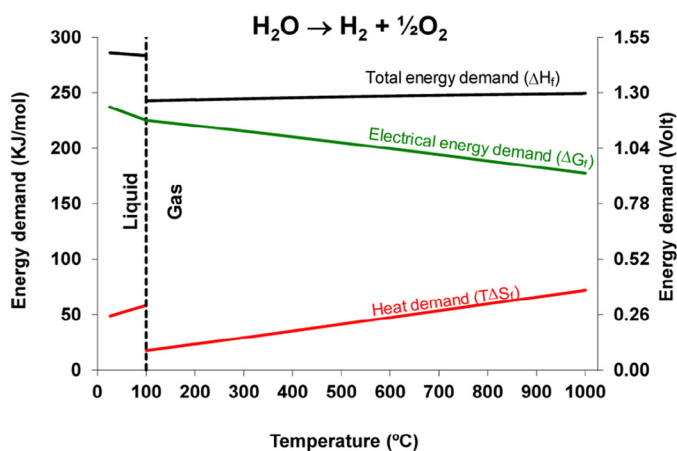


Fig. 2. Thermodynamics for  $\text{H}_2\text{O}$  electrolysis at atmospheric pressure. Reprinted from reference 32 with permission of American Chemical Society.

key-step in CO<sub>2</sub> recycling scenarios, provided suitably stable electrocatalysts are developed. The main features of co-electrolysis are discussed in [Section 5](#).

Although the high temperature operation of SOEs comes with inherent advantages, it is also the source of degradation and lack of stability, which have to be solved before solid oxide electrolysis can be commercialized on a large scale [[14,19,20](#)].

Finally, a new trend in the alkaline electrolysis emerged in the last years, based on polymeric membranes with anionic (OH<sup>-</sup>) conductivity, also known as anion exchange membranes (AEM). This innovative technology, named as solid alkaline electrolysis, appears to be promising, since it can combine positive features of both alkaline and PEM electrolysis. In the frame of the present review, solid alkaline electrolysis will be discussed together with conventional alkaline electrolysis for consistency reasons. However, since this technology is a hybrid between alkaline and PEM electrolysis (due to the polymeric form of the AEM), other reviews have classified it as a subcategory of PEM electrolyzers. Non-noble metal catalysts can be used in this technology since the kinetics of the oxygen evolution reaction is better in alkaline media than in acidic media (PEM electrolysis), while the solid form of the membrane can provide the mechanical integrity for operation under differential pressures within a compact and scalable cell design. However, several issues (such as high cost and poor ionic conductivity of the polymeric membranes, susceptibility to degradation) need to be solved before this technology can be applied [[31,39,40](#)].

## *2.1. Requirements for electrocatalysts*

Targeting efficient large-scale electrolysis, abundant, stable and active materials should be developed. The practical considerations on the development of electrocatalysts are different for the three electrolysis technologies, due to special requirements related mainly with the acidity/alkalinity of the environment and the operating temperature.

On the fundamental level, the main requirements for a well-performing electrocatalyst are:

- (i) low intrinsic overpotential for the desired reaction (hydrogen or oxygen evolution),
- (ii) high active surface which facilitates both good accessibility to the reactants and sufficiently fast removal of products (gases, liquids, ions),
- (iii) high electrical conductivity (providing pathways for electrons),
- (iv) proper chemical stability (compatibility with the electrolyte),
- (v) electrochemical stability (i.e. not being corroded at high overpotentials),
- (vi) good mechanical stability (especially for high temperature electrolysis).

In addition to these requirements, which ensure high overall system efficiency, commercialization also requires long-term stability and low capital costs in order to compete with the conventional non-sustainable processes. The following sections present the status of electrocatalyst development for anodic and cathodic reactions in the different types of electrolysis.

## **3. Anodes for water electrolysis: electrocatalysts for the oxygen evolution reaction**

Oxygen evolution is the bottleneck in the electrolysis of water. Both in alkaline and PEM electrolyzers, the main energy losses are due to high overpotentials occurring at the anode, as a result of the sluggish kinetics of the oxygen evolution reaction (OER).

It is well established that IrO<sub>2</sub> and RuO<sub>2</sub> are the most active materials for OER during water electrolysis. RuO<sub>2</sub> suffers from deactivation

both in acidic and alkaline environments (due to dissolution), while IrO<sub>2</sub> is the catalyst which shows the best trade-off between catalytic activity and stability both in alkaline and acidic media [[9](#)]. However, since iridium is one of the least abundant elements on earth, the use of more abundant materials with lower cost is desired. This has been achieved in alkaline electrolysis by the use of transition metal catalysts, but it remains a challenge in PEM electrolysis.

As discussed in detail in [Section 3.1](#), oxides of transition metals (Ni, Co, Fe, Mn) are stable at high pH and thus are promising materials for alkaline electrolysis, while research is mostly focused on the optimization of their microstructure. Perovskite materials have recently also gained much attention in alkaline electrolysis.

On the contrary, the acidic nature of the electrolyte in PEM electrolysis limits the choice of suitable metals, and thus this technology still relies on the use of platinum group metals. Aiming at lower cost, research efforts in this field mainly focus on minimizing the use of IrO<sub>2</sub> by replacing it partially by more abundant elements. The developments in this direction are discussed in [Section 3.2](#).

In solid oxide electrolysis, the anode suffers from one of the major degradation issues in this technology, i.e. the delamination of the oxygen electrode caused by the high oxygen partial pressures at the electrode/electrolyte interface [[41](#)], which leads to a large increase in the polarization resistance for the oxygen oxidation reaction [[42,43](#)]. Perovskite materials are typically used in the oxygen electrode of solid oxide electrolyzers, and evaluated in [Section 3.3](#).

The present review deals with concepts on heterogeneous electrocatalysis for the electrochemical water splitting by metal oxides on electrode surfaces. Recent advances have been presented in the last years also in the field of homogeneous water-oxidation catalysis [[44](#)]. Several complexes have been developed [[45–47](#)], while Thomsen et al. [[48](#)] recently reported grafting of such metal-organic complexes onto the electrode support. According to Dau et al. [[49](#)] homogeneous and heterogeneous catalytic systems for water splitting share structural and functional characteristics and unifying concepts with combined properties will play a role in the future. However, further discussion on homogeneous water oxidation is beyond the scopes of the present article.

## *3.1. Alkaline electrolyzers*

### *3.1.1. Ni, Co, Fe, Mn oxides*

Even though noble-metal oxides (IrO<sub>2</sub>, RuO<sub>2</sub>, PtO<sub>2</sub>, RhO<sub>2</sub>) are the most active materials for the oxygen evolution reaction (OER), low cost transition metal oxides are typically used in alkaline electrolysis due to their abundance and relatively high activity and stability. Thus, nickel, cobalt and iron-based electrodes have been extensively studied in the last years in alkaline electrolysis, while manganese oxides have received some attention as well [[9](#)].

Already in 1981 Hall [[50](#)] noted that Ni-based materials can play a key role as oxygen evolution catalysts in alkaline electrolysis. Until today, Ni-based oxides are widely used since they show good activity and have high resistance to corrosion in the alkaline media [[9](#)]. It has been suggested that several molecular layers of NiO are lying directly on the metal surface due to exposure to air, while a compact Ni(OH)<sub>2</sub> layer (covering the outermost NiO layer) is in contact with the alkaline solution [[9,51](#)]. It is well established that potential cycling can cause transformations in the nickel-based electrodes [[52](#)] between phases with different oxidation states and crystallinities [[53,54](#)]. Upon continuous cycling in potential, the top hydrous nickel oxide film is growing, which is responsible for enhanced activity toward OER [[55](#)].

Except from nickel oxide, cobalt and iron oxides are also efficient oxygen evolution catalysts in alkaline media. A comparative study of Lyons and Brandon [[56](#)] on oxidized Ni, Co and Fe anodes showed that a similar mechanism for OER occurs. Oxidized Ni was found to be the most efficient electrocatalyst for OER, while oxidized

Fe is the least efficient. The activity was correlated with the number of d electrons in the metal cation. In a recent study, Andersen et al. [57] deposited a series of metal oxides ( $\text{MnO}_2$ ,  $\text{Co}_3\text{O}_4$ ,  $\text{NiO}$ ,  $\text{CuO}$ ,  $\text{Fe}_x\text{O}_y$ ) on nitrogen-doped carbon nanotubes; they too found that the most active catalyst for OER in alkaline media is  $\text{NiO}$ .

Combining Ni with a second element has shown significant improvements in electrode performance. The preparation method can have a significant effect on the morphology of OER electrocatalysts, thus affecting both the activity and the stability during oxygen evolution [58] while the nature of the substrate also can affect the OER performance. Perez-Alonso et al. [59] prepared several Ni–Fe electrodes on different substrates (i.e. nickel foam, stainless steel mesh, nickel mesh, nickel sheet) and found that both the Ni/Fe composition and the nature of the substrate can control the activity for OER. As shown in Fig. 3b, using nickel foam and steel mesh as substrates enabled deposition of thin but homogeneous electrodes (as evidenced by the SEM images of Fig. 3a) and hence OER activity is larger compared to the case of nickel sheet and nickel mesh. Furthermore, the incorporation of  $\text{Fe}_2\text{O}_3$  in the layer enhanced the OER activity significantly. In agreement with this, amorphous Ni–Fe oxide nanoparticles supported on carbon ( $\text{Ni}_{y}\text{Fe}_{1-y}\text{O}_x/\text{C}$ ) have also been reported to exhibit higher performance than  $\text{NiO}_x/\text{C}$  [60].

Addition of Co and Fe can result in reduced overpotential losses, with  $\text{NiFe}(\text{OH})_2$  as a particularly promising material [61]. Trześniewski et al. [62] carried out a systematic spectroelectrochemical study of the OER activity of  $\text{Ni}(\text{Fe})\text{OOH}$ . Surface enhanced Raman spectroscopy results showed that  $\text{Ni}(\text{Fe})\text{OOH}$  gets charged before the reaction starts, and that those negatively charged sites act as OER precursors. The authors propose that the formation of those “active oxygen” sites, of which the chemical identity is yet unclear, occurs via a deprotonation process, which strongly depends on the pH of the electrolyte and thus has an important effect on catalytic activity in strongly alkaline environments.

Zhang et al. [63] co-deposited Co and Ni as hydroxides on a nickel plate by cathodic electrodeposition and found that the Co content affects the activity for OER (optimal Co loading was between 42 and 47%), but does not change the reaction mechanism. Wang et al. [64]

investigated the OER in alkaline medium on a  $\text{Ni}(\text{OH})_2$  electrode modified by cobalt coating, and found that the presence of cobalt can increase the OER activity promoting full charge of the electrode.

Chi et al. [65] have found that Ni–Co alloys have better electrocatalytic properties for oxygen evolution compared to pure Ni. Ternary alloys have also been used. For example, Plata-Torres et al. [66] prepared several metallic alloys containing Ni, Co and Fe by mechanical alloying. They found that Ni–Co–Mo alloys had better activity toward OER compared to Co–Ni, Co–Mo and Ni–Mo alloys. Continuous potential cycling altered the surface active sites of the Ni–Co–Mo alloys thus increasing OER activity. However, the same treatment was not effective for Ni–Co–Mo–Fe alloys. Sadiek et al. [67] achieved enhanced OER activity using glassy carbon and Au electrodes modified with binary catalysts composed of nickel oxide nanoparticles and cobalt oxide nanoparticles. The binary-modified electrodes exhibited better activity and stability compared to the individual oxide-modified electrodes.

From the early investigations on oxygen evolution catalysts for use in metal air batteries and alkaline water electrolysis, nickel cobaltite ( $\text{NiCo}_2\text{O}_4$ ), which is a type of spinel oxide, has been proposed as a material with good performance [68]. Investigations in the following years with  $\text{NiCo}_2\text{O}_4$  as OER catalysts have shown that the preparation method has a significant effect both on the electrocatalytic activity [69–71] and on the mechanical properties [70].

Spinel type oxides have been widely investigated for OER in alkaline media. Oxygen evolution on  $\text{NiCo}_2\text{O}_4$  and  $\text{Co}_3\text{O}_4$  films prepared by spray pyrolysis has been reported to follow similar mechanistic paths and Singh et al. [72] reported that the reaction occurs preferentially on the Co(IV) sites. However, this is in contradiction with more recent studies where the Co oxidation state is Co(II) and Co(III), such as cobalt hydroxide,  $\text{Co}(\text{OH})_2$ , cobalt oxyhydroxide,  $\text{CoOOH}$  and cobalt oxide;  $\text{Co}_3\text{O}_4$  have in general shown sufficient electrocatalytic activity for the OER [73]. The efficiency of the spinel type  $\text{Co}_3\text{O}_4$  can be also enhanced by the incorporation of additional metal ions, such as Zn [74], Cu [75–77], Fe [78], Mn [79]. Similarly, enhancement of the spinel oxide  $\text{NiCo}_2\text{O}_4$  has been reported by Fe substitution in the A-site ( $\text{Fe}_x\text{Ni}_{1-x}\text{Co}_2\text{O}_4$ ) [80]. Tan et al. [81] used

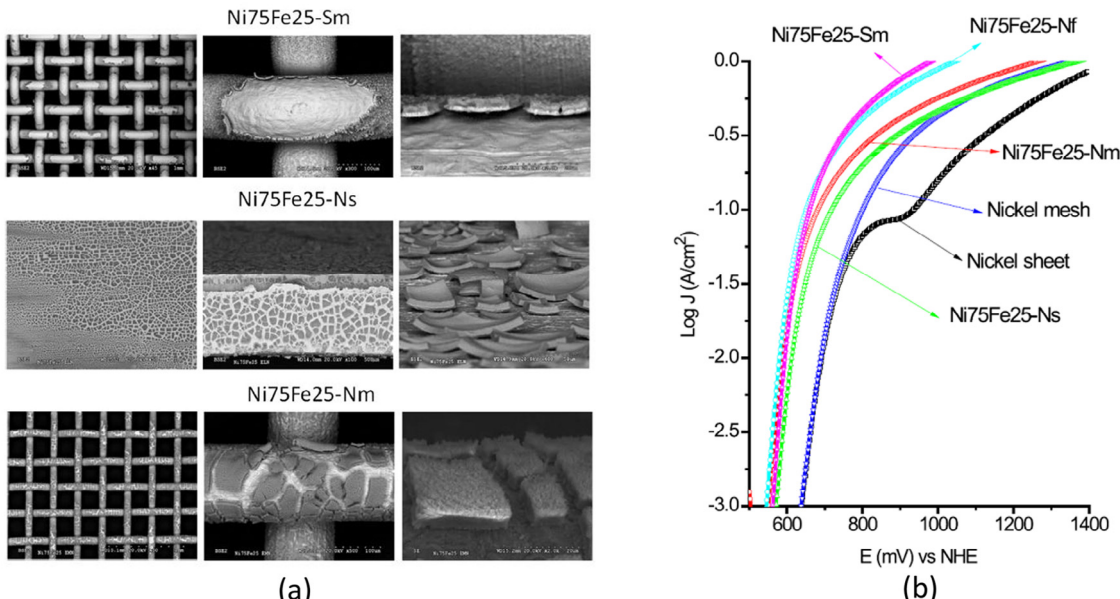


**Fig. 3.** (a) SEM images of the Ni<sub>75</sub>Fe<sub>25</sub> (Ni/Fe ratio of 75/25) on three different supports: stainless steel mesh (Sm, upper panel), nickel sheet (Ns, intermediate panel), nickel mesh (Nm, lower panel), (b) anodic steady-state polarization curves of Ni<sub>75</sub>Fe<sub>25</sub> electrocatalysts on the different supports. Scan rate = 1 mV s<sup>-1</sup>, KOH = 30 wt%. (a) shows a higher amount of discontinuities on the film structures when the meshes are used as substrates. (b) shows that the bare substrates exhibit moderate OER activity, lower than that of the Ni/Fe-modified electrodes. Nickel foam and steel mesh as substrates reduce the overpotentials, while this is not the case for nickel sheet or mesh substrates. Reprinted from reference 59 with permission of Elsevier.

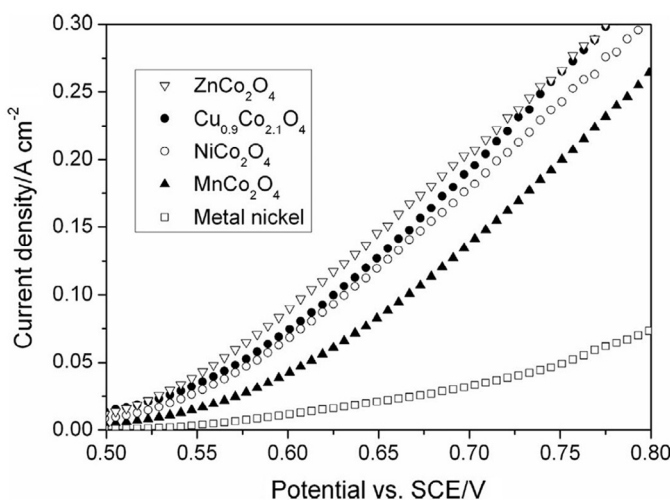


**Fig. 4.** Steady-state polarization curves for the OER in 1 M KOH. Reprinted from reference 81 with permission of Elsevier.

the co-precipitation method to synthesize a series of partially substituted cobaltite spinels  $M_xCo_{3-x}O_4$  ( $M = Ni, Cu, Zn, Mn$ ) and investigated their electrocatalytic properties for OER in 0.1 M KOH. The results of this study (Fig. 4) showed that all the cobaltite spinel electrodes have better performance than the metal Ni electrode at given potentials, while the  $ZnCo_2O_4$  and  $Cu_{0.9}Co_{2.1}O_4$  electrodes outperform  $NiCo_2O_4$  and  $MnCo_2O_4$  for OER. The high performance of  $ZnCo_2O_4$  is attributed to its high Co surface content, according to XPS findings. Finally, all the cobaltites of this study showed excellent stability after operation for 200 hours at  $0.1 A\text{ cm}^{-2}$  [81].

New mixed oxides with molecular formula  $MMoO_4$  ( $M: Mn, Fe, Co, Ni$ ) and  $M_2(MoO_4)_3$  ( $M: Fe, Cr$ ) have been recently developed as active OER catalysts. Substituted ternary oxides were found to be more active than Co-based spinel oxides [82–90]. Regarding manganese-based oxides, recent detailed [91] investigation for OER activity showed that in addition to the oxidation states, structural changes, such as concentration of oxygen point defects and length of the Mn–O bond, also play a significant role on the activity, since crystalline  $\alpha$ - $Mn_2O_3$  has better performance compared to  $Mn_3O_4$ .

All these studies have clearly shown that Ni-based oxides outperform Fe, Co and Mn-based materials. The activity of Ni and nickel hydroxides can be further increased by doping with a second element (Fe has been identified as the best choice) or by selecting proper substrates (nickel foam has exhibited superior activity). Recently, Diaz-Moralez et al. [92] attempted to rationalize the OER activity of doped Ni-based double hydroxides, in order to fundamentally investigate the improving effect of Cr, Mn, and Fe on the catalytic activity of the Ni-based double hydroxides and the deleterious effect of Co, Cu, and Zn. According to their DFT-based analysis, the effects of Fe, Mn, and Cr doping are different, as Fe and Mn are the active sites in  $NiFeOOH$  and  $NiMnOOH$  while Ni is the active site in  $NiCrOOH$ . Their computational results were compared with experimental data and suggested Ni–Fe double hydroxide as the most promising material, the activity and stability of which could be higher than that of  $IrO_2$ , depending on the preparation method. However, according to McGrory et al. [93], the activity of transition metal oxides is inferior compared to  $IrO_2$ . Following a benchmarking protocol for evaluating OER catalysts in terms of catalytic activity, stability, electrochemically active surface area, Faradaic efficiency, the authors of this study found that a current density of  $10 mA/cm^2$  can be achieved at overpotentials of  $0.35$ – $0.43 V$  using  $NiO_x$ ,  $CoO_x$ ,  $NiFeO_x$ ,  $NiLaO_x$ ,  $NiCuO_x$ ,  $NiCeO_x$ ,  $CoFeO_x$ ,  $CoP$ , while the same current density is achieved at overpotential of  $0.32 V$  for the case of  $IrO_2$ .

However, the significantly lower cost of Ni-based materials compared to  $IrO_2$  can compensate this small difference in activity. Furthermore, the same study reported a gradual loss in the OER of activity of  $IrO_2$  after 2 hours operation at  $10 mA/cm^2$ , thus suggesting that development of highly active and stable OER catalysts is still an open challenge.

### 3.1.2. Perovskites

Perovskites, mixed metal oxides of the general formula  $ABO_3$ , are materials with high structural stability and a wide range of possible compositions, as the A and/or B cations can partly be substituted by additional elements of different valences and/or sizes. Owing to their interesting properties and tunability with respect to composition, they have received widespread attention for applicability in catalysis [94–98].

In the perovskite structure  $ABO_3$ , A is the larger and B is the smaller cation. Cation A can be a lanthanide, alkaline or alkaline-earth element and the cation B is a metallic element with 3d, 4d or 5d configuration. In this structure, shown in Fig. 5, A and O form a cubic closest packing and B is contained in the octahedral voids in the packing, thus the B cation is 6-fold coordinated and the A is 12-fold coordinated by oxygen anions.

Partial substitution of the cations introduces vacancies in the materials, and this offers the possibility to tune the physicochemical properties and in particular the catalytic activity of the materials [84–88]. In general, substitution of the A-site mainly affects the ability of oxygen sorption, while substitution of the B-site influences the reactivity of the sorbed oxygen [94,99–101].

Bockris and Otagawa were the first to report the activity of perovskites for OER in 1984 [102]; they related it with the weak bond of  $OH^-$  on the surface of the catalyst. Since then, several perovskites with the  $ABO_3$  structure have been tested for OER and ORR in alkaline media, mainly as bifunctional catalysts for batteries. The majority of the studies involve materials of the type  $LaMO_3$  ( $M: Ni, Mn, Co, Fe$ ). Among them, lanthanum cobaltites,  $LaCoO_3$ , have shown interesting OER activity, which can be further improved by substitution, e.g. by Sr or Ca for La in the A-site or by Fe, Mn and Ir for Co in the B-site [100,103–110].

In parallel with experimental studies, several theoretical approaches have focused on identifying the intrinsic material characteristics that control activity. In 1980 Matsumoto et al. [111,112] correlated a broad  $\sigma^*$  band in the lattice and a high

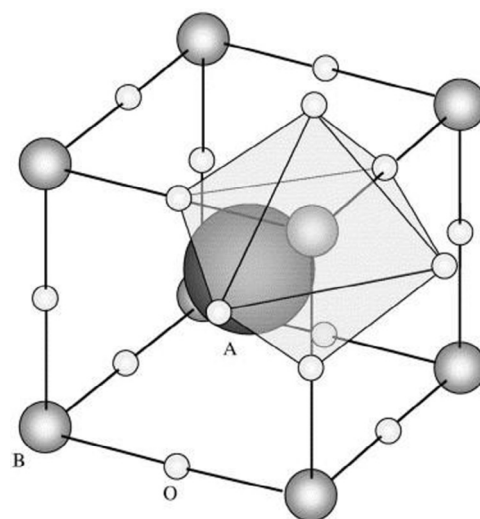


**Fig. 5.** Structure of  $ABO_3$  perovskite oxide. Reprinted from reference 94 with permission of Elsevier.

oxidation state of the B cation with a high activity for oxygen electrocatalysis. Afterward, Trasatti in 1984 [113] proposed a volcano-shaped relation between the overpotential and the enthalpy change of the lower-to-higher oxide transition. Bockris and Otagawa [102] tried to correlate the electrocatalytic activity with chemical bonding properties. Their experimental results, using various  $\text{ABO}_3$  perovskites with La in the A site and several transition metals (Ni, Co, Fe, Mn, Cr, V) in the B site, showed that the electrocatalytic activity increases as the B–OH bond strength decreases and as the number of electrons occupying the antibonding orbitals of B–OH increases. Moreover, they observed increase in the catalytic activity with the weakening of the M–O bonding in the lattice (thus with the introduction of oxygen vacancies), in consistency with the predictions of Trasatti [113] that the degree of nonstoichiometry significantly affects the electrocatalytic activity.

Several years later in 2011, Man et al. [114] used first principles calculations for modeling the thermochemistry of electrochemical reactions. According to this method, a prerequisite for the ideal catalyst (which should be able to facilitate water oxidation at potential just above the equilibrium one) is that the different charge transfer steps have reaction free energies of the same magnitude at zero potential. Since this prerequisite does not apply to

real catalysts, Man et al. [114] created free energy diagrams for OER at standard conditions on selected perovskites which show different binding strengths and estimated the size of the potential-determining step for each material. They thus [114] concluded that the OER activity of a wide range of oxides (perovskites, spinels, rutile, rock salt, bixbyite) is related to the difference in binding energies between the reaction intermediates  $\text{HOO}^*$  and  $\text{HO}^*$ . They proposed the parameter ( $\Delta G_{\text{O}^*} - \Delta G_{\text{HO}^*}$ ), i.e. the difference between the adsorption energies of  $\text{O}^*$  and  $\text{HO}^*$ , as an indicator for the universal description of activity in oxygen electrocatalysis. As shown in Fig. 6b, Suntivich et al. [115] examined systematically a decade of transition metal oxides and showed a volcano-type dependence of the OER activity with the occupancy of the 3d orbitals with  $e_g$  symmetry for the transition metal. The shapes of the 3d orbitals are illustrated in Fig. 6b [116,117]. Vojdovic and Nørskov [118] worked further in these directions and proposed that the oxygen adsorption energies are also related with the  $t_{2g}$  levels (Fig. 7).

These findings opened the way for the design of materials with targeted properties to maximize the OER activity. According to the findings of Suntivich et al. [115] the maximum OER activity would require  $e_g$  occupancy close to unity and high B-site oxygen covacency. In the  $\text{LaMO}_3$  series, M = Cr, Mn, Fe, Co or Ni, the formal

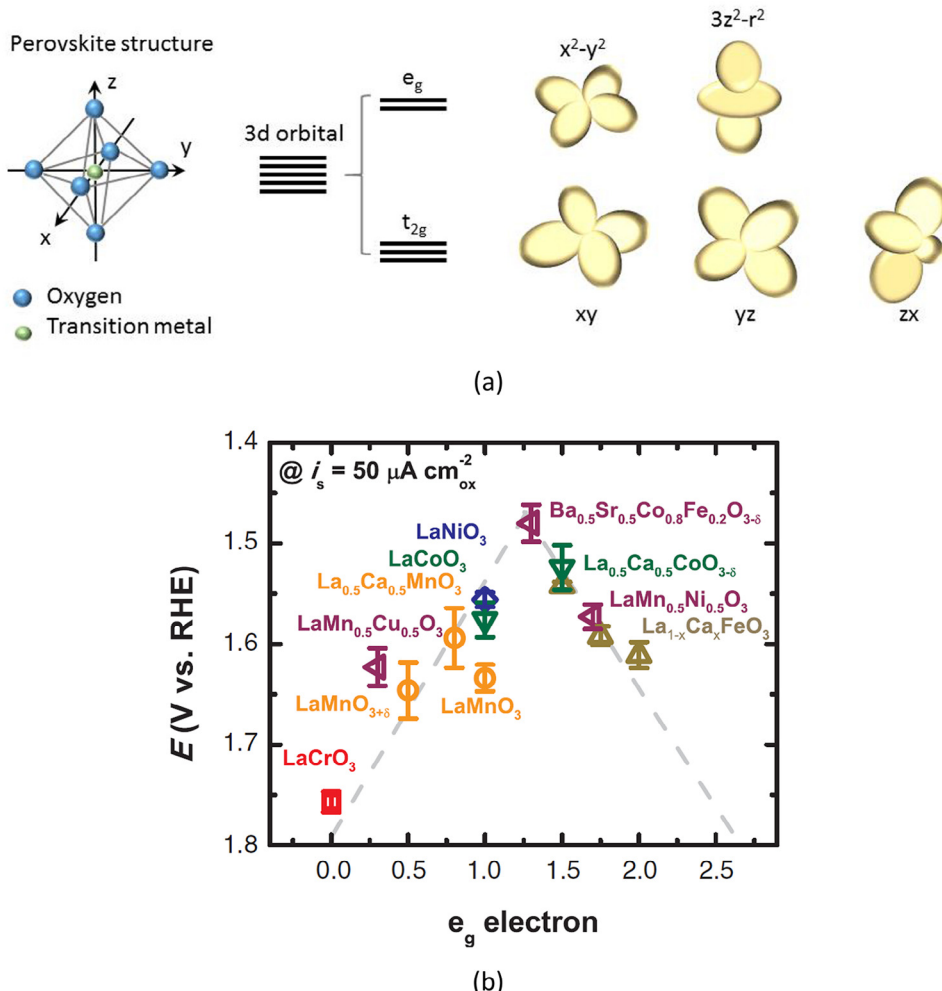


**Fig. 6.** (a) The B cations (typically transition metal) in the perovskite structure are at the center of the oxygen octahedron. The 3d orbitals fall into two groups:  $e_g$  orbitals consist of the 3d orbitals  $x^2-y^2$  and  $z^2$ , while the  $xy$ ,  $yz$  and  $xz$  constitute the  $t_{2g}$  orbitals. The  $t_{2g}$  orbitals have lower overlap with the neighboring 2p orbitals of the oxygen ions, and thus they have lower energy because the Coulomb energy is lower. The 3d orbitals  $x^2-y^2$ ,  $xy$ ,  $yz$  and  $xz$  have four lobes centered in the plane indicated in the orbital label (e.g. the lobes of the  $x^2-y^2$  lie along the x and y axes). The 3d orbital  $z^2$  has a unique shape with two lobes along the z axis and a belt centered in the xy plane. Adapted from reference 117. (b) The relation between overpotential at  $50 \mu\text{A cm}^{-2}$  and the occupancy of the  $e_g$ -symmetry electron of the transition metal B in the  $\text{ABO}_3$  structure.  $x = 0$ , 0.25 and 0.5 for  $\text{La}_{1-x}\text{Ca}_x\text{FeO}_3$ . Reprinted from reference 115 with permission of The American Association for the Advancement of Science.

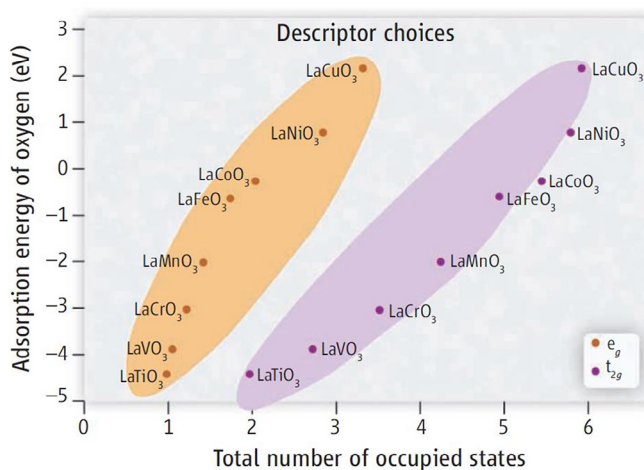


**Fig. 7.** The descriptor choices as proposed by Vojvodic and Nørskov [116] using DFT calculations on the basis of the findings of Suntivich et al. [113]. Figure shows that the  $t_{2g}$  symmetry occupation or the adsorption energy of oxygen can be also a descriptor (OER activity increases with high  $t_{2g}$  occupation). Reprinted from reference 118 with permission of The American Association for the Advancement of Science.

occupation of the 3d orbitals in the most active oxides is:  $\text{LaCoO}_3$  ( $t_{2g}^4 e_g^2 \leftrightarrow t_{2g}^5 e_g^1$ ),  $\text{LaMnO}_3$  ( $t_{2g}^3 e_g^1$ ) and  $\text{LaNiO}_3$  ( $t_{2g}^6 e_g^1$ ), (Table 2) [119,120]. The central role played by the electron density localized on the  $e_g$  orbitals, close to one, is manifested. The fact that the highest occupied orbitals,  $e_g$ , participate in  $\sigma$ -bonding with the surface-anion adsorbates explains their relevance [121]. In an octahedral coordination, the d orbitals fall into two groups: three  $t_{2g}$  orbitals, that have lower overlap with the neighboring 2p orbitals of the oxygen ions (Fig. 8A), and thus they are more stable because the Coulomb energy is lower and the  $e_g$  orbitals that are oriented toward the oxygen atoms (Fig. 8B).

A material with stoichiometry  $\text{Ba}_{0.5}\text{Sr}_{0.5}\text{Co}_{0.8}\text{Fe}_{0.2}\text{O}_{3-\delta}$  (BCSF) was identified as optimal by Suntivich et al. [115]. BSCF exhibits one order of magnitude higher intrinsic activity for OER in alkaline media than  $\text{IrO}_2$ . Similarly, high OER activity has been observed with  $\text{SrCo}_{0.8}\text{Fe}_{0.2}\text{O}_{3-\delta}$  [122,123]. Double perovskites of the form  $(\text{Ln}_{0.5}\text{Ba}_{0.5})\text{CoO}_{3-\delta}$  ( $\text{Ln}$ : Pr, Sm, Gd, Ho) have been also proposed as a family of cobalt-containing OER catalysts with high activity and stability, explained by the presence of their O p-band center neither too close nor too far from the Fermi level. The authors of this study suggest that the double perovskites have greater stability compared to BSCF, which becomes amorphous during OER [124]. A novel

**Table 2**

Electronic configuration, magnetic and electric properties, optical gap and current densities ( $I_{\text{OER}}$ ) for the  $\text{LaMO}_3$  series,  $M = \text{Cr}, \text{Mn}, \text{Fe}, \text{Co}$  or  $\text{Ni}$ .  $I_{\text{OER}}$  for OER at 2.4 V (vs Zn). Adapted from reference 126 with permission of Elsevier.

Perovskite	Electronic Configuration	Magnetic properties	Electrical properties	$\text{mA cm}^{-2}$ $I_{\text{OER}}$
$\text{LaCrO}_3$	$\begin{array}{c} \uparrow \quad \downarrow \\ \text{e}_g \\ \uparrow \quad \downarrow \end{array} \begin{array}{c} \uparrow \quad \downarrow \\ \text{t}_{2g} \\ \uparrow \quad \downarrow \end{array}$	Antiferromagnetic ( $T_{\text{Neel}} \sim 300\text{K}$ )	Insulator Optical gap $\sim 4\text{eV}$	-
$\text{LaMnO}_3$	$\begin{array}{c} \uparrow \quad \downarrow \\ \text{e}_g \\ \uparrow \quad \downarrow \end{array} \begin{array}{c} \uparrow \quad \downarrow \\ \text{t}_{2g} \\ \uparrow \quad \downarrow \end{array}$	Antiferromagnetic ( $T_{\text{Neel}} \sim 140\text{K}$ )	Semiconductor Optical gap $\sim 1,2\text{eV}$	14.3
$\text{LaFeO}_3$	$\begin{array}{c} \uparrow \quad \downarrow \\ \text{e}_g \\ \uparrow \quad \downarrow \end{array} \begin{array}{c} \uparrow \quad \downarrow \\ \text{t}_{2g} \\ \uparrow \quad \downarrow \end{array}$	Antiferromagnetic ( $T_{\text{Neel}} \sim 740\text{K}$ )	Insulator Optical gap $\sim 2,2\text{eV}$	10.0
$\text{LaCoO}_3$	IS: $\begin{array}{c} \uparrow \quad \downarrow \\ \text{e}_g \\ \uparrow \quad \downarrow \end{array} \begin{array}{c} \uparrow \quad \downarrow \\ \text{t}_{2g} \\ \uparrow \quad \downarrow \end{array}$ HS: $\begin{array}{c} \uparrow \quad \downarrow \\ \text{e}_g \\ \uparrow \quad \downarrow \end{array} \begin{array}{c} \uparrow \quad \downarrow \\ \text{t}_{2g} \\ \uparrow \quad \downarrow \end{array}$ LS: $\begin{array}{c} \uparrow \quad \downarrow \\ \text{e}_g \\ \uparrow \quad \downarrow \end{array} \begin{array}{c} \uparrow \quad \downarrow \\ \text{t}_{2g} \\ \uparrow \quad \downarrow \end{array}$	Transition from diamagnetic to paramagnetic at $T=80\text{K}$	Semiconductor Optical gap $< 1,2\text{eV}$	43.3
$\text{LaNiO}_3$	$\begin{array}{c} \uparrow \quad \downarrow \\ \text{e}_g \\ \uparrow \quad \downarrow \end{array} \begin{array}{c} \uparrow \quad \downarrow \\ \text{t}_{2g} \\ \uparrow \quad \downarrow \end{array}$	Paramagnetic	Metallic	21.4

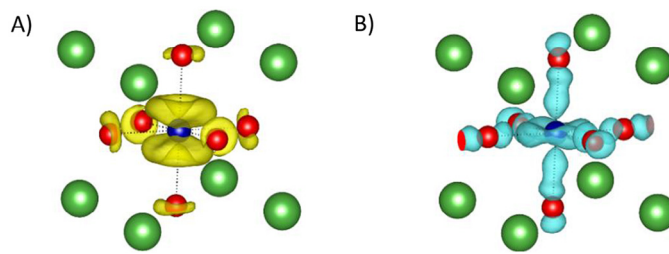


**Fig. 8.** (A) Depopulation of the  $t_{2g}$  orbitals after a low-spin ( $t_{2g}^6e_g^0$ ) to high-spin ( $t_{2g}^4e_g^2$ ) transition; and (B) relocation of the electronic density in the  $e_g$  orbitals. Electronic density obtained from DFT (GGA + U) calculations in  $\text{LaCoO}_3$ .

tetragonal ball-milled  $\text{SrNb}_{0.1}\text{Co}_{0.7}\text{Fe}_{0.2}\text{O}_{3-\delta}$  (SNCF) perovskite developed recently by Zhu et al. [125] showed excellent activity for OER in alkaline solutions. The superior performance of this material compared to BSCF was attributed to several factors, such as the presence of  $\text{Co}^{2.8+}$  with an optimal  $e_g$  orbital filling ( $t_{2g}^5e_g^{12}$ ), the good charge-transfer characteristics, high affinity for  $\text{OH}^-$  adsorption and favorable  $\text{O}_2$  desorption characteristics.

The intriguing correlation of the activity of cobaltites, usually the most active perovskites, with composition seems due to the presence of conflicting electronic interactions. Three electronic states, low-spin (LS)  $t_{2g}^6e_g^0$ , high-spin (HS)  $t_{2g}^4e_g^2$  and intermediate-spin (IS)  $t_{2g}^5e_g^1$  states, compete in stability. The electronic structure and Co–O bonds strongly depend on the dominant orbital configuration (Fig. 9) [126]. Current ab-initio calculations try to identify if the exclusive stabilization of the  $t_{2g}^5e_g^1$  electronic state for the cobalt atoms appears uniquely in the most active catalysts.

An in-depth study of the magnetic structure within the most active perovskites for oxygen evolution reaction by Gracia et al. [127] shows that the ground states preferentially settle with an extended antiferromagnetic orbital ordering. The combination of parallel and antiparallel exchange interactions appears related with the electro-catalytic activity. In their ground state, the calculated perovskites present space-separated charge transport channels depending on the spin orientation. Comparing the spin localization with reported activities, authors report a direct correlation between the maximum spin polarization accumulated on the metal/oxygen atoms, in the bulk material, and the catalytic activity. The possible implications of such observations are discussed in terms of magnetic interactions. During oxygen evolution in water electrolysis, reactants and products do not preserve spin. For triplet state oxygen to evolve, the catalyst, anode, can speed up the reaction if it is able to balance the magnetism of the oxygen molecule by extracting electrons with an opposite magnetic moment, conserving the overall spin. The presence of conflicting electronic interactions indicated

by the maximum spin polarization helps in the selective extraction of oriented electrons [127].

Another innovative recent study concerns the development of ordered oxygen-deficient perovskites with molecular level porosity ( $\text{A}_2\text{B}_2\text{O}_5$ ), which have been suggested as a promising new class of oxides for OER electrocatalysis [128]. This oxygen-deficient structure, shown in Fig. 10a for  $\text{Ca}_2\text{Mn}_2\text{O}_5$ , is described as a square pyramid of  $\text{MnO}_5$  with a zigzag structure, resulting in molecular level porosity due to the oxygen vacancy (one oxygen atom is missing from the octahedral  $\text{MnO}_6$  subunit along the directions normal to the ab plane). The oxygen-deficient  $\text{Ca}_2\text{Mn}_2\text{O}_5$  showed better OER activity than the normal  $\text{CaMnO}_3$  perovskite (Fig. 10b). The high OER activity of the former was attributed to (a) the unit cell structure, which favors the transport of  $\text{OH}^-$  ions, (b) to the electronic configuration of the B-site manganese cation with high spin electron occupying  $e_g$  orbitals, (c) to the easier formation of bonds between  $\text{Mn}^{3+}$  and  $\text{OH}^-$  through the oxygen vacancies.

Even though it has become clear from theoretical studies that the electronic structure of perovskites affects the OER activity, DFT-based material screening is an ab initio method which does not consider kinetics. Thus, this type of screening is not conclusive and represents only a first step for material optimization. Further investigations (i.e. ab-initio kinetics studies) should be performed in order to reach firm conclusions about the reaction mechanism. Finally, subtle details in the experimental procedures, such as the preparation of catalyst inks with different perovskite/carbon ratios, can result in misleading observations during experimental OER materials screening. Carbon is typically added in the catalytic ink in order to enhance the electronic conductivity of the catalytic layer. However, it has been recently reported that the presence of carbon can also enhance the OER activity of selected perovskites [129,130]. The nature of the interaction between different perovskites and carbon is still not clear, but it can be helpful for the development of more efficient OER catalyst designs. However, fundamental studies focusing on the understanding of the intrinsic properties of perovskites should be carried out with carbon-free catalytic inks. On top of this, carbon-free materials are preferable for practical applications, since carbon shows poor stability under electrolysis conditions.

### 3.1.3. Novel structures

Identifying the optimal composition for OER in alkaline electrolysis at the molecular level is one parameter, but optimizing the structure of the electrocatalyst is also key for their performance. For example, the morphology of the electrocatalyst can have profound influence on e.g. the detachment of oxygen bubbles from the surface, which in turn affects the availability of active sites [131]. Therefore, much scientific interest has been lately focused on the

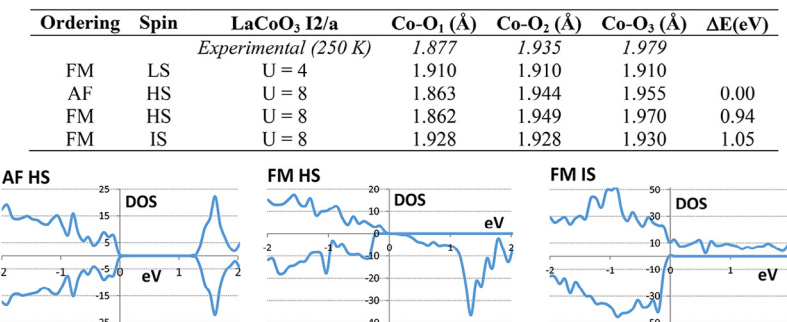


**Fig. 9.** Top: DFT (GGA + U) predictions for different  $\text{LaCoO}_3$  spin states. Bottom: Density of states (DOS) versus energy in eV for LS AFM HS, and FM IS orderings. AF: anti-ferromagnetic, FM: ferromagnetic, HS: high spin, LS: low spin. Reprinted from reference [126] with permission of Elsevier.

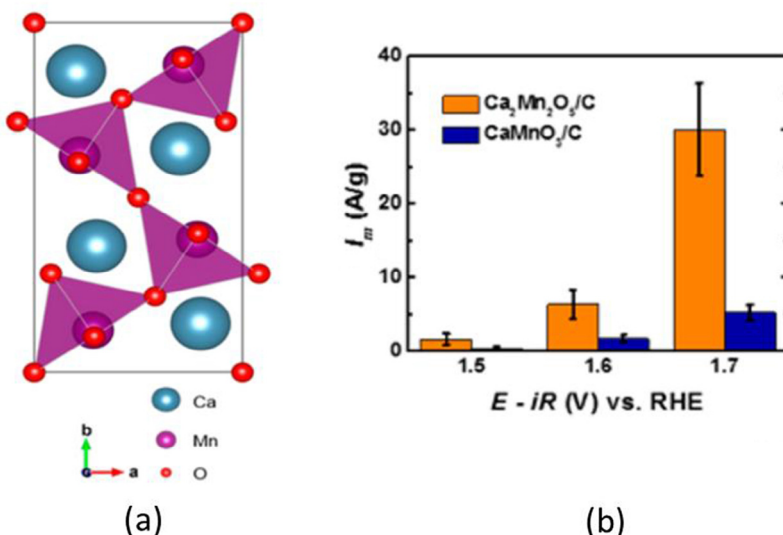


**Fig. 10.** (a) Unit cell of oxygen deficient perovskite  $\text{Ca}_2\text{Mn}_2\text{O}_5$ . The ordered oxygen vacancy along directions normal to the ab plane is shown. Normally, each Mn atom should be bonded with 6 oxygen atoms and form an octahedral. However, in the present case one oxygen is missing along the direction of the ab plane (each Mn atom is bonded with 5 oxygen atoms). Due to this oxygen vacancy, a square pyramid  $\text{MnO}_5$  subunit was obtained. (b) Comparison of the mass activities for  $\text{CaMnO}_3$  and  $\text{Ca}_2\text{Mn}_2\text{O}_5$  perovskites at various applied potentials in 0.1 M KOH. Carbon was added to the perovskite in order to increase electronic conductivity. Reprinted from reference 128 with permission of American Chemical Society.

development of novel structures that combine a large surface area with good electronic conductivity and optimal porosity.

The recent development of nickel–cobalt layered double hydroxide (LDH) nanosheets deposited onto a nickel foam support has led to electrodes with excellent performance for OER both in terms of activity and stability, related to their intrinsic layer structure and redox characteristics [132]. Wang et al. [133] developed a novel hierarchical Ni–Co oxide nanostructure, which is composed of small secondary nanosheets grown on primary nanosheet arrays. This structure allows for a  $\text{Ni}^{3+}$ -enriched surface, which facilitates the formation of  $\text{NiOOH}$  active sites and also offers high surface area. Thus these materials, showed a low overpotential of 0.34 V at  $10 \text{ mA cm}^{-2}$ , while they performed better than  $\text{Co}_3\text{O}_4$  nanorods,  $\text{Co}_3\text{O}_4$  nanosheets and Ni–Co oxide nanorods. Au/Ni $\text{Co}_2\text{O}_4$  nanoarrays have also exhibited good OER activity and high stability in the alkaline environment [134].

An innovative core–ring structure of  $\text{NiCoO}_4$  nanoplatelets has been developed by Cui et al. [135] with strong Co enrichment in the core and stoichiometric ratio of Ni:Co = 1:2. The material was introduced as an OER electrocatalyst in alkaline water electrolysis and exhibited superior performance compared to ordinary  $\text{NiCoO}_4$  and  $\text{Co}_3\text{O}_4$  prepared by alternate methods. The overpotential is 0.3 V at a current density of  $0.1 \text{ A cm}^{-2}$ . This extremely high activity is due to the increased active surface area and the large number of active surface Co atoms.

The use of carbon-based structures (nanotubes, nanosheets, nanowires, carbonaceous microspheres) as the support of OER electrocatalysts has been explored in several studies, since these materials are electronically conductive and provide large surface areas [57,136–146]. For example, the deposition of cobalt oxide nanoparticles on multiwall carbon nanotube-modified glassy carbon yields active OER electrocatalysts in alkaline media with good stability and durability, as reported by Raoof et al. [137]. Another successful example in this direction is the use of graphene oxide nanosheets as the support for dispersed Mn and Co-substituted  $\text{Fe}_3\text{O}_4$  nanoparticles [138], where the cobalt oxide and the manganese oxide ensured high oxygen evolution and reduction activity respectively, while the bulk  $\text{Fe}_3\text{O}_4$  ensured the electronic conductivity together

with the graphene nanosheets, which also reduced the external transport resistance.

An efficient, robust and economic nanostructured OER electrocatalyst was also developed by Gao et al. [147] based on  $\alpha\text{-Ni(OH)}_2$  hollow spheres. Nanoparticles of  $\alpha\text{-MnO}_2$  embedded in a matrix with abundant micropores showed also good OER activity due to improved reactants accessibility to the active sites [148]. However, Selvakumar et al. [149] showed that the optimal shape of  $\alpha\text{-MnO}_3$  is nanowires, which, compared to nanotubes and nanoparticles, showed the best performance probably due to facilitated access of the reactants to the surface.

Fe/Co metal–organic-frameworks (MOFs) have been proposed as a promising structure, since the high specific area and abundant micropores in these materials are beneficial for oxygen diffusion and catalytic sites utilization [150]. A current density of  $3 \text{ mA cm}^{-2}$  at 0.9 V vs Ag/AgCl was obtained when the MOF was mixed with carbon black, which is 79 times higher than that when only carbon black was used as reference material.

Finally, nanostructured perovskites consisting of nonstoichiometric  $\text{CaMnO}_{3-\delta}$  oxides in the form of microspheres and nanoparticles made by thermal decomposition of carbonate precursors and by the Pechini route respectively have been described by Du et al. [151]. It was found that the presence of oxygen vacancies is related to improvement in performance, with reduced overpotentials and high current densities. The oxygen-defective  $\text{CaMnO}_{3-\delta}$  with  $\delta$  close to 0.25 manifested the highest OER activity, with potential of  $\sim 1.6$  V vs RHE at  $50 \mu\text{A/cm}^2_{\text{ox}}$  normalized to electrochemical active surface area.

Ruthenium oxide,  $\text{RuO}_2$ , is one of the most active electrocatalysts for the OER, but alkaline electrolysis mainly uses transition metal catalysts due to their significantly lower cost and sufficiently high activity. However, Liang et al. focused their recent study on  $\text{RuO}_2$  and published a way to improve its stability in the alkaline environment [152]. Using wet impregnation on a  $\text{CeO}_2$  support, they prepared  $\text{RuO}_2/\text{CeO}_2$  composite electrocatalysts, where the defective nanosized  $\text{CeO}_2$  was synthesized through an explosion reaction using  $\text{Ag@CeO}_2$  core–shell nanospheres as precursors. They found that the defective  $\text{CeO}_2$ -supported  $\text{RuO}_2$  has improved OER activity

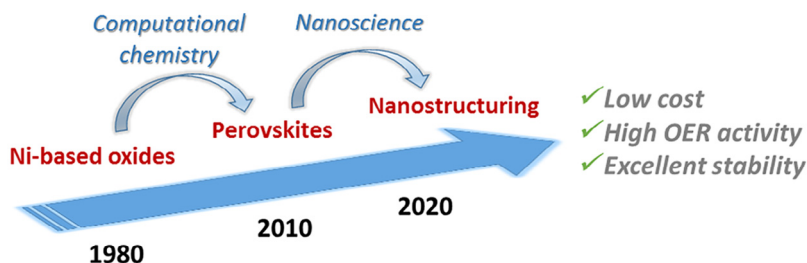


**Fig. 11.** Progress in the development of OER electrocatalysts for alkaline electrolysis, as a result of intense interaction between materials science, computational chemistry and nanoscience.

compared to pristine  $\text{RuO}_2$  and enhanced stability under alkaline conditions of 0.1 M KOH. The enhanced performance (activity and stability) was attributed to “spillover” of oxygen species from  $\text{CeO}_2$  to the  $\text{RuO}_2$  surface during the OER, which facilitates water oxidation. These results may open a new way for the employment of the highly active Ru-based materials in alkaline electrolysis. However, cost compensation with the commonly used Ni and Co based materials should be taken into account.

To conclude, several nanostructured materials have been developed and showed high OER activity, owing to their high surface area. Enhanced performance can be obtained either by nanostructuring the OER active phase or introducing the active phase into C-based structures with high surface area. The latter method could be considered as more advantageous due to simplicity in materials preparation, but on the other hand carbon materials can suffer from corrosion under OER conditions. In view of materials optimization, the first step has been taken since the progress in computational chemistry has already led to the identification of promising perovskites with high intrinsic OER activity and excellent stability. As a next step, these findings should be combined with ab-initio kinetics studies, because only such integrated studies can provide reliable conclusions for mechanistic considerations. Further developments in this field together with the recent advances in nanoscience are expected to play a key role in the design of novel OER catalysts and the replacement of Raney nickel in alkaline electrolysis (Fig. 11).

### 3.2. PEM electrolyzers

The state-of-the-art anode materials for PEM electrolysis are mixed oxides composed of  $\text{IrO}_2$  and  $\text{RuO}_2$ . The high activity of Ir and Ru has been apparent from the early investigations of water electrolysis in acidic media, since Damjakovic et al. [153] in the mid-1960s and ten years later Miles and Thomason [154] compared the OER catalytic activity of different metals and binary alloys in acidic solutions. Even though these primary investigations started from catalysts in the

metallic form, oxide films form on the surface at high anodic potentials during OER [155]. Interestingly, Ru ( $\text{RuO}_2$ ) and Ir ( $\text{IrO}_2$ ) outperform Pd, Rh, Pt, Au, Nb for OER in acidic solutions [153–156]. The lower electrocatalytic activity of Pt and Pd is caused by the high resistance oxide film that is formed on the surface of these metals;  $\text{RuO}_2$  and  $\text{IrO}_2$ , on the other hand, exhibit high electronic conductivity [20]. In these oxides, the metal–metal distance and the radius of the cation have values that allow for overlap of the inner d-orbitals that are responsible for the electron conduction [157].

Although  $\text{RuO}_2$  and  $\text{IrO}_2$  exhibit similar OER activity, Ru has the advantage of higher abundance in nature compared to Ir. However,  $\text{RuO}_2$  suffers from corrosion/dissolution during oxygen evolution in acidic environments (forming  $\text{RuO}_4$  [158]), but this can be eliminated by the use of dimensionally stable anodes (intermixing  $\text{RuO}_2$  with  $\text{TiO}_2$ ) [159]. On the other hand,  $\text{IrO}_2$  also experiences corrosion but to a much lesser extent [160,161]. Both materials have been the focus of the majority of PEM water electrolysis studies.

Aiming at more cost-affordable PEM electrolysis systems, many catalyst alternatives have been proposed lately, based mainly on three routes (Fig. 12), which are discussed in the following paragraphs:

- increasing the stability of the less expensive Ru, by using it in several binary or multi-metallic oxides (the same approach is applicable to Ir, of course),
- utilization of active supports with large surface areas for dispersing the active catalytic phase in order to decrease the catalyst loading,
- decreasing the loading of the high cost catalysts by using alternative preparation methods and catalyst structures.

#### 3.2.1. Mixed oxides

Binary oxides of the type  $\text{Ir}_x\text{Ru}_{1-x}\text{O}_2$  exhibit considerable activity and stability during OER [162–166], with  $\text{Ir}_{0.6}\text{Ru}_{0.4}\text{O}_2$  having been identified as the optimal combination by Marshall et al. [165]. Fig. 13 compares the electrochemical behavior of Pt,  $\text{IrO}_2$ ,  $\text{RuO}_2$  and

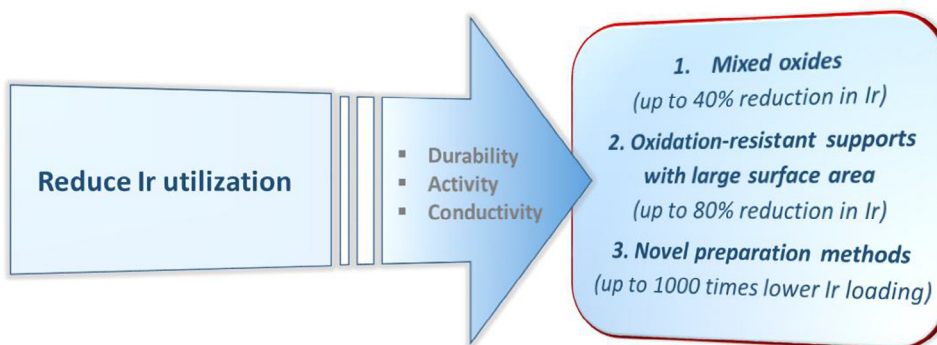


**Fig. 12.** Strategies for reducing noble metal utilization in PEM OER electrocatalysis.

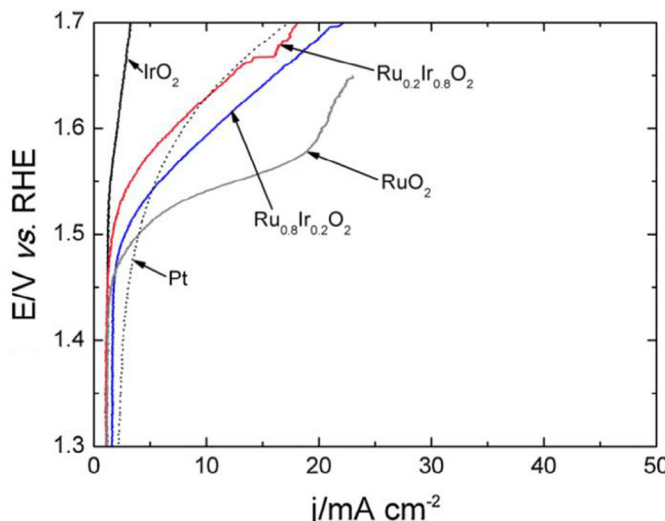


**Fig. 13.** Polarization curves with different anodes, where potential (versus the reversible hydrogen electrode (RHE)) is plotted on the y-axis and current density on the x-axis. Data were collected by varying the potential with 5 mV s<sup>-1</sup>. Electrolyte: 0.5 M H<sub>2</sub>SO<sub>4</sub>. Reprinted from reference 164 with permission of Elsevier.

IrO<sub>2</sub>–RuO<sub>2</sub> mixed oxides in an acidic supporting electrolyte (0.5 M H<sub>2</sub>SO<sub>4</sub>). The best onset potential is observed with RuO<sub>2</sub>, while the activity of Pt is much lower than that of both IrO<sub>2</sub> and RuO<sub>2</sub>. Introducing Ir in the RuO<sub>2</sub> catalyst yields sufficient electrocatalytic activity, while stability is also maintained even after prolonged operation during PEM water electrolysis at 1 A cm<sup>-2</sup> at 25 °C [164].

Suitable OER rates and sufficient stability have been also obtained with other mixed oxides, such as Ru<sub>x</sub>Ir<sub>y</sub>Ta<sub>z</sub>O<sub>2</sub> [165], Ru<sub>x</sub>Ir<sub>y</sub>Co<sub>z</sub>O<sub>2</sub> [166–168], Ru<sub>x</sub>Ir<sub>y</sub>Sn<sub>z</sub>O<sub>2</sub> [169,170], Sn<sub>x</sub>Ru<sub>1-x</sub>O<sub>2</sub> [171], Ru<sub>x</sub>Nb<sub>1-x</sub>O<sub>2</sub> [172], Ru<sub>1-x</sub>Ni<sub>x</sub>O<sub>2-y</sub> [173], Ir<sub>x</sub>Pt<sub>1-x</sub>O<sub>2</sub> [174], Ir<sub>x</sub>Sn<sub>1-x</sub>O<sub>2</sub> [175], Ir<sub>x</sub>Ti<sub>y</sub>Pt<sub>z</sub>O<sub>2</sub> [176]. Although the synergistic mechanism which accounts for the enhancement in stability and activity is not yet fully understood, alterations in the electronic structure, electronic interactions and interatomic spacing have been mentioned to play a key role in the OER reaction [21]. Even though these investigations led to the development of cheaper catalysts with favorable catalytic stability and activity, there are limits to the addition of the inexpensive metal oxides since the active surface area and the electronic conductivity decrease as the loading with cheaper metal oxides increases [177].

Neyerlin et al. [178] screened several platinum containing binary Pt–M (M: Ir, Re, Ru, Pd) and ternary Pt–Ru–M (M: Ir, Pd) catalyst libraries for their OER activity in acidic media. As shown in Fig. 14, their results revealed Pt<sub>20</sub>Ru<sub>80</sub>, Pt<sub>20</sub>Ru<sub>60</sub>Ir<sub>10</sub> and Pt<sub>20</sub>Ru<sub>70</sub>Pd<sub>10</sub> as promising OER electrocatalysts.

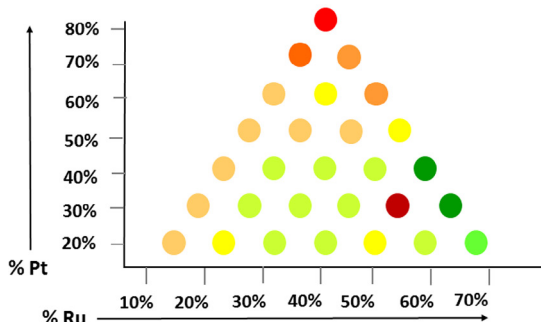


**Fig. 14.** Activity map of two ternary systems Pt–Ru–M supported on C. Left figure system Pt–Ru–Ir, Right figure system Pt–Ru–Pd. The color of the circles encodes the reactivity at 1.48 V vs RHE (red: poor activity, green: high activity). Adapted from reference 178.

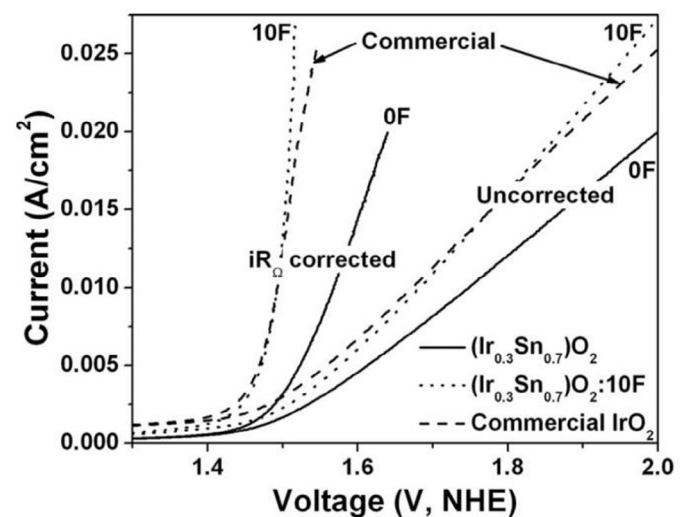
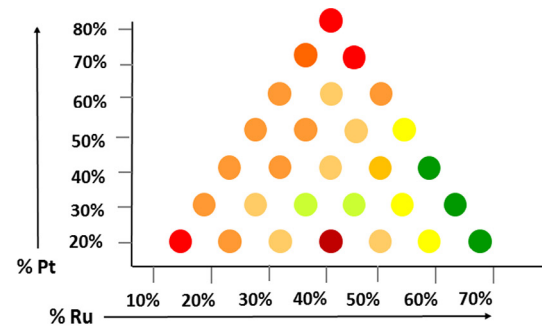


**Fig. 15.** Polarization curves for undoped and F-doped Ir<sub>0.7</sub>Sn<sub>0.3</sub>O<sub>2</sub> and also for commercial IrO<sub>2</sub>. The current density is plotted on the y-axis and the potential (versus the normal hydrogen electrode-NHE) on the x-axis. Data were collected by varying the potential with 1 mV s<sup>-1</sup>. Figure shows both the as-received potential data values (uncorrected) and the potential values after removing the ohmic-drop compensation (iR corrected). Experiments conducted in 1 N H<sub>2</sub>SO<sub>4</sub>, 40 °C. Reprinted from reference 177 with permission of The Electrochemical Society.

Fluorine doped oxides have been proposed lately as suitable low cost OER catalysts [171,177,179–181]. Kadakia et al. [177] showed that F-doped Ir<sub>0.3</sub>Sn<sub>0.7</sub>O<sub>2</sub> (10 wt% F) has better electrochemical performance, current density, polarization resistance and Tafel slope (the slope from the linear region in the plot of overpotential versus ln(i/i<sub>0</sub>), where i<sub>0</sub> is the exchange current density; unit for Tafel slope is V/dec) than the undoped binary electrocatalyst, while its performance is comparable to that of commercial IrO<sub>2</sub> (Fig. 15).

### 3.2.2. Supports for OER catalysts

To reduce the amount of precious metal in an OER catalyst, nanostructures in combination with large surface area supports can be used for increasing the catalytic activity. The support should combine high surface area with high electronic conductivity and suitable pore structure, which allows the transport of reactants and products to/from the catalytic active sites. Carbon substrates, commonly used in fuel cell technology (carbon black, graphitized carbon), suffer from corrosion under the high anodic overpotentials of OER during PEM electrolysis. Coating with Ti can prevent oxidation of the carbon paper according to Slavcheva et al. [161,182].



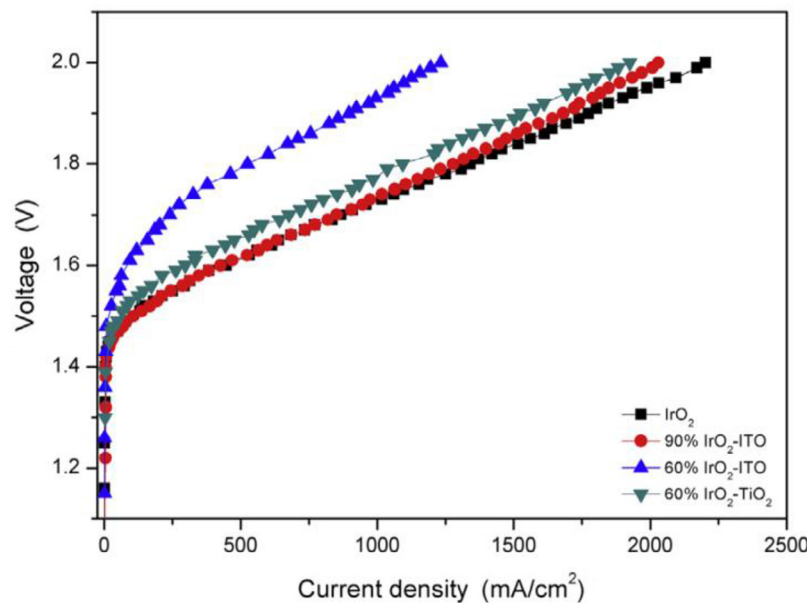


**Fig. 16.** Polarization curves during PEM water electrolysis using different  $\text{IrO}_2$ -based anodes. Cathode: 20 wt% Pt/C, T: 80 °C; electrolyte: Nafion 115. Reprinted from reference 189 with permission of Elsevier.

The same group attempted to use  $\text{IrO}_2$ -free OER catalysts by using Pt in combination with low cost transition metals instead. The bi-metallic electrocatalysts were synthesized following the sol-gel method and supported on a mechanically treated titanium-based support with a total metallic loading of 20 wt%. According to the authors, the nonstoichiometric  $\text{TiO}_x$  support enhances the OER activity of bimetallic Pt–Fe and Pt–Co catalysts compared to pure Pt, through a synergistic effect related with hypo-hyper-d-electronic interactions [183]. In general, the hypo d-electron character of the support has the ability to interact with hyper d-electron metals and the magnitude of this interaction varies when e.g. Pt is alloyed with other metals. The d-band serves as the bonding and adsorptive orbital, while electronic density defines the overall kinetics and reaction rate. Thus, this hypo-hyper d-electronic interactive effect can affect significantly catalysis and electrocatalysis [184].

Moreover, the materials were found to be stable after PEM electrolysis under  $50 \text{ mA cm}^{-2}$  at 80 °C for 6 hours. Based on the idea of the beneficial metal–support interactions, Paunovic et al. [185] prepared electrocatalysts containing a mixed Co–Ru metallic phase deposited on activated multiwall carbon nanotubes (MWCNTs) and  $\text{TiO}_2$  anatase. The presence of mixed hypo-hyper d-oxides on the catalyst's surface ( $\text{CoO}-\text{TiO}_2$ ,  $\text{RuO}_2-\text{TiO}_2$ ) was held responsible for the increased activity.

Alternative materials such as titanium carbide ( $\text{TiC}$ ) [186], tantalum carbide ( $\text{TaC}$ ) [187], silicon carbide-silicon ( $\text{SiC-Si}$ ) [188], indium tin oxide (ITO) [189] and antimony doped tin oxide (ATO) [190] have also been investigated as oxidation-resistant supports for OER, in combination with iridium catalysts. Among these systems,  $\text{TiC}$  has shown promising results since the peak current density at 1.5 V vs RHE with  $\text{Ir/TiC}$  (20% Ir) is nine times higher than that obtained with unsupported pure Ir, thus leading to significant decreases in cost [186]. Less spectacular, but still indicating ways to reduce noble metal content, is a study with silicon carbide [188]. The electrochemical activity of  $\text{IrO}_2$  was found to be improved in the presence of a Si–SiC support and the activity of samples with 80 wt % loading of  $\text{IrO}_2$  was similar to that of the unsupported catalyst. The enhancement in the performance was attributed to the improved surface properties of  $\text{IrO}_2$  in the presence of the support [188]. Polonsky et al. [187] supported  $\text{IrO}_2$  on  $\text{TaC}$ , but the oxidation of  $\text{TaC}$

by  $\text{NaNO}_3$  used in the preparation leads to the formation of a surface film of  $\text{NaTaO}_3$  with low conductivity. In order to overcome this problem, high loadings of  $\text{IrO}_2$  (higher than 50 wt %) are required.

Puthyapura et al. [189] showed that the  $\text{IrO}_2$  loading can be reduced by the use of ITO or  $\text{TiO}_2$  supports, without significant losses in catalytic activity. As shown in Fig. 16,  $\text{IrO}_2$  (60 wt%)/ $\text{TiO}_2$  shows comparable performance to unsupported  $\text{IrO}_2$ , indicating that up to at least 40% reduction in the use of  $\text{IrO}_2$  can be achieved in this way. A similar result was obtained with antimony-doped tin oxide, ATO, as the support for Ir [190].

Recently, an active and stable  $\text{IrO}_2$  catalyst supported on a novel composite support with mixed protonic–electronic conductivity was reported by Xu et al. [191]. The support was synthesized utilizing tin doped indium oxides and proton conducting phosphates and then structured with 3D-ordered hexagonal arrays using polystyrene spheres as a colloidal template. This composite support had a favorable specific surface area of  $180 \text{ m}^2\text{g}^{-1}$ . The thus obtained supported  $\text{IrO}_2$  catalyst showed five times higher catalytic activity for OER compared to pure  $\text{IrO}_2$  catalysts during PEM water electrolysis at 80–170 °C. The stability of the catalyst was verified during a long-term testing under  $0.35 \text{ A cm}^{-2}$  at 130 °C for 1150 hours.

### 3.2.3. Alternative preparation methods and novel structures

OER is a structure-sensitive reaction; according to investigations of OER activity with  $\text{RuO}_2$  electrodes sintered at different temperatures, it appears that the catalytic behavior is controlled by both the catalyst particle size and the electronic conduction mode [192,193]. Thus, prerequisite for highly active catalysts is the presence of optimum-sized crystalline particles (ensuring enough active sites) which are in good contact with each other (improving electrical conductivity). Moreover, a crystalline tetragonal structure for  $\text{IrO}_2$  and  $\text{RuO}_2$  is preferable for achieving high activity.

Numerous methods have been followed for the synthesis of these oxides in the form of powders, such as polyol method, Adams fusion, sol-gel, hydrolysis, precipitation [162–183,185–191]. Alternative preparations have been reported as well. Slavcheva et al. [161] introduced magnetron-sputter deposition of thin films as OER catalysts in PEM electrolysis. Such films represent active and stable catalysts, also mechanically, and with minimal metal loading

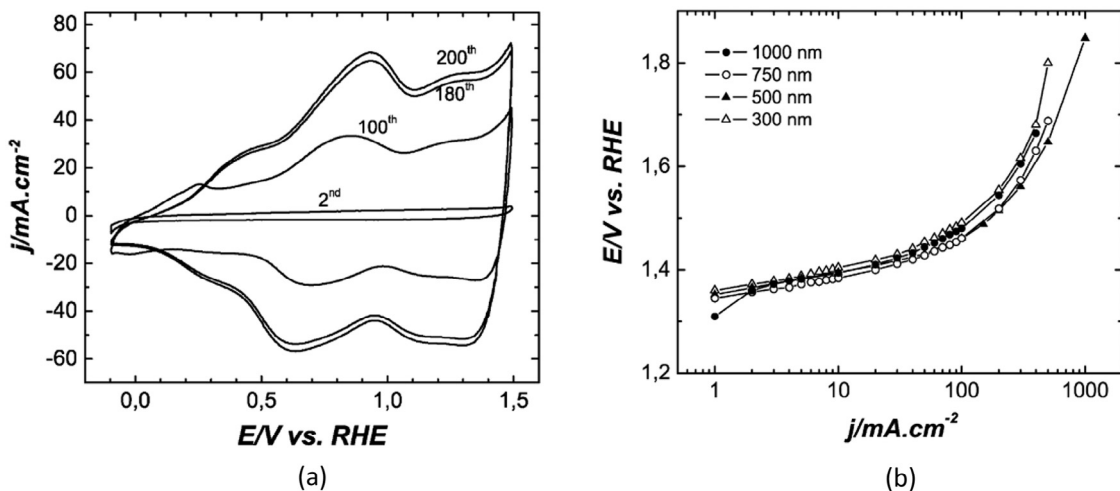


**Fig. 17.** (a) Consecutive cyclic voltammetry curves (200 scans) of a 1000 nm thick film showing the progressive oxidation of Ir to IrO<sub>2</sub>. Scan rate 100 mV s<sup>-1</sup>, T: 20 °C. (b) Steady-state polarization curves during water electrolysis using IrO<sub>2</sub> films of different thicknesses. T: 80 °C. Reprinted from reference 161 with permission of Elsevier.

[161,182,194,195]. In these studies, thin Ir films were sputter-deposited onto a carbon substrate; continuous cyclovoltammetric treatment resulted in anodically formed IrO<sub>2</sub> films (Fig. 17a) [161]. The steady-state polarization curves in Fig. 17b show that oxygen evolution initiates at 1.3 V. Both these results and long-term stability tests under 0.3 A·cm<sup>-2</sup> at 80 °C indicated that the film with 500 nm thickness has the best performance.

Finally, the introduction of novel core-shell structures in OER catalysts for PEM electrolysis appears of great interest. Nong et al. [196,197] describe an Ir catalyst formed by an electrochemically dealloyed IrNi core and IrO<sub>x</sub> shell. By combining this core-shell catalyst with a mesoporous corrosion-resistant oxide support of antimony doped tin oxide (ATO) they obtained an efficient OER catalyst, stable (for 20 hours) in the acidic environment. As shown in Fig. 18, the combined catalyst has both the advantages of the core-shell architectures and the durability benefits of an oxide support.

### 3.3. Solid oxide electrolysis

#### 3.3.1. SOE with O<sup>2-</sup> conducting oxides

A major problem, limiting the lifetime of anode materials in solid oxide electrolyzers, is the delamination of the oxygen electrode from the electrolyte (typically yttria-stabilized zirconia (YSZ)). It is the main reason for degradation and corresponds to physical damages of the electrode at the anode-electrolyte interface. Anode delamination causes the reduction of the electrochemically active area and increased ohmic losses. The exact source of this delamination is yet unclear, but several processes have been identified as responsible for it, such as morphological changes in the electrode and grain boundary porosity development in the electrolyte [198–202]. Poisoning of the anode due to chromium present in the steel of interconnect materials has been also suspected to play a role [203]; however, this possibility was excluded since anode delamination was also observed after operation without chromium-containing elements [201].

Several approaches have been proposed in order to mitigate the problem of delamination, such as (a) the application of alternating current voltage pulses [204], (b) the addition of small amounts of oxides with cations exhibiting multiple valence states to the electrolyte, to increase electronic conductivity and thus decreases the tendency of delamination of the anode [205], (c) the modification of YSZ by sol-gel coating with a discontinuous Mn–YSZ layer with submicron pores to prevent high pressure oxygen build up [206].

Similar as in solid oxide fuel cells, perovskites are used in the SOE oxygen electrodes. Among them the most common material is the composite of strontium doped lanthanum manganite (LSM) and YSZ [24]. LSM ( $La_{x}Sr_{1-x}MnO_3$ ) is used since it has good thermal and chemical compatibility with YSZ, good electronic conductivity and reasonable catalytic activity for oxygen evolution [207]. LSM–YSZ composites are used, both in order to improve activity by increasing the length of the three-phase-boundaries (LSM provides the pathway for electrons, while YSZ for oxygen ions and thus the contact region between gas-electrode-electrolyte is increased), and to improve the adhesion between the anode and the YSZ electrolyte [208].

It has been reported that LSM–YSZ anodes can be activated by cathodic polarization (fuel cell operation), while anodic current polarization (electrolysis mode) causes deactivation of LSM–YSZ anodes. The activation observed after cathodic polarization has been associated with partial reduction of LSM, but this activated state cannot

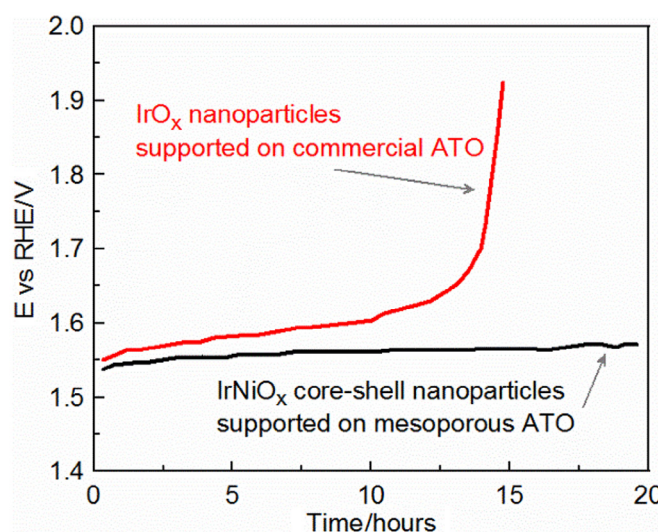


**Fig. 18.** Constant current chronopotentiometric stability measurements at a current density of 1 mA cm<sup>-2</sup> using pure IrO<sub>x</sub> nanoparticles supported on commercial antimony doped tin oxide (ATO) (red line), IrNiO<sub>x</sub> core-shell nanoparticles supported on mesoporous ATO (black line). T: 25 °C, 0.05 M H<sub>2</sub>SO<sub>4</sub>, 1600 rpm. Ir loading is 10.2 mg cm<sup>-2</sup>. Adapted from reference 196.

be maintained under anodic polarization [209–211]. Several works have been focused on the improvement of the behavior of LSM-based anodes. Detailed electrochemical impedance spectroscopy characterization of LSM–YSZ by Wang et al. [212] showed that processes related with the dissociative adsorption of oxygen along the LSM surface and with gas phase diffusion depend on the partial pressure of oxygen and on the porosity of the electrode. Yang et al. [213] showed that a porous network-like LSM–YSZ made by impregnation could have reduced electrode polarization resistance. The incorporation of Ag or Pd has been shown to improve the electrochemical performance of LSM–YSZ anodes [214,215]. Enhancement in the performance and stability has been also achieved by introducing nanoparticles of gadolinia-doped ceria (GDC) in the LSM electrode [216] or by using Pd-infiltrated LSM–GDC composites [217].

LaCoO<sub>3</sub>-based substituted perovskites have been suggested as alternative materials for the oxygen electrode of SOEs, such as La<sub>0.6</sub>Sr<sub>0.4</sub>Co<sub>0.2</sub>Fe<sub>0.8</sub>O<sub>3-δ</sub> (LSCF) [218] and La<sub>0.6</sub>Sr<sub>0.4</sub>CoO<sub>3-δ</sub> (LSC) [219]. These materials have higher ionic conductivity compared to LSM, while they also display mixed ionic and electronic conductivity and high oxygen exchange coefficients. However, both LSCF and LSC suffer from instability due to their chemical interaction with the YSZ electrolyte forming La<sub>2</sub>Zr<sub>2</sub>O<sub>7</sub> and SrZrO<sub>3</sub>. This interaction can be avoided by introducing an interlayer of GDC between LSCF and YSZ, which however causes increased ohmic losses [220]. Moreover, these materials, and in general Sr-doped perovskites suffer from poor stability due to Sr segregation and SrO precipitation to the surface, which inhibits the exchange of oxygen between the gas phase and the solid.

Zheng et al. [221] recently compared the performance of LSM, LSCF and LSC oxygen electrodes during water electrolysis and found that delamination occurred only on the LSM and LSC cells. On the other hand, Wei et al. [222] operated an SOE with LSCF anode at higher temperature (900 °C and at low current densities (0.2 A cm<sup>-2</sup>) for 20 hours, nonetheless significant poisoning of the LSCF electrode was observed sourcing from Cr contained in the interconnect materials of their cell. After long operation of a SOE with LSCF anode for 1000 hours at 800 °C under high current densities of 800 mA cm<sup>-2</sup>, Grindler et al. [223] observed changes in the conductivity of LSCF due to changes in the valence state of Co.

Other materials proposed as promising oxygen electrodes for SOEs with performance superior to that of LSM are Ba<sub>0.9</sub>Co<sub>0.5</sub>Fe<sub>0.4</sub>Nb<sub>0.1</sub>O<sub>3-δ</sub> [224], Ba<sub>0.5</sub>Sr<sub>0.5</sub>Co<sub>0.8</sub>Fe<sub>0.2</sub>O<sub>3-δ</sub> [225], SmBaCo<sub>2</sub>O<sub>5+δ</sub> [226], Sr<sub>2</sub>Fe<sub>1.5</sub>Mo<sub>0.5</sub>O<sub>6-δ</sub>–Zr<sub>0.84</sub>Y<sub>0.16</sub>O<sub>2-δ</sub> [227], Sm<sub>0.5</sub>Sr<sub>0.5</sub>CoO<sub>3</sub>–Sm<sub>0.2</sub>Ce<sub>0.2</sub>O<sub>1.9</sub> [228], Sm<sub>0.5</sub>Sr<sub>0.5</sub>CoO<sub>3</sub>–Ce<sub>0.8</sub>Sm<sub>0.2</sub>O<sub>1.9</sub> [229], La<sub>2-x</sub>Sr<sub>x</sub>Co<sub>0.5</sub>Ni<sub>0.5</sub>O<sub>4-δ</sub> [230], La<sub>2</sub>NiO<sub>4+δ</sub> and Nd<sub>2</sub>NiO<sub>4+d</sub> [231].

### 3.3.2. SOE with H<sup>+</sup> conducting oxides

The oxygen electrodes both for oxygen and proton conducting SOEs should present high porosity in order to allow the diffusion of gases and to provide sufficient active sites for oxygen evolution. In the case of proton conductors and in order to achieve high efficiency for steam electrolysis, the intrinsic rate of H<sub>2</sub>O oxidation (protons formation) should be higher than that of hydrogen production by protons; otherwise, a decrease in proton concentration within the electrolyte (due to high rates for protons recombination and hydrogen production) will lead to an increase in holes concentration (in other words, protons will dissolve in the partial prototypic conductor and will be converted to H<sub>2</sub> gas, leading to holes generation) [232]. Therefore, the development of well-performing air electrodes is of great importance in the field of proton-conducting SOEs [25].

Iwahara and coworkers [233,234] were the first to demonstrate solid oxide electrolysis with proton conduction, using Pt as the oxygen electrode. Due to the high cost of platinum, following studies introduced the use of less expensive perovskites, similar to the anodes of oxygen ion conducting cells [25], e.g. samarium

strontium cobaltites (SSC) [235], lanthanum strontium cobaltites [236] and lanthanum strontium manganites-chromites [237].

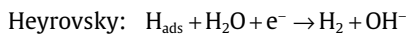
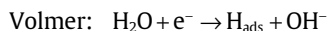
However, He et al. [238] noted that different processes/mechanisms occur in the electrolysis using oxygen-ion conductors and proton conductors and they stressed the importance of using composites with both proton and electron conductivities, in order to extend the active sites for reaction over the whole electrode area. For this purpose, composites such as BaZr<sub>0.6</sub>Co<sub>0.4</sub>O<sub>3-δ</sub> [239] and the composite materials of La<sub>0.6</sub>Sr<sub>0.4</sub>Co<sub>0.2</sub>Fe<sub>0.8</sub>O<sub>3-δ</sub>–BaZr<sub>0.5</sub>Pr<sub>0.3</sub>Y<sub>0.2</sub>O<sub>3-δ</sub> [240], La<sub>0.6</sub>Sr<sub>0.4</sub>Co<sub>0.2</sub>Fe<sub>0.8</sub>O<sub>3-δ</sub>–Ba<sub>0.5</sub>Sr<sub>0.5</sub>Co<sub>0.8</sub>Fe<sub>0.2</sub>O<sub>3-δ</sub> [241] and Co<sub>3</sub>O<sub>4</sub>-loaded La<sub>0.8</sub>Sr<sub>0.2</sub>MnO<sub>3</sub>–BaCe<sub>0.5</sub>Zr<sub>0.3</sub>Y<sub>0.16</sub>Zn<sub>0.04</sub>O<sub>3-δ</sub> [242] have been proposed.

To conclude, even though the oxygen evolution reaction during solid oxide electrolysis with oxygen-ion and proton conductors shows distinct differences in reaction mechanisms, several common requirements apply for the two cases. Both technologies rely on the use of perovskite-based composite materials, which provide both ionic and electronic conductivities and thus extend the electrocatalytically active sites all over the electrode. The additional requirements for mechanical stability (related with the high operating temperature) introduce further limitations in the choice of appropriate materials. Poor adhesion between anode and electrolyte (and thus delamination effects) is commonly the main issue of performance loss during oxygen evolution in SOE. The variety in perovskite properties which can be achieved by A, B-site substitutions is expected to lead to materials with optimized stoichiometry; however the effect of microstructure (grain size, porosity) should be thoroughly examined for further optimization.

## 4. Cathodes for water electrolysis: electrocatalysts for the hydrogen evolution reaction

The hydrogen evolution reaction (HER) on different metals is one of the most investigated electrochemical reactions. Even though well performing electrodes are currently available, further reduction of the overpotential for hydrogen evolution remains of great interest for minimizing energy consumption during water electrolysis.

In general, the mechanism of HER in alkaline media follows three steps [243,244]. The first step (Volmer reaction) includes the formation of intermediate H<sub>ads</sub> atoms, which is the rate determining step at low overpotentials. Hydrogen production then occurs following an electrochemical process (Heyrovsky reaction) and/or a chemical process (Tafel reaction):



Kinetic analysis of HER on Ni–Mo alloys has shown that at low overpotentials the reaction mechanism is a combination of the Volmer step and parallel Tafel and Heyrovsky steps, while at high overpotentials the rate of the Tafel step is negligible and the reaction proceeds through the Volmer–Heyrovsky steps [244].

Bockris was the first to investigate the kinetics of the HER reaction on various metals [245] and the effect of impurities on catalytic activity [246]; among others he observed a relation between catalytic activity (exchange current) and the work function of the metals [247]. In the period of 1950s–1970s it became apparent that the exchange current density of HER and the strength of the metal–hydrogen bond follow a so called “Volcano Curve” with the optimum at the platinum group metals (Fig. 19) [248–252]. Metals on the left adsorb H atoms too strongly, and on the right too weakly. Numerous theoretical and experimental studies have been carried out in the last 60 years focusing on the effect of electronic structure, surface electrochemistry and molecular design on HER activity [253].

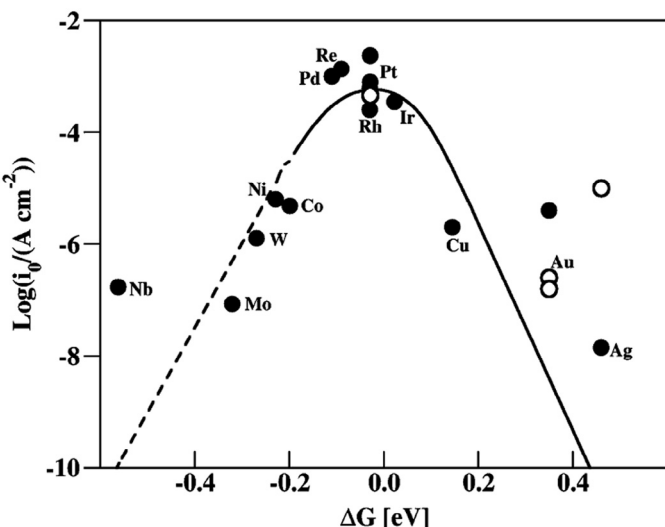


**Fig. 19.** The data points in this volcano plot are the measured exchange current density plotted against the calculated free energy of H adsorption at  $U = 0$  V. Single crystal data are indicated by open symbols. The metals on the left side have high H coverage, while the metals on the right side have low H coverage. Reprinted from reference 255 with permission of the American Chemical Society.

Recently, Nørskov et al. [254,255] used DFT calculations for electrochemical hydrogen evolution on a large number of transition metals with different substrates and suggested the binding free energy of H as the most appropriate descriptor for the HER activity. It is now well established that if the hydrogen is weakly bonded to the surface, then the HER will be limited by the adsorption step, while if hydrogen is strongly adsorbed a reaction–desorption step will limit the rate of the HER reaction. A volcano-type relationship thus describes the activity of several materials, where Pt appears as the most active material (Fig. 19).

Even though noble metal-based materials (mainly Pt) are widely chosen because of their high HER performance, their high price makes them inappropriate for large-scale applications. During the last years, various novel materials such as alloys with optimized hydrogen adsorption energy have been proposed as alternatives to Pt, while numerous investigations have focused on improving the performance by optimizing geometric factors [256]. Successful HER electrocatalysts should have high electrocatalytic activity, stable performance (no potential drift over time), chemical and electrochemical stability (long lifetime) and low cost [257]. The next paragraphs give an overview of the progress and the recent trends in materials used as HER electrocatalysts.

#### 4.1. Alkaline electrolysis

##### 4.1.1. Ni, Co, Fe based electrocatalysts

As for OER, low cost electrocatalysts based on transition metal oxides are the most typically employed materials for HER in alkaline media [256]. Among them, nickel is the most common HER electrocatalyst, owing to its low cost and high chemical stability in the alkaline environment. Nevertheless, these electrodes face problems of deactivation, since the HER activity of Ni cathodes is significantly greater on fresh electrodes than after long-term continuous operation.

Hall et al. [258], using a variety of electrochemical and physicostructural characterization techniques, investigated systematically the electrode deactivation using smooth Ni (mechanically polished electrodes with low surface area) in alkaline solutions. They found that fresh electrodes are covered by a bilayer of  $\alpha\text{-Ni(OH)}_2$

and a layer of  $\text{NiO}_x$  formed by air. For potentials lower than the reversible hydrogen electrode potential (during HER), the  $\text{NiO}_x$  layer mostly reduces to metallic Ni, while H-atoms incorporate into the bulk of the electrode material. Thus, fresh electrodes show high HER activity under cathodic polarization; however a gradual decrease in HER activity is observed after several hours of electrolysis due to nickel hydride formation. This decrease is even more pronounced under large cathodic current densities and in presence of highly concentrated alkaline solutions (typical conditions of industrialized processes) due to the large extent of hydrogen incorporation, which leads to the extensive formation of  $\alpha\text{-NiH}_x$  and  $\beta\text{-NiH}_x$ .

The same study [258] investigated also transformations occurring on the Ni electrode after repeated oxidation–reduction cycles. Transient anodic currents are typical at the cathodes of industrial electrolyzers and are generated during initiation and shut-down, causing the formation of  $\text{NiO}_x$ ,  $\alpha\text{-Ni(OH)}_2$ ,  $\beta\text{-Ni(OH)}_2$ , and  $\beta\text{-NiOOH}$ . These species are reduced back to metallic Ni on subsequent cathodic polarization during HER. However, consecutive cycles can lead to decrease in HER activity due to the development of strains and the concomitant mechanical damages on the electrode.

The presence of oxide species on the surface is critical for HER activity, since as reported by the group of Markovic [259–261], the HER activity of Ni modified by  $\text{Ni(OH)}_2$  is four times higher than for a bare Ni surface. It was proposed that  $\text{Ni(OH)}_2$  serves to enhance the water dissociation step. The same group has highlighted the importance of tailoring metal/metal oxide interfaces which can lead to a bi-functional HER mechanism. It was suggested that the oxide has an affinity to form  $\text{OH}_{\text{ads}}$  and thus promotes the dissociation of water. The thus produced hydrogen atoms are then adsorbed at the nearby metallic sites, while OH species adsorb on the metal oxide. The most suitable metal–metal oxide combination for optimal HER activity was found for  $\text{Pt}(111)\text{-Ni(OH)}_2$ , due to (a) the sufficiently high tendency of  $\text{Ni(OH)}_2$  to adsorb OH, which at the same time is not high enough to cause poisoning of the sites and (b) the optimal P–H<sub>ads</sub> energetics [259–261].

The early electrocatalytic studies identified Raney-nickel (with Zn or Al as the leachable component) as a very active HER electrocatalyst and already in the 1980s it was employed in the industrial large scale processes for hydrogen production by alkaline electrolysis [262,263]. Commercial electrolyzers still utilize Raney-nickel electrodes due to their low cost and sufficient activity, however this material suffers from substantial deactivation with time after intermittent operation for a long period, due to dissolution of the catalyst components [264]. The activity of Raney-Ni has been attributed to its hexagonal structure, which is unstable and forms the normal cubic lattice of bulk nickel [262]. The HER activity of Raney-Ni depends on the leaching conditions (concentration of the alkaline solution, temperature, time etc) [256], which in turn affect the “concentration” of Raney-Ni within the coating, the coating thickness and the amount of unleached material, i.e. Al or Zn [262].

Comparison of the HER performance of different Ni-based cathodes in 1 M NaOH was carried out by Tanaka et al. [265] and the results showed that  $\text{NiAl}_3$  outperformed  $\text{Ni}_2\text{Al}_3$ ,  $\text{NiAl}$  and  $\text{Ni}_3\text{Al}$ , due to its large surface area, the presence of micropores and the appearance of the nickel phase after leaching. The significance of the small-sized pores (which counts for larger surface area) was also highlighted by Wu et al. [266]. The same group investigated recently the HER activity and corrosion resistance during long-term water electrolysis in 6 M KOH solution, using  $\text{NiAl}_3\text{-Mo}$  (10 wt%) [267]. The improved performance of the Mo-containing electrocatalyst (Fig. 20) was related with electronic effects, since no significant changes in the pore size distribution and BET surface area of  $\text{NiAl}_3$  were observed after Mo addition. The activity for HER increased over time (Fig. 20). The authors attributed this activation to the removal of any existing oxygen layer formed during sintering in the preparation process [267].

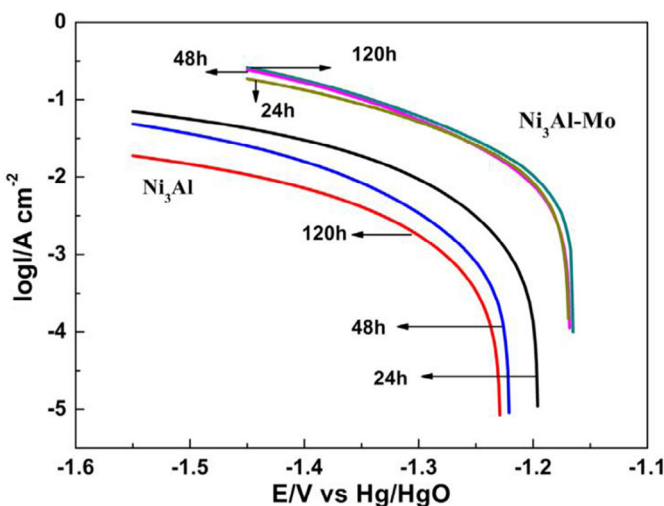


**Fig. 20.** Polarization curves for porous  $\text{Ni}_3\text{Al}-\text{Mo}$  and porous  $\text{Ni}_3\text{Al}$  electrodes after different times of continuous alkaline water electrolysis.  $\text{Ni}_3\text{Al}-\text{Mo}$  has higher activity than  $\text{Ni}_3\text{Al}$ . Furthermore, HER activity of the  $\text{Ni}_3\text{Al}$  electrode reduces as a function of electrolysis time, while for  $\text{Ni}_3\text{Al}-\text{Mo}$  a slight activation is observed after prolonged operation. Reprinted from reference 267 with permission of Elsevier.

Several metals and metal oxides have been proposed for alloying nickel in order to prevent the formation of nickel hydrides and thus improve stability, such as Fe [268], Cu [269], Ti [270], Ru [271], Mo [272], Cr [273], Pd [273], W [274], Co [275], P [276], Sn [277],  $\text{IrO}_2$  [278],  $\text{RuO}_2$  [278],  $\text{MoO}_2$  [279],  $\text{CeO}_2$  [280]. The majority of these materials is prepared by electrodeposition, while materials such as Mo or W which cannot be directly electrodeposited from aqueous solutions of their salts can be co-deposited by using appropriate complexing agents. Among the proposed nickel alloys, combinations of Ni with Mo, Co and Fe have been identified as the most promising. Although Cu is inactive by itself, Cu alloying with Ni has also received much attention, as it apparently enhances the activity of the latter [269,281,282]. It has been reported that the specific HER activity (normalized by the real Ni surface) can be up to 20% higher than that of pure Ni by the addition of 49 wt% Cu [281].

According to Jaksic et al. [184,283] based on the Brewer–Engel theory, alloying metals of the left half of the transition series in the periodic table (empty or less filled d-bands or hypo-d electronic elements) with metals of the right half of the series (more filled d-bands or hyper-d electronic elements) results in a maximum bond strength and a well pronounced synergism for HER [184,283]. In this case, the intermetallic bonding of the alloys results to reduced lattice parameters and interatomic distance, due to changes in the electronic properties of the electron orbitals of neighboring atoms which finally facilitate H desorption.

In agreement with this theory, combination of Ni with rare earth metals such as Ce [284], Y, Pr or Sm [285] and Dy [286] has resulted in active HER electrodes. Rosalbino et al. [287] synthesized ternary Co–Ni–R ( $R = \text{Y}, \text{Ce}, \text{Pr}, \text{Er}$ ) crystalline alloys and used them as electrocatalytic materials for HER in 1 M NaOH at 25 °C. All ternary alloys had superior electrocatalytic activity compared to the binary Ni–Co alloy; among them,  $\text{Co}_{57}\text{Ni}_{36}\text{Y}_{6.5}$  and  $\text{Co}_{57}\text{Ni}_{35}\text{Ce}_8$  exhibited the highest activity for HER with exchange current densities of 0.07 and 0.09 mA/cm<sup>2</sup> respectively, while the current exchange density for  $\text{Co}_{57}\text{Ni}_{47}$  was 0.05 mA/cm<sup>2</sup> [287]. The authors attributed the superior performance of these ternaries to the change of the electronic properties related to appropriate combination of d<sup>8</sup>-orbitals of Ni with d<sup>1</sup>-orbitals of Y or Ce and d<sup>7</sup>-orbitals of Co.

Arul-Raj et al. [288] compared the HER activity of various Ni alloys (Ni–Mo, Ni–Zn, Ni–W, Ni–Fe, Ni–Cr,) during alkaline water

electrolysis and showed that Ni–Mo alloys yield the best currents for hydrogen evolution. Specifically, an overpotential of 0.18 V was reached after 1500 hours of water electrolysis in 6M KOH at 300 mA/cm<sup>2</sup> at 80 °C; this was 0.3 V lower than that of a nickel cathode. Apart from the high activity, Ni–Mo electrocatalysts showed excellent resistance to corrosion and long-term stability. Further investigations were carried out to elucidate the effect of replacing part of the high-cost Mo in the Ni–Mo alloy by another element, aiming to decreased materials costs. The comparison of the HER activity of several ternaries showed the following order:  $\text{Ni}-\text{Mo}-\text{Fe} > \text{Ni}-\text{Mo}-\text{Cu} > \text{Ni}-\text{Mo}-\text{Zn} > \text{Ni}-\text{Mo}-\text{Co} > \text{Ni}-\text{Mo}-\text{W} > \text{Ni}-\text{Mo}-\text{Cr}$  [289]. In essence, partially replacing Mo (in Ni–Mo) by Fe does not lead to alterations in electrocatalytic performance, since similar overpotentials have been obtained using the ternary  $\text{Ni}-\text{Mo}-\text{Fe}$  ( $\text{Ni}_{70}\text{Mo}_{15}\text{Fe}_{15}$ ) and the binary Ni–Mo ( $\text{Ni}_{70}\text{Mo}_{30}$ ) during 1500 hours of water electrolysis. However, the Ni–Mo–Fe combination was considered from the authors as more suitable for practical applications due to significantly lower cost [289]. In agreement with this study, several other groups also identified Ni–Mo-based alloys as active electrocatalysts for alkaline HER based on non-platinum-group metals [272,290,291]. However, it turned out that the inherent oxophilicity of Mo makes this material quite pyrophoric, and thus unsuitable for any commercial application [292].

A composite  $\text{Ni}/\text{NiO}_x-\text{Cr}_2\text{O}_3-\text{C}$  electrocatalyst was proposed recently by Bates et al. [292] as a highly active HER electrocatalyst, which is also chemically stable when supported on polymeric solid alkaline membranes. The experimental results showed that the activity of this material is higher than the sum of individual HER activities from the Ni and Cr–Ox components. This, according to the authors, is the result of a synergistic effect, where at adjacent  $\text{Ni}/\text{NiO}_x$  sites the metallic Ni acts as a sink for the adsorption of intermediate hydrogen atoms and  $\text{NiO}_x$  facilitates OH adsorption, while  $\text{Cr}_2\text{O}_3$  stabilizes the composite  $\text{NiO}_x$  component under HER conditions (where  $\text{NiO}_x$  would typically reduce to Ni) [292].

As already noted, cobalt is also a promising material for alloying with nickel and in this direction, Hong et al. [293] investigated the HER activities of several electrodeposited Ni–Co alloys and found that they exhibit improved activity compared with pure Ni and Co electrocatalysts. As shown in Fig. 21,  $\text{Ni}_{49}\text{Co}_{51}$  alloy demonstrated the highest intrinsic activity for HER in alkaline media among the tested alloys. This enhancement in HER activity after alloying was related by the authors with changes in the electronic structure of

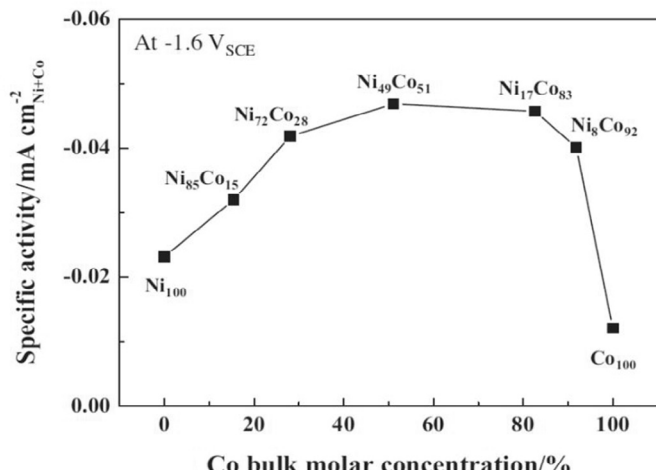


**Fig. 21.** Specific HER activities normalized by the electrochemically active surface area for  $\text{Ni}_{100}$ ,  $\text{Co}_{100}$  and several Ni–Co alloys. Data obtained under standard potential of −1.6 V vs SCE, 0.5 NaOH, 25 °C. Reprinted from reference 293 with permission of Elsevier.

Ni [293]. It was suggested that the electron-rich phase of Ni in the Ni–Co alloys is more active toward HER due to its lower hydrogen binding energy, in agreement with Nørskov's calculations [254,255].

Lupi et al. [294] tried to activate Ni–Co alloys during HER electrocatalysis by adding Mo ions into the alkaline NaOH solution. The in-situ activation led to improvement of the electrocatalytic properties of Ni–Co alloys, since the exchange current density increased two orders of magnitude. Moreover, the presence of Mo resulted in enhanced electrochemical stability in all cases. The observed enhancement in performance was attributed to the formation of Ni–Co–Mo ternary alloys on the electrode surface.

The HER activity of Fe is naturally higher than that of Ni, but Fe is unstable in the alkaline environment and thus cannot be used in commercial applications of alkaline electrolysis. However, combinations of Fe with Ni are promising and Ni–Fe alloys show better HER activity than the individual parent materials. Meguro et al. [295] prepared Fe, Ni and Ni–Fe catalysts with electrodeposition and used them for HER in 8 M NaOH solution at 90 °C. They found similar values for the Tafel slope (150 mV/dec) indicating that the mechanism of hydrogen evolution does not change upon alloying. However, enhanced HER rates were obtained using Ni–Fe alloys. Indicatively, a current density of 100 A/m<sup>2</sup> was achieved under overpotential of 0.22 V with Ni–Fe vs 0.26 V for Fe and 0.34 V for Ni. The improved performance was related with the acceleration of proton discharge (which is the rate determining step) due to charge transfer from nickel to iron by alloying. The effect of adding C in the Ni–Fe alloy was also investigated. Ni–Fe–C alloys were prepared by electrodeposition using Ni and Fe precursors while lysine was used as the carbon precursor. Carbon addition resulted in further enhancement of the HER activity of the Ni–Fe alloys. A current density of 100 A/m<sup>2</sup> is achieved upon overpotential of 0.04 with Ni–Fe–C vs 0.22 V with Ni–Fe, but after introduction of carbon a 5-fold decrease in the Tafel slope was observed, indicating alterations in the HER mechanism. XPS analysis showed that carbon addition enhances considerably the charge transfer from nickel to iron. It was thus concluded that the carbon addition accelerates the proton discharge on iron to such an extent that this step is not any longer the rate determining step (rds), with the step of H<sub>ads</sub> desorption being the rds instead. Ni–Fe–C alloys were found to be more active than Fe–C, while Ni–C showed the poorest performance. Ni–Fe–C alloys have been also used for seawater electrolysis and it was found that their activity depends on the grain size [296] and the composition of the alloy [297]. Flis-Kabulska et al. [298] also reported enhancement in HER activity (up to 80%) after introducing carbon to Ni cathodes, while in this case the carburization took place by plasma treatment in CH<sub>4</sub>/H<sub>2</sub> gas mixture at 470 °C.

A novel investigation regarding solid alkaline water electrolysis was carried out recently by Chanda et al. [299]. The author of this study synthesized NiFe<sub>2</sub>O<sub>4</sub> electrocatalysts using the co-precipitation method, and combined them with a modified (i.e. poly(2,6-dimethyl-1,4-phenylene oxide (PPO))) binder. The catalysts were then deposited on top of a nickel foam support and were used for HER in alkaline water electrolysis with a polymeric anion-selective membrane. The catalyst was found to be stable and active under operation at 50 °C under 250 mA/cm<sup>2</sup> for 140 hours (Fig. 22). In the course of water electrolysis, Fe ions in NiFe<sub>2</sub>O<sub>4</sub> were reduced, due either to cathodic potential or to the presence of hydrogen in the cathode catalytic layer. For maintaining the electrostatic balance in NiFe<sub>2</sub>O<sub>4</sub>, the oxide phase of Fe<sub>2</sub>O<sub>3</sub> which is present after catalyst synthesis is converted to iron hydroxides, thus proving the active participation of iron in the HER mechanism [299].

As already mentioned, Ni Raney electrodes exhibit high electrocatalytic activity, which however decreases over time during long-term water electrolysis [256,300]. A novel type of Raney electrode was developed by Döner et al. [301,302] by preparing Co–Zn coatings on a graphite electrode, etching in a concentrated alkaline

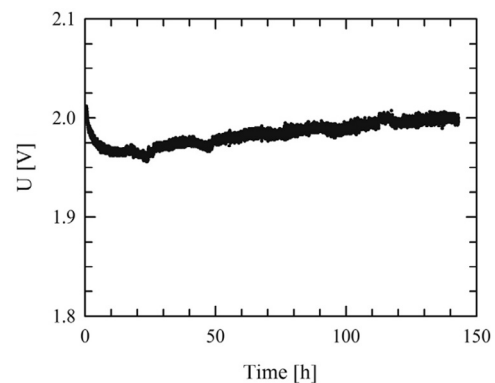


**Fig. 22.** Long-term water electrolysis. 10 wt% KOH, galvanostatic operation at 250 mA cm<sup>-2</sup>, anode: bare Ni foam, cathode: 10 mg cm<sup>-2</sup> NiFe<sub>2</sub>O<sub>4</sub> + polymer binder; electrode area 4 cm<sup>2</sup>. Reprinted from reference 299 with permission of Elsevier.

solution and finally depositing a low amount of Pt (1 mg/cm<sup>2</sup>) onto the etched Co–Zn. The resulting material is a promising HER electrocatalyst, since it presented high HER activity (10 times higher than the bare graphite) and durability and since stable performance was obtained during 120 hours of continuous water electrolysis under 100 mA cm<sup>-2</sup> in 1 M KOH at 25 °C [302].

Another recent study proposed the application of Co–W crystalline alloys of Co<sub>95</sub>W<sub>5</sub>, Co<sub>90</sub>W<sub>10</sub>, Co<sub>85</sub>W<sub>15</sub>, Co<sub>80</sub>W<sub>20</sub>, Co<sub>70</sub>W<sub>30</sub> (atomic %) as possible HER electrocatalysts [303]. In 1 M NaOH solution at 25 °C, the Co–W alloys showed better performance compared to polycrystalline Co, Ni and Ni–Mo electrocatalysts. In particular, the overpotential at a current density of 250 mA/cm<sup>2</sup> is 0.33–0.38 V for the different Co–W alloys, while this for Co and Ni is 0.46 V and 0.45 mV respectively. The authors attributed the enhanced activity of the alloys to the modifications in the electron density of states at the Fermi level of Co upon alloying with tungsten. Among the investigated alloys, Co<sub>90</sub>W<sub>10</sub> was found to yield the highest HER activity, which according to the authors coincides with an increase in the density of states at the Fermi level of the 3d Co band. This influences the proton discharge, thus enabling the Co-sites to act as a hydrogen source for the neighboring W sites, where hydrogen desorption occurs [303]. Ni–W coatings on Ni mesh also show good electrocatalytic activity for HER, which, similarly to Co–W, depends on the content of tungsten in the coatings. However, according to Tasic et al. [304], the improved electrocatalytic characteristics of Ni–W are mostly related to the high surface roughness of the coatings.

Amorphous coatings prepared by co-deposition of Fe, Ni or Co with Mo, W, P or Si have been investigated for alkaline HER. As reviewed by Safizadeh et al. [256], molybdenum and phosphorus are the most promising elements for the development of amorphous structures in alloys. Donten et al. [305] used Ni–Mo alloys and found that the amorphous/nanocrystalline structure appears when the Mo content is higher than circa 20 at %. Amorphous Fe alloys have also been investigated as cathode materials for alkaline water electrolysis [306]. It has been reported that the addition of metalloids (B and/or Si) to the Fe-based electrode material can lead to the development of low cost HER electrocatalysts, since reduction in overpotentials was observed after an activation procedure with cyclic voltammetry. Further addition of Co leads to highly active HER electrocatalysts. The overpotential with Fe–C–Si–B material can be reduced by 0.20 V compared to polycrystalline Ni, while the energy consumption for 1 N m<sup>3</sup>–H<sub>2</sub> can be reduced up to 0.48 kWh [306].

As an alternative to metals and their oxides, silicides [307–309] and nitrides [310] of transition metals have presented also good HER activities both in acidic and in alkaline environments. It has been

**Table 3**

Development status of main material families for HER electrocatalysis in alkaline media.

Material	Activity	Stability	Status
Raney Ni	Sufficient activity	Deactivation after intermittent operation	Commercially used
Ni–Co, Ni–Fe	High activity, which can be further improved upon alloying with rare earths	Better stability than Raney Ni, but still not optimal	Laboratory applications
NiFe <sub>2</sub> O <sub>4</sub>	Very high activity	Long term stability	Applied in lab-scale electrolysis with polymeric membrane
Ni–Mo	Very high activity	Long term stability	Pyrophoric material: inappropriate for commercialization
(Ni,Co)–W	High activity	Unknown	Laboratory applications
Co <sub>2</sub> Si	Very high activity	Unknown	Laboratory applications
Ni <sub>3</sub> N	High activity	Unknown	Laboratory applications

reported that both Co<sub>2</sub>Si and CoSi<sub>2</sub> present high HER activity in 0.5–2 M KOH, with current densities up to 10 times larger compared to Co [309].

To conclude, Table 3 summarizes the development status of the main material families for HER electrocatalysis in alkaline media. Raney nickel is the typical HER material used in industrial electrolysis due to its low cost and sufficiently high activity (still not optimal), even though stability issues occur due to nickel hydration after prolonged cathodic polarization. In the course of developing alternative HER catalysts, both active and stable, several materials have been proposed but not yet implemented in real systems. Several metals and/or metal oxides have been alloyed with Ni leading to well-performing catalysts as a result of electronic interactions, among them the combination of Ni–Mo–Fe seems to be promising for practical utilization. NiFe<sub>2</sub>O<sub>4</sub> is also a material with great promise, while other materials such as silicides and nitrides have been also proposed, but further detailed research is needed in this direction.

#### 4.1.2. Novel structures

The implementation of nanostructures in electrocatalytic materials has gained attention recently in order to further improve efficiency and/or reduce the loading, especially for precious metals. Some recent examples of nanostructuring alkaline HER electrocatalysts are presented in this section.

The deposition of Pd and Ru nanoparticles on the surface of Ni foam has been shown to enhance catalytic activity of the baseline material toward HER in alkaline solution [311]. At the overpotential of –0.30 V, the current densities were 21, 71 and 92 mA/cm<sup>2</sup> for unmodified, Pd-modified and Ru-modified Ni foam respectively (these values are normalized per surface area). The observed improvement is not only mainly related with the superior HER activity of both Pd and Ru, but also the increase of the electrochemically active surface for the modified materials (22-fold increase upon Pd addition, 11-fold increase upon Ru addition) is a key parameter. These findings show that modified Ni foam materials are potential cathodes for commercial alkaline electrolyzers, since enhancement in HER performance was observed with the deposition of trace amounts of the noble metals (ca. 0.1 wt% Pd or Ru), thus with minimal cost increase in the materials. Another nanostructured material promising for HER electrocatalysis under alkaline conditions was proposed by Shibli et al. [312]. In this work NiO nanoparticles (of 3 nm) were incorporated into a Ni–P matrix resulting in a four-fold reduction of overpotentials.

Carbon nanotubes, one of the major breakthroughs in nanomaterial synthesis, was coupled by McArthur et al. [313] with nanoparticles synthesis and led to the development of 3D Ni nanoparticle-decorated on multiwall carbon nanotubes electrocatalysts on which alkaline (1 M KOH) HER can occur. The thus developed material showed significant increase in electrocatalytic activity relative to a bulk Ni plate. Indicatively at overpotential of 0.10 V, the obtained current density is two orders of magnitude larger on the decorated catalyst compared to the bulk Ni.

Finally, the hydrothermal method has been proposed as a promising route for the generation of novel nanostructured alkaline HER electrocatalysts, based on the development of RuO<sub>2</sub>–NiO nanorod arrays on a Ni foam substrate [314]. These integrated materials showed enhanced surface area, small charge transfer resistance, excellent HER performance and long-term stability (after 60 hours of continuous operation). The exchange current density for the RuO<sub>2</sub>–NiO/Ni foam was reported to be two orders of magnitude higher than that of Ni foam or NiO/Ni foam catalysts. Moreover, a low value for the Tafel slope was observed (38 mV/dec) suggesting the appropriateness of this material for practical applications. This pronounced HER activity was attributed to the unique nanostructure of the material. According to the authors, the presence of nickel oxide/hydroxide on the catalyst surface promotes the dissociation of water and the formation of hydrogen intermediates, which can consecutively adsorb onto the neighboring Ru sites and recombine into molecular H<sub>2</sub> very rapidly [314]. The in situ growth technology followed in this study also led to significantly enhanced mechanical adhesion between the nanorod arrays and the Ni foam substrate. Moreover, the nanorods have the ability to supply smooth hydrogen evolution channels, thus allowing fast removal of the H<sub>2</sub> bubbles from the electrode surface. Not only these morphological characteristics play a key role for ensuring high catalytic activity, but also they are mainly responsible for the long-term stability of this material compared to conventional coated catalysts (Fig. 23).

#### 4.2. PEM electrolyzers

##### 4.2.1. Pt based electrocatalysts

Since the main challenges in PEM electrolysis are related to the OER (HER is much faster than its counter-reaction OER), research efforts are mainly focused on the development of anode electrocatalysts and less studies refer to cathode materials. In fact,

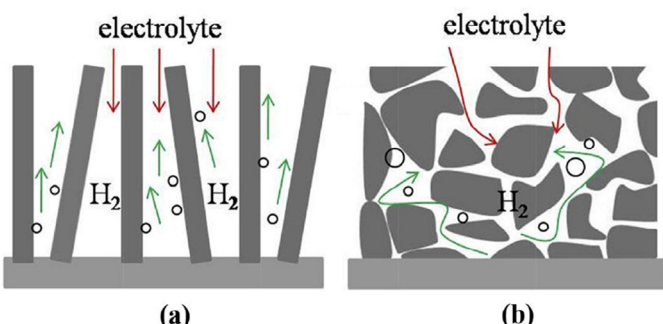


Fig. 23. Schematic representation of the morphology of RuO<sub>2</sub>–NiO/Ni foam (a) where the accumulation of H<sub>2</sub> bubbles on the surface is prevented and (b) of the conventional coated catalyst where these phenomena typically occur. Reprinted from reference 314 with permission of Elsevier.

the exchange current density for  $H^+/H_2$  on the most effective HER electrocatalyst is almost 1000 times larger than the exchange current density for  $H_2O/O_2$  on the most effective OER electrocatalysts [315].

The majority of the works on HER for PEM electrolyzers utilizes Pt-based materials [19,20,316–318], and carbon supported highly dispersed Pt nanoparticles are presently the benchmark electrocatalysts for PEM electrolysis [20]. According to Fig. 17, Pt not only yields the best HER activity, but also shows excellent stability in the acidic PEM environment. As discussed in the next paragraphs, several inorganic materials have recently drawn attention as alternative HER electrocatalysts, but their performance is still much lower compared to that of Pt-based electrocatalysts. Thus, research efforts are directed in the frame of nanotechnology aiming to the minimization of Pt loading, while maintaining high HER activity.

The catalytically active phase is typically developed in the form of dispersed nanoparticles (below 10 nm) in order to increase the surface to volume ratio and thereby reduce the loading of the high-cost Pt. The catalyst is then introduced in gas diffusion electrodes based on low-cost electronic carriers with large surface area, such as carbon black or carbon nanotubes. The nature of the electronic carrier plays an important role on the HER activity, as shown by Grigoriev et al. [316]. In their study, the same catalytic phase composed of Pt nanoparticles was dispersed on carbon black and on graphitic nanofibers and the resulted materials were used as HER electrocatalysts in a PEM electrolysis cell. During water electrolysis at  $1\text{ A cm}^{-2}$  and at  $90^\circ\text{C}$ , a voltage of 1.67 V was observed with the graphitic nanofiber, instead of 1.72 V for the case of carbon black. The enhanced performance of graphitic nanofibers can be attributed to both their lower resistivity, which facilitates electron transfer during HER, and also to their microporous structure, which favors the transport of reactant gases due to better diffusion of hydrogen [319].

#### 4.2.2. Sulphides, phosphides, carbides and nitrides

In the quest to find highly active HER electrocatalysts composed of earth-abundant materials, several sulphides, carbides and nitrides have been proposed lately as promising alternatives to the Pt cathodes. Among the thus developed materials, molybdenum sulphides (mainly  $MoS_2$ ) represent a promising class of materials for HER electrocatalysis, due to their relatively high activity (but still lower than Pt), excellent stability and low cost (Mo is about  $10^4$  times more abundant than Pt) [320–323]. The high HER activity of single trilayer  $MoS_2$  was predicted by Hinnemann et al. in 2005 [324] using DFT calculations to analyze the similarities between metallic  $MoS_2$  and effective biological HER catalysts, such as hydrogenases and nitrogenases which possess active centers consisting of Fe, Ni and Mo. The HER activity of  $MoS_2$  supported on graphite was experimentally verified by employing this catalyst on a Nafion electrolyte; reasonable activity was obtained with an overpotential of 0.1–0.2 V [324].

Furthermore, recent investigations by the group of Nørskov [325] emphasized the key role of the support on the electrocatalytic activity of  $MoS_2$ , which can result in several orders of magnitude difference in HER activity. The calculations revealed that an ideal support should exhibit optimal adhesion energy for the Mo-edge of  $MoS_2$  equal to  $-0.30\text{ eV}$ . Doped graphene and graphene supported on metals are proposed as supports with great potential to achieve high HER activities [325].

In the last ten years,  $MoS_x$ -based HER electrocatalysts have been extensively investigated and rapid progress took place in this field [321,322]. As reviewed recently by Yan et al. [321], numerous morphologies of  $MoS_x$  (such as nanoparticles, nanosheets, films, composites) have resulted in high HER efficiencies. The use of  $MoS_x$  nanoparticles has the clear advantage of the large amount of active sites, but on the other hand these materials have shown poor stability

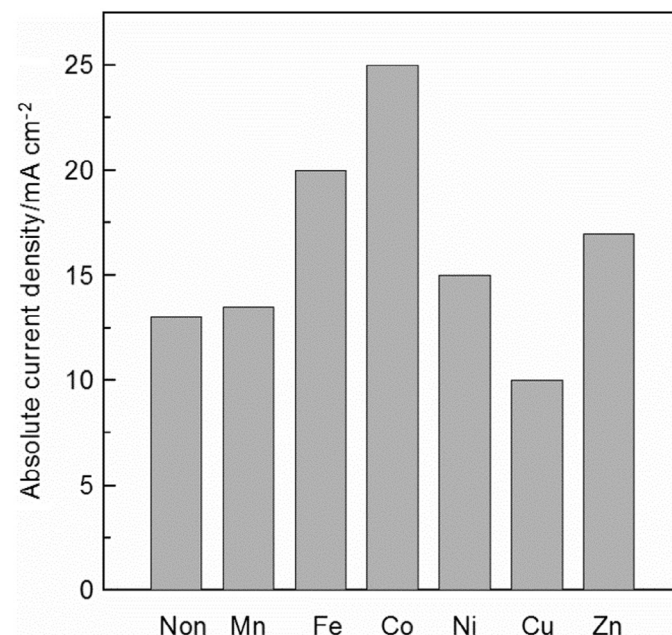


**Fig. 24.** Absolute values of current densities obtained with unpromoted and M-promoted ( $M = Mn, Fe, Co, Ni, Cu$  or  $Zn$ )  $MoS_3$  films on glassy carbon in  $pH = 0$  at  $0.20\text{ V}$  overpotential. Adapted from reference 329.

[321]. According to Xie et al. [326], the rich existence of defects in  $MoS_2$  results in partial cracking of the catalytically inert basal planes, which leads to exposure of additional active edge sites and thus to higher activity. Working in this direction, the authors of this study developed a strategy for controlling the defects in  $MoS_2$  ultrathin nanosheets and obtained materials with excellent HER activity (small onset potential of  $0.12\text{ V}$ , small Tafel slope of  $50\text{ mV/dec}$ , durability for  $>160\text{ min}$ ).  $MoS_x$  films consisting of nanoparticles [327] or nanosheets [328] have been also reported in literature, as well as amorphous  $MoS_x$  films, the activity of which has been related with the presence of more unsaturated active sites than in  $MoS_2$  single crystals or nanoparticles [321]. Doping with transition metal ions has been shown to further enhance (up to 1.8 times larger current densities were observed in acidic environment) the HER activity of amorphous  $MoS_x$  films [329]. However, as shown in Fig. 24, enhancement is observed only with selected promoter ions (Fe, Co, Ni, Zn) while doping with ions of Mn and Cu did not have any effect on HER activity.

Even though there are still remaining challenges associated with the use of  $MoS_x$  in PEM electrolysis which make them unsuitable for large-scale application, this family of materials could possibly have a place in future PEM electrolysis. A main issue related with the use of  $MoS_x$  nanoparticles, nanosheets and films for HER is the low conductivity of these materials. The use of conductive templates or supports (such as carbon nanotubes or graphene) is a method proposed to optimize conductivity [321]. Hou et al. [330] proposed the use of  $MoO_2$  nanobelts coated with nitrogen self-doped  $MoS_2$  nanosheets as an active HER electrocatalyst, where the nitrogen doping leads to enhanced conductivity as well as to a high density of spinning electro states around the N and Mo atoms in  $MoS_2$  nanosheets. The obtained core-shell type catalyst had higher HER activity (with a Tafel slope of  $47\text{ mV/dec}$ ) and durability compared to commercial Pt/catalysts [330]. Great progress was presented in a latter study of the same group, since a novel catalyst was developed [331] by growing  $MoS_2$  nanosheets on carbon fibers and then decorating  $MoS_2$  with Pt nanoparticles. The resulted composite exhibited excellent characteristics for HER electrocatalysis, with

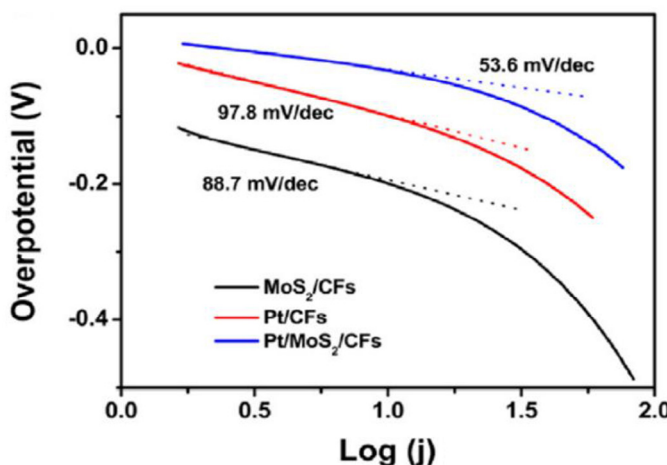


**Fig. 25.** Tafel plots for different HER electrocatalysts: MoS<sub>2</sub> nanosheets grown on carbon fibers (black), Pt nanoparticles on carbon fibers (red) and Pt nanoparticles on MoS<sub>2</sub> nanosheets grown on carbon fibers (blue). Reprinted from reference 331 with permission of Elsevier.

an overpotential of  $-5$  mV, Tafel slope of  $54$  mV/dec (Fig. 25) and excellent stability during  $10$  hours of continuous operation. The optimized performance of the composite was attributed to several factors: (i) the effective charge transfer due to the enhancement in conductivity provided by the carbon support, (ii) the high electrochemical effective surface area provided mainly by the structure of the carbon fibers (permeable channels for ion adsorption and transport), (iii) the synergistic effect between MoS<sub>2</sub> nanosheets and Pt nanoparticles, as confirmed by XPS [331].

Transition-metal phosphides form a class of materials that has been widely used as anodes in Li-ion batteries and as catalysts for the hydrodesulfurization reaction (HDS) [332]. Owing to the mechanistic similarities of HER and HDS related with the dependence of catalytic activity on the binding of hydrogen to the catalyst, the activity of these materials for HER has been lately investigated and validated. Kucernak et al. [333] investigated the role of phosphorus content in nickel phosphides on the corrosion resistance in acid and on the HER activity. The authors of this study [333] used the hydrothermal route for developing several nickel phosphides and concluded that the materials with higher phosphorus content are more stable in the acidic environment of  $0.5$  M H<sub>2</sub>SO<sub>4</sub>. Regarding HER activity, Ni<sub>2</sub>P catalysts were found to be more active than Ni<sub>12</sub>P<sub>5</sub> at  $25$  °C (current densities of  $1.27$  A/cm<sup>2</sup> and  $0.02$  A/cm<sup>2</sup> respectively at  $-0.2$  V). Pan et al. [334] synthesized monodispersed nickel phosphide nanocrystals with several different compositions following the thermal decomposition approach, where the phase-controlled synthesis was achieved by changing the molar ratio of P:Ni precursor. The nanocrystals of Ni<sub>5</sub>P<sub>4</sub> exhibited higher HER activity than Ni<sub>12</sub>P<sub>5</sub> and Ni<sub>2</sub>P nanocrystals (Fig. 26), which according to the authors can be attributed to the higher positive charge of Ni and the stronger ensemble effect of P in Ni<sub>5</sub>P<sub>4</sub> nanocrystals. The same group also published recently [335] an innovative article where carbon nanospheres were decorated by nanostructured Ni<sub>2</sub>P. The hybrids were used as HER electrocatalysts in  $0.5$  M H<sub>2</sub>SO<sub>4</sub>. A carbon content of  $40\%$  was found to be the optimal, but still HER activity is lower compared to Pt. For achieving a current density of  $10$  mA/cm<sup>2</sup>, the overpotential needed is  $0.12$  V for Ni<sub>2</sub>P-10% C,  $0.11$  V for Ni<sub>2</sub>P-20% C,  $0.92$  V for Ni<sub>2</sub>P-40% C and  $0.99$  V for Ni<sub>2</sub>P-60% C.

Several other phosphides, carbides and nitrides in combination with various novel nanostructures have been proposed lately as promising low-cost HER electrocatalysts with tolerance in acidic media. Table 4 gives a comparison for the HER activity of various

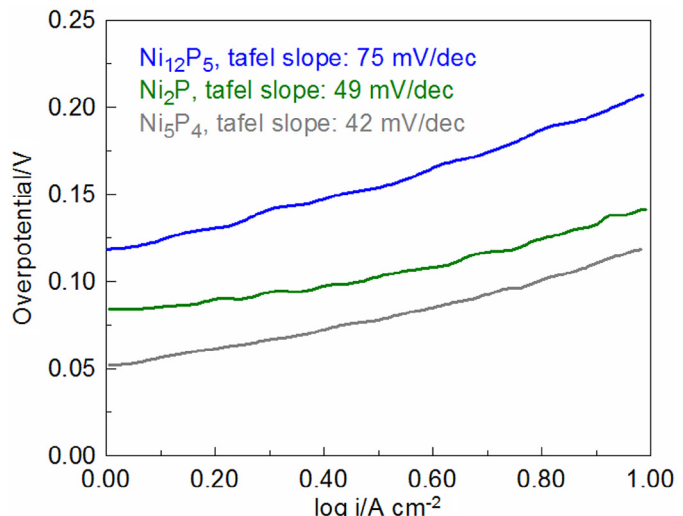


**Fig. 26.** Tafel plots for different HER electrocatalysts: Ni<sub>12</sub>P<sub>5</sub> (blue), Ni<sub>2</sub>P (green), Ni<sub>5</sub>P<sub>4</sub> (gray),  $0.5$  M H<sub>2</sub>SO<sub>4</sub>,  $25$  °C. Adapted from reference 334.

recently developed materials [326–350]. Indicatively, excellent performance and stability has been observed using FeP nanoparticles on candle soot [339], WP<sub>2</sub> nanorods [344], molybdenum phosphor-sulphide [343], CoP nanocrystals on carbon nanotubes [340], porous C<sub>3</sub>N<sub>4</sub> nanolayers with nitrogen-doped graphene sheets [345], a novel bimetallic carbide nanowire structure where nanosized Mo<sub>2</sub>C particles were integrated onto a highly conductive WC backbone [346], WC nanopowder for high temperature PEM electrolysis [350], nanostructured mixed close-packed Co<sub>0.6</sub>Mo<sub>1.4</sub>N<sub>2</sub> [347], Mo<sub>2</sub>C and Mo<sub>2</sub>N nanoparticles [348].

#### 4.2.3. Other materials

While most of the materials developments are focused on sulphides, phosphides, carbides and nitrides, other individual materials have been also investigated as possible anodes for PEM electrolysis. Grigoriev et al. [351] proposed that Pd could be advantageously used as an alternative to Pt for HER in PEM water electrolyzers, however alloying is required since pure Pd forms hydrides which lead to instability and degradation issues. The alloying of Pd with the low cost element Bi at ca.  $70$  at % was shown to suppress Pd hydride formation and thus improve long term stability during HER, while the HER activity is similar to that of pure Pd [352].

Perovskitic materials have been also used as HER electrocatalysts in  $0.1$  M H<sub>2</sub>SO<sub>4</sub>. The effect of using different B-site metals on lanthanum based perovskites (LaMO<sub>3</sub>) was investigated by Galal et al. [349]. The catalytic activity was found to follow the order LaFeO<sub>3</sub> > LaCoO<sub>3</sub> > LaNiO<sub>3</sub> > LaMnO<sub>3</sub>. The superior performance of LaFeO<sub>3</sub> could be related with the fact that Fe itself has higher HER activity compared to Co, Ni and Mn [353].

Co nanoparticles encapsulated in nitrogen-doped carbon were used recently as potential HER catalysts in a wide range of pH. It was found that the interactions between Co nanoparticles and surface carbon nanoshells resulted in high HER activities. To achieve current density of  $10$  mA/cm<sup>2</sup> the overpotential needed is  $0.2$  V, much lower compared to the  $0.4$  V needed for Fe nanoparticles encapsulated in nitrogen-doped carbon and to the  $0.6$  V for the multiwalled carbon nanotubes [354]. Another recently published interesting and promising work utilizes HER electrocatalysts based on MoO<sub>2</sub>-graphene composites [355]. High HER activity ( $50$  mV/dec Tafel slope) was observed together with a low onset overpotential of  $0.2$  V. The optimized structure of this material, responsible for the high HER activity, is based on the synergistic effects of MoO<sub>2</sub> nanoparticles

**Table 4**Comparison of performance of various HER electrocatalysts in 0.5 M H<sub>2</sub>SO<sub>4</sub>.

Catalyst	Tafel slope (mV/dec)	Exchange current density (mA/cm <sup>2</sup> )	Current density i (mA/cm <sup>2</sup> )	Overpotential at current density i (mV)	Reference
Amorphous MoS <sub>3</sub> film	40	0.0013	2	170	[329]
MoS <sub>2</sub> nanoparticles on graphene	41	–	10	150	[337]
Defect-rich MoS <sub>2</sub> nanosheets	50	0.009	10	180	[326]
Pt–MoS <sub>2</sub> nanosheets on carbon fibers	53.6	–	10	35	[331]
CoS <sub>2</sub> nanowire	51.6	0.015	10	145	[338]
FeP on candle soot	58	0.22	10	112	[339]
FeP nanowires*	38	0.42	10	55	[336]
CoP on carbon nanotubes	57	0.13	10	115	[340]
CoP nanowires	51	0.288	10	67	[341]
CoP nanoparticles	50	0.13	20	85	[342]
Ni <sub>5</sub> P <sub>4</sub> nanocrystals	42	0.057	10	105	[334]
NiP <sub>2</sub> on carbon nanospheres	46	0.49	–	–	[335]
Mo/P/S	50	0.2	–	–	[343]
WP <sub>2</sub> nanorods	52	0.013	10	148	[344]
C <sub>3</sub> N <sub>4</sub> layers on nitrogen-doped graphene	49	0.43	10	80	[345]
Mo <sub>2</sub> C–WC nanowire	56	0.0047	80	184	[346]
Co <sub>0.6</sub> Mo <sub>1.4</sub> N <sub>2</sub>	–	0.000015	10	200	[347]
Mo <sub>2</sub> N	100	–	10	381	[348]
Mo <sub>2</sub> C	56	–	10	198	[348]
Mo <sub>2</sub> C on carbon nanotubes	55	0.014	1	63	[349]

\* In 0.1M HClO<sub>4</sub>.

with graphene, the high conductivity (mainly due to graphene) and the high number of active sites due to the structural characteristics.

Inspired by the broad use of Ni in alkaline electrolysis, Wang et al. [356] attempted the use of Ni based alloys in acidic HER electrocatalysis. Alloying was essential in order to ensure stability in the acidic environment and NiMoZn alloys were synthesized and evaluated as HER electrocatalysts. Their work identified the essential role of Zn in boosting the intrinsic electrocatalytic activity. Zn concentration of 1–3 at % results in high HER activities, 10 and 1.5 times higher compared to Ni and NiMo alloy nanoparticles respectively. The optimal alloy with 2at% Zn has also presented excellent stability in the acidic electrolyte of 0.5 M H<sub>2</sub>SO<sub>4</sub> during an accelerated stability test (1000 sweeps between 0 and –0.4 V vs Ag/AgCl, 0.1 V/s) where the material has experienced conditions between extreme (30 mA/cm<sup>2</sup>) and normal (10 mA/cm<sup>2</sup>) working conditions.

In conclusion, several materials have been developed and investigated as HER electrocatalysts in acidic media as alternatives to the high-cost Pt. The majority of these materials belong to the main families of sulphides, phosphides, carbides and nitrides, but also other individual materials (metallic alloys, perovskites) have been proposed. Among these materials, MoS<sub>x</sub> seems to be the most promising candidate in terms of activity and stability in the acidic environment. Recent studies have shown that the main obstacle for commercialization of MoS<sub>x</sub>, which is the poor electronic conductivity, could be overcome utilizing advances in nanotechnology, such as the core-shell structures.

#### 4.3. Solid oxide electrolyzers (SOEs)

##### 4.3.1. SOE with O<sup>2–</sup> conducting oxides

As already discussed for the case of OER, the materials used in SOEs are typically based on the already mature technology of solid oxide fuel cells, even though the working conditions, especially at the hydrogen electrode side, are quite different between the two technologies. Thus, the ceramo-metallic cermet Ni–YSZ (YSZ: ZrO<sub>2</sub> stabilized with 8 mol% Y<sub>2</sub>O<sub>3</sub>) is typically used as the hydrogen electrode in large scale SOEs [357–360]. The nickel component in the two-phase cermet is employed due to its high activity, electronic conductivity and low cost. The presence of the ceramic phase (YSZ) in the cermet provides prevention of Ni from sintering, good adhesion between the electrode and the electrolyte, thermal expansion coefficient which is acceptably close to that of the other cell

components, while YSZ also provides pathways for oxygen ion transport deep into the porous electrocatalytic layer thus leading to large length of the three-phase-boundaries.

However, degradation in the performance of Ni–YSZ during prolonged steam electrolysis has been reported and was ascribed to cracks in Ni–YSZ [361], aggregation of Ni due to the high temperature and the high humidity [362], relocation of Ni [363], varying surface roughness of the Ni particles [364], poisoning from impurities in the material [365], crystallographic transformation of YSZ [366]. Moreover, metallic nickel can be oxidized to NiO during the steam electrolysis, resulting in loss of electronic conductivity in the cermet and consequently to degradation of the performance of the electrode and even delamination from the electrolyte surface. In order to prevent such Ni oxidation, significant concentration of hydrogen gas (as a reducing agent) is typically added to the gas stream [367].

Thus, efforts have been focused on the development of novel materials with high activity and stability in order to replace Ni–YSZ cathodes in SOEs. The combination of highly dispersed Ni with samaria-doped ceria was first proposed [368], but nowadays all the research efforts are directed on the development of novel perovskitic materials.

Substituted lanthanum chromates are commonly investigated as cathodes for steam SOEs. Yang and Irvine [369] in 2008 were the first to introduce (La<sub>0.75</sub>Sr<sub>0.25</sub>)<sub>0.95</sub>Mn<sub>0.5</sub>Cr<sub>0.5</sub>O<sub>3</sub> as the cathode of a steam electrolysis cell operated in the temperature range of 750–1000 °C without the need of having a flow of a reducing agent gas over the electrode. Aiming at higher electrocatalytic activity, loading of active Fe [370] or Ni [371] into the composite La<sub>0.75</sub>Sr<sub>0.25</sub>Cr<sub>0.5</sub>Mn<sub>0.5</sub>O<sub>3–δ</sub>–Ce<sub>0.8</sub>Sm<sub>0.2</sub>O<sub>2–δ</sub> cathode has been proposed. The Ni-loading of the perovskite-based composite resulted in a 20% increase in Faradaic efficiency for 3%H<sub>2</sub>O/5%H<sub>2</sub>/Ar and to 11% increase for 3% H<sub>2</sub>O/Ar, due to the synergetic effect of the catalytically active Ni phase and the redox-stable perovskite. Promising performance was observed for the Fe-loaded composite when either 3% H<sub>2</sub>O/5% H<sub>2</sub>/Ar or 3% H<sub>2</sub>O/Ar was supplied for the electrolysis at 800 °C. Moreover, the Fe-loaded composite showed stable performance during the first hour of continuous operation under 1.5 V at 800 °C; a decrease of ca 15% in performance was however observed after 15 hours of continuous electrolysis.

A novel perovskite chromate cathode with anchored nickel nanoparticles was proposed recently as a potential fuel

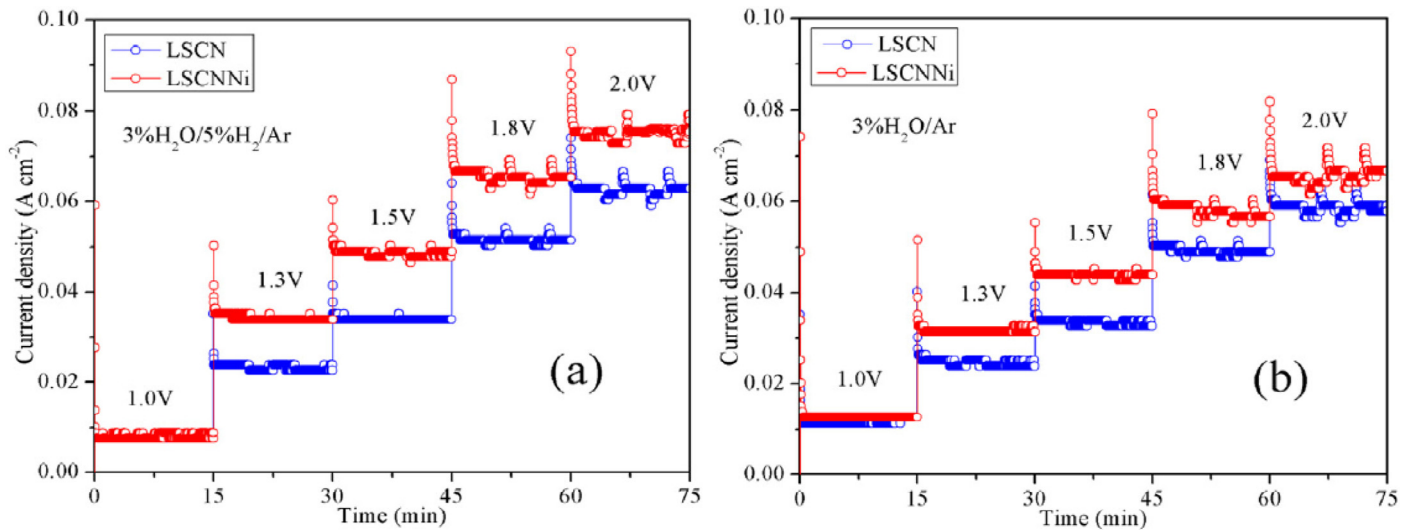


**Fig. 27.** Effect of loading Ni in  $(La_{0.75}Sr_{0.25})_{0.95}(Cr_{0.8}Ni_{0.2})_{0.95}Ni_{0.05}O_{3-\delta}$  cathode on the performance during electrolysis in 3%H<sub>2</sub>O/5%H<sub>2</sub>/Ar (a) and 3%H<sub>2</sub>O/Ar (b). T: 800 °C, electrolyte: YSZ, anode: LSM/YSZ. Reprinted from reference 372 with permission of Elsevier.

electrode for the steam electrolysis in oxygen-ion solid oxide electrolyzers [372]. In this work catalytic Ni nanoparticles were introduced in a perovskite which was A-site deficient, i.e.  $(La_{0.75}Sr_{0.25})_{0.95}(Cr_{0.8}Ni_{0.2})_{0.95}Ni_{0.05}O_{3-\delta}$ . As shown in Fig. 27, when Ni is loaded in the composite, higher current densities are observed during steam electrolysis at 800 °C either in presence or in absence of hydrogen in the stream. The Ni-loaded composite exhibited sufficiently stable performance during continuous electrolysis of 3% H<sub>2</sub>O/Ar at 1.5 V, with a slight decrease (below 10%) in current density (not shown here).

Even though these studies [370–372] showed that loading of substituted lanthanum chromites with an active metallic phase can lead to enhanced performance of steam electrolysis, slight degradation over time was observed in all cases under prolonged operation, mainly due to chemical and structural changes of the perovskitic phase.

Qin et al. [373] synthesized a Fe-doped titanate of  $(La_{0.2}Sr_{0.8})_{0.9}Ti_{0.9}Fe_{0.1}O_{3-\delta}$  with A-site deficiency and B-site excess and their experimental results showed that this material can be a potential cathode for oxygen-ion conducting SOEs. Doping with Fe led to improvement in electrocatalytic activity of the titanate, similarly with the cases of doping of chromates [370–372]. Specifically, the current efficiency of the Fe-loaded perovskite was enhanced by 20% compared to the bare perovskite in a wide range of applied potentials, both in presence and in absence of H<sub>2</sub> in the water steam. Interestingly, the Fe-doped titanate showed excellent stability when direct steam electrolysis was performed at 1.4 V in 3% H<sub>2</sub>O/Ar at 800 °C for 24 hours, thus suggesting that the anchored interface between the Fe nanocatalyst and the perovskitic substrate is beneficial to the thermal stability and the high-temperature catalytic activity.

The same group used the concept of metal doping also on lanthanum vanadates [374] and loaded  $La_{0.7}Sr_{0.3}VO_3$  with Fe and Ni, which resulted in improved electrolysis (up to 20% increase in current efficiency) compared to the undoped perovskite. However, the stability of this material during long-term operation was not discussed in their work.

To conclude, the typical Ni–YSZ composite used in SOEs suffers from poor stability under the operating conditions of electrolysis which results to several structural damages. In the course of developing alternative SOE cathodes, perovskites have gained much attention. Appropriate materials should offer good chemical stability in presence of steam and hydrogen, compatibility with the other

cell components, good thermal expansion characteristics and electronic (or mixed ionic-electronic) conductivity. Substituted lanthanum chromates, titanates and vanadates have been proposed and it has been found that the addition of an active metallic phase (e.g. Ni, Fe) can lead to enhanced performance; however stability is still a main challenge related to SOEs.

#### 4.3.2. SOE with H<sup>+</sup> conducting oxides

A basic difference between proton and oxygen ion conducting SOEs is the fact that the electrode at the HER side is exposed only to hydrogen gas (evolving during electrolysis) in the first case, while reactant steam water is also present in the second case. This operational difference allows the use of nickel-based materials as hydrogen electrodes in proton conducting SOEs, since they do not suffer from reoxidation (and subsequent degradation due to the loss of electronic conductivity) as in the case of oxygen-conducting SOEs [235]. Moreover, apart from its low cost and high electrical conductivity, nickel has exhibited good chemical compatibility with the majority of the existing proton-conducting oxides at high temperatures in solid oxide fuel cell applications, with electrolytes such as  $Ba_3Ca_{1.18}Nb_{1.82}O_{9-\delta}$  [375],  $BaZr_{0.8}Y_{0.2}O_{3-\delta}$  [376–378],  $BaZr_{0.1}Ce_{0.7}Y_{0.2}O_{3-\delta}$  [379],  $BaZr_{0.3}Ce_{0.5}Y_{0.2}O_{3-\delta}$  [380],  $BaCe_{0.85}Y_{0.15}O_{3-\delta}$  [381],  $Y_{0.8}Ca_{0.2}BaCo_{0.4}O_{7-\delta}$  [382].

Hydrogen electrodes are typically composed of nickel-ceramic cermets (and not pure Ni), in order to ensure high length of three-phase-boundaries (TPBs) and thus to provide an extended reaction zone, but also in order to enhance adhesion to the electrolyte [24,383]. Successful steam electrolysis at 700 °C has been achieved using nickel-based ceramo-metallic cermets, such as  $Ni-BaCe_{0.5}Zr_{0.3}Y_{0.16}Zn_{0.04}O_{3-\delta}$  [237,243] and  $Ni-BaCe_{0.5}Zr_{0.3}Y_{0.2}O_{3-\delta}$  [238].

These materials have exhibited sufficient intrinsic activity and stability, thus optimization of the hydrogen electrodes for proton-conducting SOEs should focus mainly on the microstructure of the nickel-based composites rather than on the development of new alternative materials. High porosity of the electrode structure is advantageous for facilitating the gas diffusion, but on the other hand the macro-pores can increase the contact resistance between the electrolyte and the hydrogen electrode and also decrease the TPB length. In order to ensure high porosity while simultaneously keeping a high TPB area and good electrolyte/electrode contact, a thin and relatively dense functional layer is typically added between the electrolyte and the porous external electrode film [24,383].

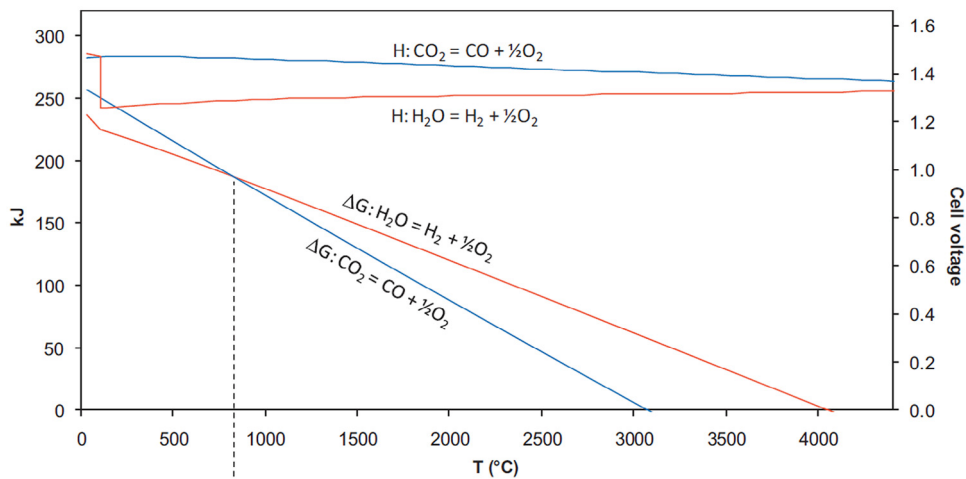


**Fig. 28.** Thermodynamics of  $\text{CO}_2$  and  $\text{H}_2\text{O}$  splitting reactions. The electrochemical cell potential that corresponds to the energy input is given in the right axis. The dashed line indicates the temperature where  $\text{H}_2\text{O}/\text{CO}_2$  co-electrolysis can occur. Reprinted from reference 390 with permission of Elsevier.

## 5. High temperature $\text{CO}_2/\text{H}_2\text{O}$ co-electrolysis

### 5.1. Operation and mechanisms

SOEs have the advantageous capability of producing syngas directly via the co-electrolysis of  $\text{CO}_2$  and  $\text{H}_2\text{O}$ . SOE co-electrolysis units are expected to play a crucial role in the future for the production of synthetic fuels from water and  $\text{CO}_2$  with the use of intermittent renewable energy sources. The syngas produced during co-electrolysis can be subsequently transformed into synthetic fuels [384–390].

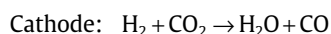
This can thus lead to significant reduction in the cost of a total system for  $\text{CO}_2$ -recycled fuel production process, since the need for a reverse water–gas-shift reactor is eliminated [390,391]. Pozzo et al. [392] proposed a novel process plant design by integrating a dimethyl ether (DME) synthesis unit with a woody biomass gasifier and a high-temperature co-electrolysis unit. According to their calculations, the utilization of the co-electrolysis unit can lead to a two-fold enhancement in biomass-to-liquid plant efficiency compared to conventional plants [392].

According to thermodynamics (Fig. 28), the co-electrolysis of  $\text{CO}_2$  and  $\text{H}_2\text{O}$  should be carried out at temperatures between 700 and 900 °C, where the energy demands for the two electrolytic processes are similar. Numerous studies have demonstrated the feasibility of co-electrolysis both in laboratory scale using single cells [32–35,393–405] and in large-scale using stacks of cells [406–411].

In the cathode of such cells, two electrochemical reactions occur simultaneously at the triple phase boundary, i.e.  $\text{H}_2\text{O}$  and  $\text{CO}_2$  electrochemical reductions. The oxygen ions produced by these electrochemical reactions are transferred through an oxygen ion-conducting membrane (typically YSZ) to the anode, where oxygen gas is formed. Thus, the electrochemical reactions that take place in solid oxide co-electrolysis are:



Moreover, the reversible water gas shift (RWGS) catalytic reaction also takes place at the cathode:



It thus appears that at the cathode of the electrolyzer, CO can be produced either electrochemically by the dissociation of  $\text{CO}_2$ , or catalytically via the RWGS reaction. Controversial observations

have been presented in the literature regarding the actual contribution of electrochemistry and catalysis in the total CO production. Most of the studies report that  $\text{CO}_2/\text{H}_2\text{O}$  co-electrolysis performs slightly worse (10%) than  $\text{H}_2\text{O}$  electrolysis (CO is mainly produced electrochemically and RWGS has a small contribution) [393,394,398,400,401,406], while a few studies report that  $\text{CO}_2/\text{H}_2\text{O}$  electrolysis has the same performance as  $\text{H}_2\text{O}$  electrolysis (CO is totally produced catalytically via the RWGS) [405,410].

These discrepancies regarding the CO production route can be related to the actual differences in the studied systems, since according to recent findings [32,394,412], the contribution of the electrochemical and catalytic routes on the total CO production can be significantly affected both by the structural characteristics of the electrode–catalyst (porosity, particle size, ionic conductivity, thickness), but also by the operating conditions (gas composition, temperature, operation at limiting currents).

Li et al. [412] developed a theoretical model considering the catalytic and electrochemical reactions and mass and charge transport properties in order to predict the competitive behavior of catalytic and electrochemical routes for CO production during  $\text{CO}_2/\text{H}_2\text{O}$  co-electrolysis. According to this study, the heterogeneous catalytic reactions take place near the outer surface of the cathode and they are 20–100 times faster than the electrochemical reactions, which take place at the three-phase-boundaries (close to the electrolyte). The model predicts that heterogeneous catalysis is limited by mass transfer, while electrochemistry is limited by charge transfer. Thus, modifications in the porosity and particle size of the cathode could enhance mass transport and thus promote the  $\text{CO}_2$  reaction through the catalytic route, resulting in experimentally obtained polarization curves of  $\text{CO}_2/\text{H}_2\text{O}$  co-electrolysis close to that of  $\text{H}_2\text{O}$  electrolysis. Similarly, increase in the ionic conductivity of the cathode is related to improved charge transfer, and thus promotes the electrochemical route of  $\text{CO}_2$  reduction, leading to polarization curves of  $\text{CO}_2/\text{H}_2\text{O}$  co-electrolysis similar to those of  $\text{CO}_2$  electrolysis. Operating conditions influence both mass and charge transfer, however not at the same extent (e.g. electrochemical reactions are more sensitive to temperature changes).

### 5.2. Materials for co-electrolysis

The majority of the studies on high temperature  $\text{CO}_2/\text{H}_2\text{O}$  co-electrolysis utilize Ni–YSZ composite cathodes, similarly to the case of steam electrolysis [32,34,393–401,413].

It is well established that co-electrolyzers encounter stability issues, while the degradation depends strongly on the current density. Several studies have shown that the degradation is much faster when the cell is operated at higher current densities [397–399,401]. Indicatively, Sun et al. [397,398] investigated the durability of  $\text{CO}_2/\text{H}_2\text{O}$  co-electrolysis at 800 °C with 60% reactant utilization and observed an overall cell voltage degradation rate of 0.2 mV/h under operation at 1 A/cm<sup>2</sup>, while at 1.5 A/cm<sup>2</sup> the degradation rate increases to 0.8 mV/h. Electrochemical characterization has shown that the initial cell degradation (for the first 200 hours) is due to increase in the polarization resistance and is weakly dependent on the applied current, while the long term degradation (after >200 hours of operation) exhibits strong dependence on current density and it is related to increase in the serial resistance indicating structural changes at the electrodes [397,398]. Degradation was attributed both to the oxygen electrode (LSM) and to the cathode electrode (Ni-YSZ). The microstructural changes that took place after prolonged co-electrolysis at different current densities were investigated with SEM. In the Ni-YSZ electrode, passivation and blocking of the TPBs by impurities were the main causes for degradation. As a result, Ni grain growth and loss of Ni percolation and loss in the Ni-YSZ contact were observed, which were more pronounced with increasing current density [398,400]. Formation of carbon during co-electrolysis can also take place on electrodes with low porosity and can lead to degradation phenomena (due to the subsequent volume expansion and nickel dusting), finally resulting in electrode delamination [34].

Alternative cathode materials have also been used for  $\text{CO}_2/\text{H}_2\text{O}$  electrolysis. Sr-doped  $\text{LaVO}_3$  (LSV) perovskite was used together with  $\text{CeO}_2$  and Pd as a composite cathode and was successfully employed in co-electrolysis. It was found that different mechanisms occur depending on the presence of Pd in the LSV- $\text{CeO}_2$  composite, since Pd addition was reported to inhibit the electrochemical  $\text{CO}_2$  reduction, while promoting the RWGS reaction for CO production [35]. No degradation was observed in the performance of the LSV- $\text{CeO}_2$ -Pd composite after continuous co-electrolysis under 0.5 A/cm<sup>2</sup> for 10 hours, while this was not the case when dry  $\text{CO}_2$  electrolysis was attempted with the same system, where microstructural changes such as the coating of YSZ of an LSV coating caused severe degradation due to loss of the catalytically active site for  $\text{CO}_2$  reduction [35].

Efficient co-electrolysis has been also demonstrated with a  $\text{La}_{0.2}\text{Sr}_{0.8}\text{TiO}_{3+\delta}$  cathode, where the flow of a reducing gas (e.g. H<sub>2</sub>) or the pre-reduction of the electrode was necessary. Faradaic efficiencies of 85% for  $\text{H}_2\text{O}$  electrolysis and 25% for  $\text{CO}_2$  electrolysis were achieved at 700 °C [403]. Instead of Ni-YSZ cathode, composites of  $(\text{La}_{0.75}\text{Sr}_{0.25})_{0.97}(\text{Cr}_{0.5}\text{Mn}_{0.5})\text{O}_{3-\delta}-\text{Gd}_{0.1}\text{Ce}_{0.9}\text{O}_{1.95}$  [404] have been proposed, suffering however from difficulties in steam diffusion at least under the exact operating conditions. Recently, it was shown that the addition of Cu by impregnation on  $\text{La}_{0.75}\text{Sr}_{0.25}\text{Cr}_{0.5}\text{Mn}_{0.5}\text{O}_{3-\delta}$  (LSCM) can lead to a 6-fold enhancement in activity during  $\text{H}_2\text{O}$  electrolysis due to the improved electronic conductivity of the Cu-doped LSCM. Moreover, the Cu-doped perovskite showed excellent activity during  $\text{CO}_2/\text{H}_2\text{O}$  co-electrolysis and stability for more than 50 hours of operation at 0.3 A/cm<sup>2</sup> at 750 °C [33].

To sum up,  $\text{CO}_2-\text{H}_2\text{O}$  co-electrolysis offers a potentially feasible and environmentally friendly way for the production of synthesis gas. Despite its yet unproven durability at high current densities, this technology is very promising for future commercialization. Most reports on this process have been performed with Ni-YSZ composites, the typical cathode material of SOEs. However, nickel is a well-known catalyst for forming solid carbon through the dissociation of carbon containing gases and disproportionation of CO. Carbon deposition is a typical degradation source of co-electrolyzers, while most degradation phenomena arise from the fact that Ni-based materials are typically subsequent to structural damages due to volume expansion, as observed also with high temperature water

electrolyzers. However, the operation and degradation mechanisms during co-electrolysis are much more complex compared to water electrolysis, since both catalytic and electrocatalytic reactions take place at the cathode. Further fundamental investigations on identifying the exact mechanisms are expected to provide useful input for the design of more active and stable materials. At present, only few works have investigated the possibility of using materials alternative to Ni-YSZ as cathodes for co-electrolysis. As in the case of water electrolysis, ceramic materials with electronic conductivity would fit better to the conditions that occur in the cathode (not extremely reducing) and would result in better performance. In this direction, these few attempts have been focused on using perovskites with different stoichiometries and on the possibility of combining perovskites with a metallic phase (e.g. Cu, Pd).

## 6. Outlook and summary

Hydrogen can serve as a chemical carrier for storing excess power generated by renewable energy sources and it can be subsequently utilized in several processes contributing to the realization of a carbon-neutral energy scenario. Hydrogen can be used as a fuel on-demand (in internal combustion engines and in fuel cells) having zero post-combustion emissions. Alternatively, hydrogen can be used as a reducing agent for the recycling and valorization of point-source  $\text{CO}_2$  and its conversion to fine chemicals or fuels, thus leading to an overall reduction in the fossil fuel consumption.

One should not forget that electrolysis of water produces O<sub>2</sub> as well, which in pure form is a valuable chemical. Future developments as the electrification of the chemical industry will undoubtedly lead to environments where at least part of the generated O<sub>2</sub> can be used in production processes. Another area where both hydrogen and oxygen are valuable assets is in the coal-to-liquids industry, which is rapidly growing in China [414]. By integrating renewable electricity with coal technology, oxygen can be used in the gasification process, while hydrogen can be added to the synthesis gas, which has inherently low H<sub>2</sub>/CO ratio when obtained from coal. In this way the  $\text{CO}_2$ -producing water gas shift process can be minimized. Hence integrating electrolysis with coal technology has significant potential for reducing the negative environmental impact associated with the use of coal [415].

Water electrolysis is a viable technology for hydrogen production due to its high efficiency and low environmental impact. Even though water electrolysis is a proven technology of which the concept has been demonstrated two centuries ago, the large-scale implementation of electrolyzers for renewable H<sub>2</sub> production is hampered by the low abundance of active and stable electrocatalysts, and their inability to deal with fluctuating conditions. Research efforts are mainly directed to the development of electrocatalysts, which are free (or with reduced amounts) of noble metals. Finally, the EU energy roadmap envisages an integrated network of electrolyzers operating in conjunction with renewable energy sources. Therefore, stability in the performance during the intermittent operation of a daily cycle and long lifetime are required.

Depending on the type of the electrolyte used (i.e. alkaline liquids, polymeric membranes, solid oxide ceramics), the electrolysis technologies are classified accordingly. The three types of water electrolyzers share the same operational principles, however distinct differences exist in terms of operational conditions and thus in the selection of proper materials. Low temperature electrolysis offers numerous advantages related with simple cell design, quick start-up and safe operation. On the other hand, the high temperature during solid oxide electrolysis may offer higher efficiencies using low-cost materials. Moreover, thermodynamics allows the simultaneous co-electrolysis of  $\text{CO}_2$  and  $\text{H}_2\text{O}$  for direct production of syngas (H<sub>2</sub> + CO), a process of great interest that could lead to significant reductions in  $\text{CO}_2$  emissions.

This review provides a survey of the recent progress in the development of active and stable electrocatalysts with minimal cost, for the three technologies of water electrolysis (alkaline, PEM, SOE).

The discussion in this article is limited to concepts on heterogeneous electrocatalysis. However, homogeneous and heterogeneous catalytic systems for water splitting share structural and functional characteristics. As an example, detailed XPS and XAS studies under electrochemical conditions over prolonged reaction times using iridium-based catalyst precursors have shown that structural modifications of the ligand framework play an important role in the catalytic activity [416]. This can be ascribed to an iridium oxide deposit developed during the decomposition of the precursor [417]. It thus appears that for such cases homogeneous and heterogeneous water splitting are two facets of the same process, i.e. water oxidation on an  $\text{IrO}_2$  like surface, which forms in a sort of self-assembling process. Therefore, direct comparison and combination of the two fields would be of great interest and could lead to significant improvements of both approaches.

Our article is structured in two main parts, which concern the hydrogen and the oxygen electrode respectively. For each case, the basic requirements and the degradation issues of electrocatalysts vary depending on the type of electrolysis. The electrocatalytic activity and stability are subjected to both the nature of the electrocatalysts and their structural characteristics. These issues are discussed by pointing out the progress in designing optimized materials with selected characteristics, the current limitations and obstacles in materials development and the promising directions for future research. The main outcome of our review can be summarized as follows:

### 6.1. Alkaline electrolysis

Water electrolysis in liquid alkaline media takes place at temperatures below 100 °C and is the simplest and most mature among the three electrolysis technologies. Even though it is the least efficient electrolysis method, alkaline electrolysis has already found industrial applications.

Low cost electrocatalysts mainly based on nickel alloys are typically used both in the anodic and the cathodic compartment of alkaline electrolyzers. Research efforts are directed at (i) increased durability and reliability, since both anodic and cathodic electrocatalysts exhibit deactivation after long-term operation, (ii) improved electrocatalytic activity, mainly for the oxygen evolution reaction of which the kinetics are not favored in alkaline media.

To meet these needs, research lines follow two main routes. The first one aims at the development of novel efficient and stable materials, either by doping Ni, Co, or Fe based electrocatalysts with other elements or by investigating alternative materials. In the latter case, perovskites have shown promise. Theoretical studies are now identifying relevant descriptors for HER and OER activity to reveal the targeted characteristics (for example binding energies of reaction intermediates, occupancy of 3d orbitals with  $e_g$  symmetry) for maximizing electrocatalytic activity. A new aspect in oxygen evolution that has not had much attention so far in both catalysis [418] and electrocatalysis [127] is in how far magnetic properties of the catalyst can facilitate the formation of  $\text{O}_2$ . This molecule, which is in the (magnetically ordered) triplet state, is likely to form most readily when spin-oriented precursors (O, or OH) are brought together in the right orientation. Such fundamental insights based on descriptors should then be complemented with kinetic studies for rigorously investigating the mechanistic pathway of the reaction under realistic conditions in order to lead to the rational design of highly efficient electrocatalysts (mainly for the oxygen evolution reaction).

The second route is related with the recent advances in the field of nanotechnology. Several 2D or 3D nanostructures of Ni and Co based materials have resulted in an evolution of electrocatalysts with

optimized characteristics (surface area, porosity, conductivity) which also exhibit high efficiency and long-term stability. Advances in materials nanostructuring are expected to lead to significant improvements in electrocatalysts performance due to enhanced chemical stability, surface area, catalyst utilization or bubble management.

### 6.2. PEM electrolysis

The use of solid polymeric membranes with protonic conductivity for water electrolysis at temperatures below 100 °C is advantageous since it allows for compact, robust and stackable cell designs with minor safety issues. However, the acidic environment in PEM electrolyzers hinders the kinetics of the redox reactions and introduces the requirement of using expensive noble metal catalysts thus limiting the commercialization of this technology.

The main challenges in PEM electrolysis are related to the OER, since HER is a much faster reaction.  $\text{RuO}_2$  and  $\text{IrO}_2$  exhibit high OER activity; however,  $\text{RuO}_2$  suffers from corrosion/dissolution during oxygen evolution in acidic environments, while  $\text{IrO}_2$  is more stable but is less abundant and thus a very expensive material. The development of efficient OER electrocatalysts with reduced price follows three distinct research directions. The first direction utilizes the relatively less expensive Ru-based materials and aims to ensure sufficient chemical stability by the incorporation of other elements, such as Ir or Sn. The second and third directions both focus on decreasing the loading of the high cost catalysts (Ir). The second direction aims to the development of large surface area supports (such as  $\text{TiO}_2$ ,  $\text{TiC}$ ,  $\text{TaC}$ ) for introducing the catalytic phase there into. Finally, the third approach aims to reduce the utilization of noble metal catalysts by employing alternative preparation methods (e.g. sputter deposition) and novel catalyst structures (e.g. core–shell structures).

Regarding the cathode where HER takes place, the state-of-the-art electrocatalyst consists of highly dispersed Pt nanoparticles on carbon supports. Although Pt is characterized by its high cost, low Pt loadings are typically required for HER in PEM electrolysis and thus this catalyst can be considered as appropriate even for large scale applications. However, novel nanostructures may contribute in the future to the further minimization of the Pt loading. Efforts on developing alternative inorganic materials as alternative HER electrocatalysts (sulphides, phosphides, carbides and nitrides) are currently carried out. Among them,  $\text{MoS}_2$  has been identified as a promising material, but its performance is still lower compared to that of the Pt-based state-of-the-art electrocatalysts, due to poor stability and low electronic conductivity. However, the introduction of this material into novel nanostructures may lead to advances in this field.

### 6.3. Solid oxide electrolysis (SOE)

High temperature steam water electrolysis can provide high efficiency, with lower total cost compared to conventional low temperature electrolysis due to favorable thermodynamics and kinetics. Moreover the operation temperatures of SOEs open up the opportunity of the simultaneous electrolysis of  $\text{CO}_2$  and  $\text{H}_2\text{O}$  for the production of synthesis gas. However, in viable systems the heat should be generated renewably (by heat from the sun or a nuclear power plant) or supplied from the waste heat of exothermic processes.

SOE technology relies on the use of solid oxide ceramics as electrolytes. These oxides typically have the ability of conducting oxygen ions ( $\text{O}^{2-}$ ), but recently oxides with protonic ( $\text{H}^+$ ) conductivity have been also realized.

Even though kinetics is favored at the operation temperature range of SOEs, difficulties occur in the selection of appropriate

catalyst–electrode materials due to a number of degradation and stability issues and this is the main reason that this technology is still in the R&D stage.

Composite materials are typically used, where the electrocatalytic active phase is mixed with the ceramic phase of the electrolyte, in order not only to maximize the length of the three-phase-boundaries (and thus increase electrocatalytic activity), but also to improve mechanical stability (by ensuring better adhesion between the electrode and the electrolyte). Perovskitic oxides are typical materials used as electrocatalysts for the oxygen electrode, due to their numerous advantageous characteristics such as high catalytic activity, good thermal compatibility with the ceramic oxide electrocatalyst and high electronic conductivity. Even though well performing materials have been identified, there is still on-going research for the identification of alternative perovskites with mixed ionic–electronic conductivity (for further extending the reaction zone) and with better chemical compatibility with the electrolyte oxides and interconnect materials.

Regarding the hydrogen electrode, Ni-based composites are the most common materials used in SOE. The use of proton-conducting SOEs is a promising approach, since hydrogen is produced in a separated chamber, which among all eliminates problems from Ni reoxidation due to the presence of water. For the case of proton-conducting SOE, sufficient performance has been already achieved and optimization is only needed regarding the microstructure for further enhancing catalytic properties. On the other hand, for the case of O<sup>2-</sup>-conducting SOE, Ni-based composites suffer from deactivation not only after intermittent operation in steam electrolysis, but also during H<sub>2</sub>O/CO<sub>2</sub> co-electrolysis and thus the development of alternative materials is necessary, a field in which perovskitic materials are again expected to find application in the future.

## Acknowledgement

SynCat@DIFFER, Syngaschem BV and SynCat@Beijing gratefully acknowledge financial support by Synfuels China Technology Co. Ltd.

## References

- [1] Acar C, Dincer I. Comparative assessment of hydrogen production methods from renewable and non-renewable methods. *Int J Hydrogen Energy* 2014;39:1–12.
- [2] Hussein AK. Applications of nanotechnology in renewable energies – a comprehensive overview and understanding. *Renew Sustain Energy Rev* 2015;42:460–76.
- [3] Chen J, Yang D, Song D, Jiang J, Ma A, Hu MZ, et al. Recent progress in enhancing solar-to-hydrogen efficiency. *J Power Sources* 2015;280:649–66.
- [4] Mazloomi K, Gomes C. Hydrogen as an energy carrier: prospects and challenges. *Renew Sustain Energy Rev* 2012;16:3024–33.
- [5] Ball M, Wietschel M. The future of hydrogen – opportunities and challenges. *Int J Hydrogen Energy* 2009;34:615–17.
- [6] Veziroglu T, Macario R. Fuel cell vehicles: state of the art with economic and environmental concerns. *Int J Hydrogen Energy* 2011;36:25–43.
- [7] Ibrahim H, Ilincă A, Perron J. Energy storage systems – characteristics and comparisons. *Renew Sustain Energy Rev* 2008;12:1221–50.
- [8] Rand DAJ. A journey on the electrochemical road to sustainability. *J Solid State Electrochem* 2011;15:1579–622.
- [9] Fabbri E, Habereeder A, Waltar K, Kötz R, Schmidt TJ. Developments and perspectives of oxide-based catalysts for the oxygen evolution reaction. *Catal Sci Technol* 2014;4:3800–21.
- [10] Cipriani G, Di Dio V, Genduso F, La Cascia D, Liga R, Miceli R, et al. Perspective on hydrogen energy carrier and its automotive applications. *Int J Hydrogen Energy* 2014;39:8482–94.
- [11] Fayaz H, Saidur R, Razali N, Anuar FS, Saleman AR, Islam MR. An overview of hydrogen as a vehicle fuel. *Renew Sustain Energy Rev* 2012;16:5511–28.
- [12] Hua T, Ahluwalia R, Eudy L, Singer G, Jermer B, Asselin-Miller N, et al. Status of hydrogen fuel cell electric buses worldwide. *J Power Sources* 2014;269:975–93.
- [13] van de Loosdrecht J, Niemantsverdriet JW. Synthesis gas to hydrogen, methanol and synthetic fuels. In: Schoegl R, editor. *Chemical energy storage*. Berlin: De Gruyter; 2013. p. 443–57.
- [14] Rostrup-Nielsen J, Christiansen LJ. Concepts in syngas preparation. *Catalytic science series*. London: Imperial College Press; 2011.
- [15] Balat M, Balat M. Political, economic and environmental impacts of biomass-based hydrogen. *Int J Hydrogen Energy* 2009;34:3589–603.
- [16] Holladay JD, Hu J, King DL, Wang Y. An overview of hydrogen production technologies. *Catal Today* 2009;139:244–60.
- [17] Barbir F. PEM electrolysis for production of hydrogen from renewable energy sources. *Sol Energy* 2005;78:661–9.
- [18] Kato T, Kubota M, Kobayashi N, Suzuki Y. Effective utilization of by-product oxygen from electrolysis hydrogen production. *Energy* 2005;30:2580–95.
- [19] Zeng K, Zhang D. Recent progress in alkaline water electrolysis for hydrogen production and applications. *Prog Energy Combust Sci* 2010;36:307–26.
- [20] Carmo M, Fritz DL, Mergel J, Stolten D. A comprehensive review on PEM water electrolysis. *Int J Hydrogen Energy* 2013;38:4901–34.
- [21] Aricò AS, Siracusano S, Briguglio N, Baglio V, Di Blasi A, Antonucci V. Polymer electrolyte membrane water electrolysis: status of technologies and potential applications in combination with renewable power sources. *J Appl Electrochem* 2013;43:107–18.
- [22] Hauch A, Ebbesen SD, Jensen SH, Mogensen M. Highly efficient high temperature electrolysis. *J Mater Chem* 2008;18:2331–40.
- [23] Ni M, Leung MKH, Leung DYC. Technological development of hydrogen production by solid oxide electrolyzer cell (SOEC). *Int J Hydrogen Energy* 2008;33:2337–54.
- [24] Laguna-Bercero MA. Recent advances in high temperature electrolysis using solid oxide fuel cells: a review. *J Power Sources* 2012;203:4–16.
- [25] Bi L, Boulfrad S, Traversa E. Steam electrolysis by solid oxide electrolysis cells (SOECs) with proton-conducting oxides. *Chem Soc Rev* 2014;43:8255–70.
- [26] Grigoriev SA, Kuleshov NV, Grigoriev AS, Millet P. Electrochemical characterization of high-temperature proton exchange membrane fuel cell using doped-poly benzimidazole as solid polymer electrolyte. *J Fuel Cell Sci Technol* 2015;12:31004–8.
- [27] Morfopoulou CI, Andreopoulou AK, Daletou MK, Neophytides SG, Kallitsis JK. Cross-linked high temperature polymer electrolytes through oxadiazole bond formation and their applications in HT PEM fuel cells. *J Mater Chem A Mater Energy Sustain* 2013;1:1613–22.
- [28] Papadimitriou KD, Georghiou M, Neophytides SG, Kallitsis JK. Covalent cross-linking in phosphoric acid of pyridine based aromatic polyethers bearing side double bonds for use in high temperature polymer electrolyte membrane fuel cells. *J Membr Sci* 2013;433:1–9.
- [29] Todd D, Schwager M, Merida W. Thermodynamics of high-temperature, high-pressure water electrolysis. *J Power Sources* 2014;269:424–9.
- [30] Ganley JC. High temperature and pressure alkaline electrolysis. *Int J Hydrogen Energy* 2009;34:3604–11.
- [31] Parrondo J, Arges CG, Niedzwiecki N, Anderson EB, Ayers KE, Ramani V. Degradation of anion exchange membranes used for hydrogen production by ultrapure water electrolysis. *RSC Adv* 2014;4:9875–9.
- [32] Ebbesen SD, Jensen SH, Hauch A, Mogensen MB. High temperature electrolysis in alkaline cells, solid proton conducting cells and solid oxide cells. *Chem Rev* 2014;114:10697–734.
- [33] Udagawa J, Aquiar P, Brandon NP. Hydrogen production through steam electrolysis: model-based steady state performance of a cathode-supported intermediate temperature solid oxide electrolysis cell. *J Power Sources* 2007;166:127–36.
- [34] Kim SW, Kim H, Yoon KJ, Lee JH, Kim BK, Choi W, et al. Reactions and mass transport in high temperature co-electrolysis of steam/CO<sub>2</sub> mixtures for syngas production. *J Power Sources* 2015;280:630–9.
- [35] Xing R, Wang Y, Zhu Y, Liu S, Jin C. Co-electrolysis of steam and CO<sub>2</sub> in a solid oxide electrolysis cell with La<sub>0.75</sub>Sr<sub>0.25</sub>Cr<sub>0.25</sub>Mn<sub>0.5</sub>O<sub>3-δ</sub>-Cu ceramic composite electrode. *J Power Sources* 2015;274:260–4.
- [36] Tao Y, Ebbesen SD, Mogensen MB. Carbon deposition in solid oxide cells during co-electrolysis of H<sub>2</sub>O and CO<sub>2</sub>. *J Electrochem Soc* 2014;161:F337–43.
- [37] Yoon SE, Song SH, Choi J, Ahn JY, Kim BK, Park JS. Co-electrolysis of steam and CO<sub>2</sub> in a solid oxide electrolysis cell with ceramic composite electrodes. *Int J Hydrogen Energy* 2014;39:5497–504.
- [38] Xu J, Yang Y, Li YW. Fischer-Tropsch synthesis process development: steps from fundamentals to industrial practices. *Curr Opin Chem Eng* 2013;2:354–62.
- [39] Pan J, Chen C, Li Y, Wang L, Tan L, Li G, et al. Constructing ionic highway in alkaline polymer electrolytes. *Energy Environ Sci* 2014;4:354–60.
- [40] Varcoe JR, Atanassov P, Dekel DR, Herring AM, Hickner MA, Kohl PA, et al. Anion-exchange membranes in electrochemical energy systems. *Energy Environ Sci* 2014;7:3135–91.
- [41] Sharma VI, Yildiz B. Degradation mechanism in La<sub>0.8</sub>Sr<sub>0.2</sub>CoO<sub>3</sub> as contact layer on the solid oxide electrolysis anode. *J Electrochem Soc* 2010;157:B441–8.
- [42] Mawdsley JR, Carter JD, Kropf AJ, Yildiz B, Maroni VA. Post-test evaluation of oxygen electrodes from solid oxide electrolysis stacks. *Int J Hydrogen Energy* 2009;34:4198–207.
- [43] Sohal MS, O'Brien JE, Stoops CM, Sharma VI, Yildiz B, Virkar A. Degradation issues in solid oxide cells during high temperature electrolysis. *J Fuel Cell Sci Technol* 2011;9:11017.
- [44] Thomsen JM, Huang DL, Crabtree RH, Brudvig GW. Iridium-based complexes for water oxidation. *Dalton Trans* 2015;44:12452–72.
- [45] Joya KS, Subbaiyan NK, Souza FD, de Groot HJM. Surface-immobilized single-site iridium complexes for electrocatalytic water splitting. *Angew Chem Int Ed Engl* 2012;124:9739–43.
- [46] Fillol JL, Codolà Z, Garcia-Bosch I, Gómez L, Pla JJ, Costas M. Efficient water oxidation catalysts based on readily available iron coordination complexes. *Nat Chem* 2011;3:807–13.

- [47] Barnett SL, Goldberg KI, Mayer JM. A soluble copper-bipyridine water oxidation electrocatalyst. *Nat Chem* 2012;4:498–502.
- [48] Thomsen JM, Sheehan SW, Hashmi SM, Campos J, Hintermair U, Crabtree RH, et al. Electrochemical activation of  $Cp^*$  iridium complexes for electrode-driven water-oxidation catalysis. *J Am Chem Soc* 2014;136:13826–34.
- [49] Dau H, Limberg C, Reier T, Risch M, Roggan S, Strasser P. The mechanism of water oxidation: from electrolysis via homogeneous to biological catalysts. *ChemCatChem* 2010;2:724–61.
- [50] Hall DE. Electrodes for alkaline water electrolysis. *J Electrochim Soc* 1981;128:740–6.
- [51] Juodkazis K, Juodkazyte J, Vilkauskaitė R, Jasulaitiene V. Nickel surface anodic oxidation and electrocatalysis of oxygen evolution. *J Solid State Electroch* 2008;12:1469–79.
- [52] Lyons MEG, Brandon M. The oxygen evolution reaction on passive oxide covered transition metal electrodes in aqueous alkaline solution: part 1 – Nickel. *Int J Electroch* 2008;3:1386–424.
- [53] Kibria MF, Mridha MS. Electrochemical studies of the nickel electrode for the oxygen evolution reaction. *Int J Hydrogen Energy* 1996;21:179–82.
- [54] Bode H, Dehmelt K, Witte J. Zur Kenntnis der Nickelhydroxidelektrode – Über das Nickel (II)-hydroxidhydrat. *Electrochim Acta* 1966;11:1079–87.
- [55] Godwin IJ, Lyons MEG. Enhanced oxygen evolution at hydrous nickel oxide electrodes via electrochemical ageing in alkaline solution. *Electrochim Commun* 2013;32:39–42.
- [56] Lyons MEG, Brandon M. A comparative study of the oxygen evolution reaction on oxidized nickel, cobalt and iron electrodes in base. *J Electroanal Chem* 2010;641:119–30.
- [57] Andersen NI, Serov A, Atanassov P. Metal oxides/CNT nano-composite catalysts for oxygen reduction/oxygen evolution in alkaline media. *Appl Catal B* 2015;163:623–7.
- [58] Seetharaman S, Balaji R, Ramya K, Dhathathreyan KS, Velan M. Electrochemical behavior of nickel-based electrodes for oxygen evolution reaction in alkaline water electrolysis. *Ionics* 2014;20:713–20.
- [59] Perez-Alonso FJ, Adan C, Rojas S, Pena MA, Fierro JLG. Ni/Fe electrodes prepared electrodeposition method over different substrates for oxygen evolution reaction in alkaline medium. *Int J Hydrogen Energy* 2014;39:5204–12.
- [60] Qiu Y, Xin L, Li W. Electrocatalytic oxygen evolution over supported small amorphous Ni-Fe nanoparticles in alkaline electrolyte. *Langmuir* 2014;30:7893–901.
- [61] Li X, Walsh FC. Nickel based electrocatalysts for oxygen evolution in high current density, alkaline water electrolyzers. *Phys Chem Chem Phys* 2011;13:1162–7.
- [62] Trześniewski BJ, Diaz-Morales O, Vermaas DA, Longo A, Bras W, Koper MTM, et al. In situ observation of active oxygen species in Fe-containing Ni-based oxygen evolution catalysts: the effect of pH on electrochemical activity. *J Am Chem Soc* 2015;137:15112–21.
- [63] Zhang Y, Cao X, Yuan H, Zhang W, Zhou Z. Oxygen evolution reaction on Ni hydroxide film electrode containing various content of Co. *Int J Hydrogen Energy* 1999;24:529–36.
- [64] Wang X, Luo H, Yang H, Sebastian PJ, Gamboa SA. Oxygen catalytic evolution reaction on nickel hydroxide electrode modified by electroless cobalt coating. *Int J Hydrogen Energy* 2004;29:967–72.
- [65] Chi B, Li J, Yang J, Gong Y, Wang N. Deposition of Ni-Co by cyclic voltammetry method and its electrocatalytic properties for oxygen evolution reaction. *Int J Hydrogen Energy* 2005;30:29–34.
- [66] Plata-Torres M, Torres-Huerta AM, Domínguez-Crespo MA, Arce-Estrada EM, Ramírez-Rodríguez C. Electrochemical performance of crystalline Ni-Co-Mo-Fe electrodes obtained by mechanical alloying on the oxygen evolution reaction. *Int J Hydrogen Energy* 2007;32:4142–52.
- [67] Sadiq IM, Mohammad AM, El-Sharke ME, El-Deab MS, El-Anadouli BE. Enhanced electrolytic generation of oxygen gas at binary nickel oxide–cobalt oxide nanoparticle-modified electrodes. *J Solid State Electroch* 2013;17:871–9.
- [68] Tseung ACC, Jasem S. Oxygen evolution on semiconducting oxides. *Electrochim Acta* 1977;22:31–4.
- [69] Wu G, Li N, Zhou DR, Mitsuo K, Xu BQ. Anodically electrodeposited Co + Ni mixed oxide electrode: preparation and electrocatalytic activity for oxygen evolution in alkaline media. *J Solid State Chem* 2004;177:3682–92.
- [70] Bocca C, Barbucci A, Delucchi M, Cerisola G. Nickel-cobalt oxide-coated electrodes: influence of the preparation technique on oxygen evolution reaction (OER) in an alkaline solution. *Int J Hydrogen Energy* 1999;24:21–6.
- [71] Chi B, Lin H, Li J, Wang N, Yang J. Comparison of three preparation methods of  $NiCo_2O_4$  electrodes. *Int J Hydrogen Energy* 2006;31:1210–14.
- [72] Singh RN, Hamdani M, Koenig JF, Poillerat G, Gautier JL, Chartier P. Thin films of  $Co_3O_4$  and  $NiCo_2O_4$  obtained by the method of chemical spray pyrolysis for electrocatalysis. III. The electrocatalysis of oxygen evolution. *J Appl Electroch* 1990;20:442–6.
- [73] Liu YC, Koza JA, Switzer JA. Conversion of electrodeposited  $Co(OH)_2$  to  $CoOOH$  and  $Co_3O_4$  and comparison of their catalytic activity for the oxygen evolution reaction. *Electrochim Acta* 2014;140:359–65.
- [74] Liu X, Chang Z, Luo L, Xu T, Lei X, Liu J, et al. Hierarchical  $Zn_xCo_{3-x}O_4$  nanoarrays with high activity for electrocatalytic oxygen evolution. *Chem Mater* 2014;26:1889–95.
- [75] Grewe T, Dang X, Weidenthaler C, Schuth F, Tuysuz H. Design of ordered mesoporous composite materials and their electrocatalytic activities for water oxidation. *Chem Mater* 2013;25:4926–35.
- [76] Bikkarolla SK, Papakonstantinou P.  $CuCo_2O_4$  nanoparticles on nitrogenated graphene as highly efficient oxygen evolution catalyst. *J Power Sources* 2015;281:243–51.
- [77] Wu X, Scott K. *J Mater Chem* 2011;21:12344–51.
- [78] Grawe T, Deng X, Tuysuz H. Influence of Fe doping on structure and water oxidation activity of nanocast  $Co_3O_4$ . *Chem Mater* 2014;26:3162–8.
- [79] Ma TY, Dai S, Jaroniec M, Qiao SZ. Synthesis of highly active and stable spinel-type oxygen evolution electrocatalysts by a rapid inorganic self-template method. *Chem Eur J* 2014;20:12669–76.
- [80] Chanda D, Hnat J, Paidar M, Bouzek K. Evolution of physicochemical and electrocatalytic properties of  $NiCo_2O_4$  ( $AB_2O_4$ ) spinel oxide with the effect of Fe substitution at the A site leading to efficient anodic  $O_2$  evolution in an alkaline environment. *Int J Hydrogen Energy* 2014;39:5713–22.
- [81] Tan Y, Wu C, Li H, Li J, Chi B, Pu J, et al. Insight the effect of surface Co cations on the electrocatalytic oxygen evolution properties of cobaltite spinels. *Electrochim Acta* 2014;121:183–7.
- [82] Srirapu VKVP, Sharma CS, Awasthi R, Singh RN, Sinha ASK. Copper-iron-molybdenum mixed oxides as efficient oxygen evolution electrocatalysts. *Phys Chem Chem Phys* 2014;16:7385–93.
- [83] Singh RN, Singh JP, Singh A. Electrocatalytic properties of new spinel-type  $MMoO_4$  ( $M = Fe, Co$  and  $Ni$ ) electrodes for oxygen evolution in alkaline solutions. *Int J Hydrogen Energy* 2008;33:4260–4.
- [84] Singh RN, Madhu, Awasthi R, Sinha ASK. Preparation and electrochemical characterization of a new  $NiMoO_4$  catalyst for electrochemical  $O_2$  evolution. *J Solid State Electroch* 2009;13:1613–19.
- [85] Singh RN, Awasthi R, Sinha ASK. Electrochemical characterization of a new binary oxide of Mo with Co for  $O_2$  evolution in alkaline solution. *Electrochim Acta* 2009;54:3020–5.
- [86] Srirapu VKVP, Kumar M, Awasthi R, Singh RN, Sinha AS. Manganese molybdate and its Fe-substituted products as new efficient electrocatalysts for oxygen evolution in alkaline solutions. *Int J Hydrogen Energy* 2013;38:13587–95.
- [87] Singh RN, Madhu, Awasthi R, Tiwari SK. Iron molybdates as electrocatalysts for  $O_2$  evolution reaction in alkaline solutions. *Int J Hydrogen Energy* 2009;34:4693–700.
- [88] Singh RN, Kumar M, Sinha AS. Novel  $Fe_xCr_{2-x}(MoO_4)_3$  electrocatalysts for oxygen evolution reaction. *Int J Hydrogen Energy* 2012;37:15117–24.
- [89] Kumar M, Awasthi R, Sinha ASK, Singh RN. New ternary Fe, Co and Mo mixed oxide electrocatalysts for oxygen evolution. *Int J Hydrogen Energy* 2011;36:8831–8.
- [90] Kumar M, Awasthi R, Pramanick AK, Singh RN. New ternary mixed oxides of Fe, Co and Mo for enhanced oxygen evolution. *Int J Hydrogen Energy* 2011;36:12698–705.
- [91] Ramírez A, Hillebrand P, Stellmach D, May MM, Bogdanoff P, Fiechter S. Evaluation of  $MnO_x$ ,  $Mn_2O_3$  and  $Mn_3O_4$  electrodeposited films for the oxygen evolution reaction of water. *J Phys Chem C* 2014;118:14073–81.
- [92] Diaz-Morales O, Ledezma-Yanez I, Koper MTM, Calle-Vallejo F. Guidelines for the rational design of Ni-based double hydroxide electrocatalysts for the oxygen evolution reaction. *ACS Catal* 2015;5:5380–7.
- [93] MacCrory CCL, Jung S, Peters J, Jaramillo TF. Benchmarking heterogeneous electrocatalysts for the oxygen evolution reaction. *J Am Chem Soc* 2013;135:16977–87.
- [94] Tanaka H, Misra M. Advances in designing perovskite catalysts. *Curr Opin Solid State Mater Sci* 2001;5:381–7.
- [95] Zhu J, Li H, Zhong L, Xiao P, Xu X, Yang X, et al. Perovskite oxides: preparation, characterizations and applications in heterogeneous catalysis. *ACS Catal* 2014;4:2917–40.
- [96] Pena MA, Fierro JLG. Chemical structures and performance of perovskite oxides. *Chem Rev* 2011;101:1981–2017.
- [97] Royer S, Duprez D, Can F, Courtois X, Batiot-Dupeyrat C, Laassiri S, et al. Perovskites as substitutes of noble metals for heterogeneous catalysis: dream or reality. *Chem Rev* 2014;114:10292–368.
- [98] Ishihara T, editor. *Perovskite oxide for solid oxide fuel cells (fuel cells and hydrogen energy)*. New York: Springer Science and Business Media; 2009.
- [99] Zhang HM, Shimizu Y, Miura N, Yamazoe N. Oxygen sorption and catalytic properties of  $La_{1-x}Sr_xCo_{1-y}Fe_yO_3$  perovskite-type oxides. *J Catal* 1990;121:432–40.
- [100] Zhang S, Huang K, Huang C, Huang H, Liu S, Fan M. Preparation of silver-modified  $La_{0.6}Ca_{0.4}CoO_3$  binary electrocatalyst for bi-functional air electrodes in alkaline medium. *J Power Sources* 2011;196:4019–25.
- [101] Wang ZL, Xu D, Xu JJ, Zhang XB. Oxygen electrocatalysts in metal-air batteries: from aqueous to nonaqueous electrolytes. *Chem Soc Rev* 2014;43:7746–86.
- [102] Bockris JOM, Otagawa T. The electrocatalysis of oxygen evolution on perovskites. *J Electrochim Soc* 1984;131:290–302.
- [103] Seo MH, Park HW, Lee DU, Park MG, Chen Z. Design of highly active perovskite oxides for oxygen evolution reaction by combining experimental and ab initio studies. *ACS Catal* 2015;5:4337–44.
- [104] Oh MY, Jeon JS, Lee JJ, Kim P, Nahm KS. The bifunctional catalytic activity of perovskite  $La_{0.6}Sr_{0.4}CoO_3-\delta$  for oxygen reduction and evolution reactions. *RSC Adv* 2015;5:19190–8.
- [105] Miyahara Y, Miyazaki K, Fukutsuka T, Abe T. Catalytic roles of perovskite oxides in electrochemical oxygen reactions in alkaline media. *J Electrochim Soc* 2014;161:F694–7.
- [106] Okhuma H, Uechi I, Imanishi N, Hirano A, Takeda Y, Yamamoto O. Carbon electrode with perovskite-oxide catalyst for aqueous electrolyte lithium-air secondary batteries. *J Power Sources* 2013;223:319–24.

- [107] Malkhandi S, Yang B, Manohar AK, Manivannan A, Surya Prakash GK, Narayanan SR. Electrocatalytic properties of nanocrystalline calcium-doped lanthanum cobalt oxide for bifunctional oxygen electrodes. *J Phys Chem Lett* 2012;3:967–72.
- [108] Chang YM, Wu PW, Wu CY, Hsieh YC. Synthesis of  $\text{La}_{0.6}\text{Ca}_{0.4}\text{Co}_{0.8}\text{Ir}_{0.2}\text{O}_3$  perovskite for bi-functional catalysis in an alkaline electrolyte. *J Power Sources* 2009;189:1003–7.
- [109] Bursell M, Pirjamali M, Kiros Y.  $\text{La}_{0.6}\text{Ca}_{0.4}\text{CoO}_3$ ,  $\text{La}_{0.1}\text{Ca}_{0.9}\text{MnO}_3$  and  $\text{LaNiO}_3$  as bifunctional oxygen electrodes. *Electrochim Acta* 2002;47:1651–60.
- [110] Rincón RA, Ventosa E, Tietz F, Masa J, Seisel S, Kuznetsov V, et al. Evaluation of perovskites as electrocatalysts for the oxygen evolution reaction. *ChemPhysChem* 2014;15:2810–16.
- [111] Matsumoto Y, Yamada S, Nishida T, Sato E. Oxygen evolution on  $\text{La}_{1-x}\text{Sr}_x\text{Fe}_{1-y}\text{CoO}_3$  series oxides. *J Electrochem Soc* 1980;127:2360–4.
- [112] Matsumoto Y, Sato E. Oxygen evolution on  $\text{La}_{1-x}\text{Sr}_x\text{MnO}_3$  electrodes in alkaline solutions. *Electrochim Acta* 1979;24:421–3.
- [113] Trasatti S. Electrocatalysis in the anodic evolution of oxygen and chlorine. *Electrochim Acta* 1984;29:1503–12.
- [114] Mai IC, Su HY, Calle-Vallejo F, Hansen HA, Martinez JL, Inoglu NG, et al. Universality in oxygen evolution electrocatalysis on oxide surfaces. *ChemCatChem* 2011;3:1159–65.
- [115] Suntivich J, May KJ, Gasteiger HA, Goodenough JB, Shao-Horn Y. A perovskite oxide optimized for oxygen evolution catalysis from molecular orbital principles. *Science* 2011;334:1383–5.
- [116] Zundhal DS, DeCoste DJ. Chemical principles. 7th ed. Belmont: Brooks/Cole; 2013.
- [117] Jin K, Ge C, Lu H, Yang G. Research on the photoelectric effect in perovskite oxide heterostructures. In: Chen L, Dai N, Jiang X, Jin K, Liu H, Zhao H, editors. Advances in condensed matter optics. Leck: CPI Books GmbH; 2015. p. 191–230.
- [118] Vojvodic A, Nørskov JK. Optimizing perovskites for the water-splitting reaction. *Science* 2011;334:1355–6.
- [119] Lopez K, Park G, Sun HJ, An JC, Eom S, Shim J. Electrochemical characterizations of  $\text{LaMO}_3$  ( $M = \text{Co, Mn, Fe and Ni}$ ) and partially substituted  $\text{LaNi}_x\text{M}_{1-x}\text{O}_3$  ( $x = 0.25$  or  $0.5$ ) for oxygen reduction and evolution in alkaline solution. *J Appl Electrochem* 2015;45:313–23.
- [120] Kremenić G, Nieto JML, Tascón JMD, Tejeda LG. Chemisorption and catalysis on  $\text{LaMO}_3$  oxides. *J Chem Soc Faraday Trans 1* 1985;81:939–49.
- [121] Goodenough JB. Covalency criterion for localized vs collective electrons in oxides with the perovskite structure. *J Appl Phys* 1966;37:1415–22.
- [122] Risch M, Grimaud A, May KJ, Stoerzinger KA, Chen TJ, Mansour AN, et al. Structural changes of cobalt-based perovskites upon water oxidation investigated by EXAFS. *J Phys Chem C* 2013;117:8628–35.
- [123] May KJ, Carlton CE, Stoerzinger KA, Risch M, Suntivich J, Lee YL, et al. Influence of oxygen evolution during water oxidation on the surface of perovskite oxide catalysts. *J Phys Chem Lett* 2012;3:3264–70.
- [124] Grimaud A, May KJ, Carlton CE, Lee YL, Risch M, Hong WT, et al. Double perovskites as a family of highly active catalysts for oxygen evolution in alkaline solution. *Nat Commun* 2013;4:2439.
- [125] Zhu Y, Zhou W, Chen ZG, Chen Y, Su C, Tade MO, et al.  $\text{SrNb}_{0.1}\text{Co}_{0.7}\text{Fe}_{0.2}\text{O}_{3-\delta}$  as a next-generation electrocatalyst for oxygen evolution in alkaline solution. *Angew Chem Int Ed Engl* 2015;54:3897–901.
- [126] Gracia J, Escuin M, Mallada R, Navascués N, Santamaría J. Nano-heaters: new insights on the outstanding deposition of dielectric energy on perovskite nanoparticles. *Nano Energy* 2016;20:20–8.
- [127] Lim T, Niemantsverdriet JW, Gracia J. Layered antiferromagnetic ordering in the most active perovskite catalysts for oxygen evolution reaction. *ChemCatChem* 2016;doi:10.1002/cctc.201600611R1.
- [128] Kim J, Yin X, Tsao KC, Fang S, Yang H.  $\text{Ca}_2\text{Mn}_2\text{O}_5$  as oxygen-deficient perovskite electrocatalyst for oxygen evolution reaction. *J Am Chem Soc* 2014;136:14646–9.
- [129] Mohamed R, Cheng X, Fabbri E, Leveque P, Kötz R, Conrad O, et al. Electrocatalysis of perovskites: the influence of carbon on the oxygen evolution activity. *J Electrochem Soc* 2015;162:F579–86.
- [130] Nishio K, Molla S, Okugaki T, Nakanishi S, Nitta I, Kotani Y. Oxygen reduction and evolution reactions of air electrodes using a perovskite oxide as an electrocatalyst. *J Power Sources* 2015;278:645–51.
- [131] Ahn SH, Choi I, Park HY, Hwang SJ, Yoo SJ, Cho E, et al. Effect of morphology of electrodeposited Ni catalysts on the behavior of bubbles generated during the oxygen evolution reaction in alkaline water electrolysis. *Chem Commun* 2013;49:9323–5.
- [132] Jiang J, Zhang A, Li L, Ai L. Nickel-cobalt layered double hydroxide nanosheets as high-performance electrocatalyst for oxygen evolution reaction. *J Power Sources* 2015;278:445–51.
- [133] Wang HY, Hsu YY, Chen R, Chan TS, Chen HM, Liu B. Oxygen evolution reaction:  $\text{Ni}^{3+}$ -induced formation of active  $\text{NiOOH}$  on the spinel  $\text{Ni-Co}$  oxide surface for efficient oxygen evolution reaction. *Adv Energy Mater* 2015;5:1500091–9.
- [134] Lu X, Liu J, Li Y, Li Y, Sun X.  $\text{Au}/\text{NiCo}_2\text{O}_4$  arrays with high activity for water oxidation. *ChemCatChem* 2014;6:2501–6.
- [135] Cui B, Lin H, Li JB, Li X, Yang J, Tao J. Core-ring structured  $\text{NiCo}_2\text{O}_4$  nanoplatelets: synthesis, characterization and electrocatalytic applications. *Adv Funct Mater* 2008;18:1440–7.
- [136] Cheng Y, Tian Y, Fan X, Liu J, Yan C. Boron doped multi-walled carbon nanotubes as catalysts for oxygen reduction reaction and oxygen evolution reaction in alkaline media. *Electrochim Acta* 2014;143:291–6.
- [137] Raoof JB, Chekin F, Ehsani V. Cobalt oxide nanoparticle-modified carbon nanotubes as an electrocatalyst for electrocatalytic evolution of oxygen gas. *Bull Mater Sci* 2015;38:135–40.
- [138] Zhan Y, Xu C, Lu M, Liu Z, Lee JY. Mn and Co co-substituted  $\text{Fe}_3\text{O}_4$  nanoparticles on nitrogen-doped reduced graphene oxide for oxygen electrocatalysis in alkaline solution. *J Mater Chem A Mater Energy Sustain* 2014;2:16217–23.
- [139] Cheng Y, Liu C, Cheng HM, Jiang SP. One pot synthesis of metal-carbon nanotubes network hybrids as highly efficient catalysts for oxygen evolution reaction of water splitting. *ACS Appl Mater Interfaces* 2014;6:10089–98.
- [140] Su Y, Zhu Y, Jiang H, Shen J, Yang X, Zou W, et al. Cobalt nanoparticles embedded in N-doped carbon as an efficient bifunctional electrocatalyst for oxygen reduction and evolution reactions. *Nanoscale* 2014;6:15080–9.
- [141] Chekin F, Tahermansouri H, Besharat MR. Nickel oxide nanoparticles prepared by gelatin and their application toward the oxygen evolution reaction. *J Solid State Electrochem* 2014;18:747–53.
- [142] Ma TY, Dai S, Jaroniec M, Qiao SZ. Metal-organic framework derived hybrid  $\text{Co}_3\text{O}_4$ -carbon porous nanowire arrays as reversible oxygen evolution electrodes. *J Am Chem Soc* 2014;136:13925–31.
- [143] Zhang X, Xiao Q, Zhang Y, Jiang X, Yang Z, Xue Y, et al.  $\text{La}_2\text{O}_3$  doped carbonaceous microspheres: a novel bifunctional electrocatalyst for oxygen reduction and evolution reactions with ultrahigh mass activity. *J Phys Chem C* 2014;118:20229–37.
- [144] Wang H, Li Z, Li G, Peng F, Yu H.  $\text{Co}_3\text{S}_4/\text{NCNTs}$ : a catalyst for oxygen evolution reaction. *Catal Today* 2015;245:74–8.
- [145] Zhang Y, Xiao Q, Guo X, Zhang X, Xue Y, Jing L, et al. A novel electrocatalyst for oxygen evolution reaction based on rational anchoring of cobalt carbonate hydroxide hydrate on multiwall carbon nanotubes. *J Power Sources* 2015;278:464–72.
- [146] Yu X, Xu P, Hua T, Han A, Liu X, Wu H, et al. Multiwalled carbon nanotubes supported porous nickel oxide as noble metal-free electrocatalysts for efficient water oxidation. *Int J Hydrogen Energy* 2014;39:10467–75.
- [147] Gao M, Sheng W, Zhuang Z, Fang Q, Gu S, Jiang J, et al. Efficient water oxidation using nanostructured  $\alpha$ -nickel-hydroxide as an electrocatalyst. *J Am Chem Soc* 2014;136:7077–84.
- [148] Yin F, Li G, Wang H. Hydrothermal synthesis of  $\alpha\text{-MnO}_2/\text{MIL}-101(\text{Cr})$  composite and its bifunctional electrocatalytic activity for oxygen reduction/evolution reactions. *Catal Commun* 2014;54:17–21.
- [149] Selvakumar K, Senthil Kumar SM, Thangamuthu R, Kruthika G, Murugan P. Development of shape engineered  $\alpha\text{-MnO}_2$  materials as bi-functional catalysts for oxygen evolution reaction and oxygen reduction reaction in alkaline medium. *Int J Hydrogen Energy* 2014;39:21024–36.
- [150] Wang H, Yin F, Li G, Chen B, Wang Z. Preparation, characterization and bifunctional catalytic properties of MOF (Fe/Co) catalyst for oxygen reduction/evolution reactions in alkaline electrolyte. *Int J Hydrogen Energy* 2014;39:16179–86.
- [151] Du J, Zhang T, Cheng F, Chu W, Wu Z, Chen J. Nonstoichiometric perovskite  $\text{CaMnO}_{3-\delta}$  for oxygen evolution electrocatalysis with high activity. *Inorg Chem* 2014;53:9106–14.
- [152] Liang F, Yum Y, Zhou W, Xu X, Zhu Z. Highly defective  $\text{CeO}_2$  as a promoter for efficient and stable water oxidation. *J Mater Chem A Mater Energy Sustain* 2015;3:634–40.
- [153] Damjanovic A, Dey A, Bockris JOM. Electrode kinetics of oxygen evolution and dissolution on Rh, Ir and Pt-Rh alloy electrodes. *J Electrochem Soc* 1966;113:739–46.
- [154] Miles MH, Thomason MA. Periodic variations of overvoltages for water electrolysis in acid solutions from cyclic voltammetric studies. *J Electrochem Soc* 1976;123:1459–61.
- [155] Park S, Shao Y, Liu J, Wang Y. Oxygen electrocatalysts for water electrolyzers and reversible fuel cells: status and perspective. *Energy Environ Sci* 2012;5:9331–44.
- [156] Miles MH, Klaus EA, Gunn BP, Locker JR, Serafin WE. The oxygen evolution reaction on platinum, iridium, ruthenium and their alloys at 80°C in acid solutions. *Electrochim Acta* 1978;23:521–6.
- [157] Trasatti S, Buzzanca G. Ruthenium dioxide: a new interesting electrode material. Solid state structure and electrochemical behaviour. *J Electroanal Chem* 1971;29:A1–5.
- [158] Kötz R, Lewerenz HJ, Stucki S. XPS studies of oxygen evolution on Ru and  $\text{RuO}_2$  anodes. *J Electrochem Soc* 1983;130:825–9.
- [159] Trasatti S. Electrocatalysis: understanding the success of DSA. *Electrochim Acta* 2000;45:2377–85.
- [160] Hackwood S, Schiavone LM, Dautremont-Smith WC, Beni G. Anodic evolution of oxygen on sputtered iridium oxide films. *J Electrochem Soc* 1981;128:2569–73.
- [161] Slavcheva E, Radev I, Bliznakov S, Topalov G, Andreev P, Budevski E. Sputtered iridium oxide films as electrocatalysts for water splitting via PEM electrolysis. *Electrochim Acta* 2007;52:3889–94.
- [162] Kötz R, Stucki S. Stabilization of  $\text{RuO}_2$  by  $\text{IrO}_2$  for anodic oxygen evolution in acid media. *Electrochim Acta* 1986;31:1311–16.
- [163] Cheng J, Zhang H, Chen G, Zhang Y. Study of  $\text{Ir}_x\text{Ru}_{1-x}\text{O}_2$  oxides as anodic electrocatalysts for solid polymer electrolyte water electrolysis. *Electrochim Acta* 2009;54:6250–6.
- [164] Mamaca N, Mayousse E, Arrii-Clacens S, Napporn TW, Servat K, Guillet N, et al. Electrochemical activity of ruthenium and iridium based catalysts for oxygen evolution reaction. *Appl Catal B* 2012;111–112:376–80.

- [165] Marshall AT, Sunde S, Typpkin M, Tunold R. Performance of a PEM water electrolysis cell using  $\text{Ir}_x\text{Ru}_y\text{Ta}_z\text{O}_2$  electrocatalysts for the oxygen evolution electrode. *Int J Hydrogen Energy* 2007;32:2320–4.
- [166] Siracusano S, van Dijk N, Payne-Johnson E, Baglio V, Arico AS. Nanosized  $\text{IrO}_x$  and  $\text{IrRuO}_x$  electrocatalysts for the  $\text{O}_2$  evolution reaction in PEM water electrolyzers. *Appl Catal B* 2015;164:488–95.
- [167] Corona-Guinto JL, Gardeno-Garcia L, Martinez-Casillas DC, Sandoval-Pineda JM, Tamayo-Meza P, Silva-Casarín R, et al. Performance of a PEM electrolyzer using RuIrCo<sub>x</sub> electrocatalysts for the oxygen evolution electrode. *Int J Hydrogen Energy* 2013;38:12667–73.
- [168] Gonzalez-Huerta RG, Ramos-Sánchez G, Balbuena PB. Oxygen evolution in Co-doped  $\text{RuO}_2$  and  $\text{IrO}_2$ : experimental and theoretical insights to diminish electrolysis overpotential. *J Power Sources* 2014;268:69–76.
- [169] Marshall AT, Haverkamp RG. Electrocatalytic activity of  $\text{IrO}_2\text{-RuO}_2$  supported on Sb-doped  $\text{SnO}_2$  nanoparticles. *Electrochim Acta* 2010;55:1978–84.
- [170] Hutchings R, Müller K, Kötz R, Stucki S. A structural investigation of stabilized oxygen evolution catalysts. *J Mater Sci* 1984;19:3987–94.
- [171] Kadakia K, Datta MK, Velikokhatnyi Ol, Jampani P, Park SK, Chung SJ, et al. High performance fluorine doped (Sn, Ru)O<sub>2</sub> oxygen evolution reaction electro-catalysts for proton exchange membrane based water electrolysis. *J Power Sources* 2014;245:362–70.
- [172] Puthiyapura VK, Pasupathi S, Basu S, Wu X, Su H, Varagunapandian N, et al.  $\text{Ru}_x\text{Nb}_{1-x}\text{O}_2$  catalysts for the oxygen evolution reaction in proton exchange membrane water electrolyzers. *Int J Hydrogen Energy* 2013;38:8605–16.
- [173] Macounová K, Jirkovský J, Makarova MV, Franc J, Krtík P. Parallel oxygen and chlorine evolution on  $\text{Ru}_{1-x}\text{Ni}_x\text{O}_2$  nanostructured electrodes. *Electrochim Acta* 2008;53:6126–34.
- [174] Papazisi KM, Siokou A, Balomenou S, Tsiplikides D. Preparation and characterization of  $\text{Ir}_x\text{Pt}_{1-x}\text{O}_2$  anode electrocatalysts for the oxygen evolution reaction. *Int J Hydrogen Energy* 2012;37:16642–8.
- [175] Marshall A, Børresen B, Hagen G, Typpkin M, Tunold R. Preparation and characterisation of nanocrystalline  $\text{Ir}_x\text{Sn}_{1-x}\text{O}_2$  electrocatalytic powders. *Mater Chem Phys* 2005;94:226–32.
- [176] Da Silva LA, Alves VA, Trasatti S, Bootds JFC. Surface and electrocatalytic properties of ternary oxides  $\text{Ir}_{0.5}\text{Ti}_{0.7-x}\text{Pt}_x\text{O}_2$ . Oxygen evolution from acidic solution. *J Electroanal Chem* 1997;427:97–104.
- [177] Kadakia KS, Jampani P, Velikokhatnyi Ol, Datta MK, Chyng SJ, Poston JA, et al. Nanostructured (Ir, Sn)O<sub>2</sub>-F – oxygen evolution reaction anode electrocatalyst powders for PEM based water electrolysis. *J Electrochem Soc* 2014;161:F868–75.
- [178] Neyerlin KC, Bugosh G, Forgie R, Liu Z, Strasser P. Combinatorial study of high-surface-area binary and ternary electrocatalysts for the oxygen evolution reaction. *J Electrochem Soc* 2009;156:B363–9.
- [179] Kadakia KS, Jampani P, Velikokhatnyi Ol, Datta MK, Park SK, Hong DH, et al. Nanostructured F doped  $\text{IrO}_2$  electro-catalyst powders for PEM based water electrolysis. *J Power Sources* 2014;269:855–65.
- [180] Kadakia KS, Datta MK, Velikokhatnyi Ol, Jampani P, Kumta PN. Fluorine doped (Ir, Sn, Nb)O<sub>2</sub> anode electro-catalyst for oxygen evolution via PEM based water electrolysis. *Int J Hydrogen Energy* 2014;39:664–74.
- [181] Velikokhatnyi Ol, Kadakia KS, Datta MK, Kumta PN. Fluorine-doped  $\text{IrO}_2$ : a potential electrocatalyst for water electrolysis. *J Phys Chem C* 2013;117:20542–7.
- [182] Slavcheva E, Radev I, Topalov G, Budevski E. Sputtered electrocatalysts for PEM electrochemical energy converters. *Electrochim Acta* 2007;53:362–8.
- [183] Stoyanova A, Borisov G, Lefterova E, Slavcheva E. Oxygen evolution on Ebonex-supported Pt-based binary compounds in PEM water electrolysis. *Int J Hydrogen Energy* 2012;37:16515–21.
- [184] Jakšić MM. Hypo-hyper-d-electronic interactive nature of interionic synergism in catalysis and electrocatalysis for hydrogen reactions. *Int J Hydrogen Energy* 2001;26:559–78.
- [185] Paunovic P, Gogovska DS, Popovski O, Stoyanova A, Slavcheva E, Lefterova E, et al. Preparation and characterization of Co-Ru/TiO<sub>2</sub>/MWCNTs electrocatalysts in PEM hydrogen electrolyzer. *Int J Hydrogen Energy* 2011;36:9405–14.
- [186] Ma L, Sui S, Zhai Y. Preparation and characterization of Ir/TiC catalyst for oxygen evolution. *J Power Sources* 2008;177:470–7.
- [187] Polonsky J, Petrushina IM, Christensen E, Bouzek K, Prag CB, Andersen JET, et al. Tantalum carbide as a novel support material for anode electrocatalysts in polymer electrolyte membrane water electrolyzers. *Int J Hydrogen Energy* 2012;37:2173–81.
- [188] Nikiforov AV, Tomás-García AL, Petrushina IM, Christensen E, Bjerrum NJ. Preparation and study of  $\text{IrO}_2\text{/SiC-Si}$  supported anode catalyst for high temperature PEM steam electrolyzers. *Int J Hydrogen Energy* 2011;36:5797–805.
- [189] Puthiyapura VK, Pasupathi S, Su H, Liu X, Pollet B, Scott K. Investigation of supported  $\text{IrO}_2$  as electrocatalyst for the oxygen evolution reaction in proton exchange membrane water electrolyser. *Int J Hydrogen Energy* 2014;39:1905–13.
- [190] Puthiyapura VK, Mamlouk M, Pasupathi S, Pollet BG, Scott K. Physical and electrochemical evaluation of ATO supported  $\text{IrO}_2$  catalyst for proton exchange membrane water electrolyser. *J Power Sources* 2014;269:451–60.
- [191] Xu J, Aili D, Li Q, Christensen E, Jensen JO, Zhang W, et al. Oxygen evolution catalysts on supports with a 3-D ordered array structure and intrinsic proton conductivity for proton exchange membrane steam electrolysis. *Energy Environ Sci* 2014;7:820–30.
- [192] Natarajan V, Basu S, Scott K. Effect of treatment temperature on the performance of RuO<sub>2</sub> anode electrocatalyst for high temperature proton exchange membrane water electrolyzers. *Int J Hydrogen Energy* 2013;38:16623–30.
- [193] Tunold R, Marshall AT, Rasten E, Typpkin M, Owe LE, Sunde S. Materials for electrocatalysis of oxygen evolution process in PEM water electrolysis cells. *ECS Trans* 2010;25(23):103–17.
- [194] Labou D, Slavcheva E, Schnakenberg U, Neophytides S. Performance of laboratory polymer electrolyte membrane hydrogen generator with sputtered iridium oxide anode. *J Power Sources* 2008;185:1073–8.
- [195] Sapountzi FM, Divane SC, Papaioannou EI, Souentie S, Vayenas CG. The role of Nafion content in sputtered  $\text{IrO}_2$  anodes for low temperature PEM water electrolysis. *J Electroanal Chem* 2011;662:116–22.
- [196] Nong HN, Oh HS, Reier T, Willinger E, Willinger MG, Petkov V, et al. Oxide-supported  $\text{IrNiO}_x$  core-shell particles as efficient, cost-effective and stable catalysts for electrochemical water splitting. *Angew Chem Int Ed Engl* 2015;54:2975–9.
- [197] Nong HN, Gan L, Willinger E, Teschner D, Strasser P.  $\text{IrO}_x$  core-shell nanocatalysts for cost- and energy-efficient electrochemical water splitting. *Chem Sci* 2014;5:2955–63.
- [198] Keane M, Mahapatra MK, Verma A, Singh P. LSM-YSZ interactions and anode delamination in solid oxide electrolysis cells. *Int J Hydrogen Energy* 2012;37:16776–85.
- [199] Kaiser A, Monreal E, Koch A, Stoltzen D. Reactions at the interface  $\text{La}_{0.5}\text{Ca}_{0.5}\text{MnO}_3\text{-YSZ}/\text{Al}_2\text{O}_3$  under anodic current. *Ionicics* 1996;2:184–9.
- [200] Lim H, Virkar AV. A study of solid oxide fuel cell stack failure by inducing abnormal behavior in a single cell test. *J Power Sources* 2008;185:790–800.
- [201] Momma A, Kato T, Kaga Y, Nagata S. Polarization behavior of high temperature solid oxide electrolysis cells (SOEC). *J Ceram Soc Jpn* 1997;105:369–73.
- [202] Chen K, Jiang SP. Failure mechanism of (La, Sr)MnO<sub>3</sub> oxygen electrodes of solid oxide electrolysis cells. *Int J Hydrogen Energy* 2011;36:10541–9.
- [203] Hino R, Haga K, Aita H, Sekite K. R&D on hydrogen production by high-temperature electrolysis of steam. *Nucl Eng Des* 2004;233:363–75.
- [204] Rashkeen SN, Glazoff M. Control of oxygen delamination in solid oxide electrolyzer cells via modifying operational regime. *Appl Phys Lett* 2011;99:173506.
- [205] Virkar AV. Mechanism of oxygen electrode delamination in solid oxide electrolyzer cells. *Int J Hydrogen Energy* 2010;35:9527–43.
- [206] Li N, Keane M, Mahapatra MK, Singh P. Mitigation of the delamination of LSM anode in solid oxide electrolysis cells using manganese-modified YSZ. *Int J Hydrogen Energy* 2013;38:6298–303.
- [207] Hamedani HA, Dahmen K-H, Li D, Garmestani H. Effect of spray parameters on the microstructure of  $\text{La}_{1-x}\text{Sr}_x\text{MnO}_3$  cathode prepared by spray pyrolysis. In: Singh P, Bansal NP, editors. Advances in solid oxide fuel cells IV. New Jersey: John Wiley & Sons, Inc.; 2009. p. 139–46.
- [208] Yang C, Coffin A, Chen F. High temperature solid oxide electrolysis cell employing porous structured ( $\text{La}_{0.75}\text{Sr}_{0.25}\right)_{0.95}\text{MnO}_3$  with enhanced oxygen electrode performance. *Int J Hydrogen Energy* 2010;35:3221–6.
- [209] Wang WS, Huang YY, Jung SW, Vohs JM, Gorte RJ. A comparison of LSM, LSF and LSCo for solid oxide electrolyzer anodes. *J Electrochem Soc* 2006;153:A2066–70.
- [210] Marina OA, Pederson LR, Williams MC, Coffey GW, Meinhardt KD, Nguyen CD. Electrode performance in reversible solid oxide fuel cells and energy conversion. *J Electrochem Soc* 2007;154:B452–9.
- [211] Wang W, Jiang SP. Effect of polarization on the electrode behavior and microstructure of (La, Sr)MnO<sub>3</sub> electrodes of solid oxide fuel cells. *J Solid State Electrochem* 2004;8:914–22.
- [212] Wang J, Zhang Y, Liang T, Deng C, Xu J. Effect of oxygen partial pressure on the electrochemical impedance of  $\text{La}_{0.8}\text{Sr}_{0.2}\text{MnO}_{3-\delta}\text{Zr}_{0.92}\text{Y}_{0.08}\text{O}_2$  porous composite anodes in solid oxide electrolysis cell. *J Power Sources* 2012;208:415–20.
- [213] Yang CH, Jin C, Coffin A, Chen FL. Characterization of infiltrated ( $\text{La}_{0.75}\text{Sr}_{0.25}\right)_{0.95}\text{MnO}_3$  as oxygen electrode for solid oxide electrolysis cells. *Int J Hydrogen Energy* 2010;35:5187–93.
- [214] Sholklapper TZ, Radmilovic V, Jacobson CP, Visco SJ, De Jonghe LC. Nanocomposite Ag-LSM solid oxide fuel cell electrodes. *J Power Sources* 2008;175:206–10.
- [215] Liang F, Chen J, Jiang SP, Chi B, Pu J, Jian L. Development of nanostructured and palladium promoted (La, Sr)MnO<sub>3</sub>-based cathodes for intermediate-temperature SOFCs. *Electrochim Solid-State Lett* 2008;11:B213–16.
- [216] Chen KF, Ai N, Jiang SP. Development of (Ce,Gd)O<sub>2</sub>-impregnated (La, Sr)MnO<sub>3</sub> anodes of high temperature solid oxide electrolysis cells. *J Electrochem Soc* 2010;157:P89–94.
- [217] Chen KF, Ai N, Jiang SP. Enhanced electrochemical performance and stability of (La,Sr)MnO<sub>3</sub>-(Gd, Ce)O<sub>2</sub> oxygen electrodes of solid oxide electrolysis cells by palladium infiltration. *Int J Hydrogen Energy* 2012;37:1301–10.
- [218] Fan H, Keane M, Singh P, Han MF. Electrochemical performance and stability of lanthanum strontium cobalt ferrite oxygen electrode with gadolinia doped ceria barrier layer for reversible solid oxide fuel cell. *J Power Sources* 2014;268:634–9.
- [219] Tao YK, Shao J, Wang JX, Wang WG. Synthesis and properties of  $\text{La}_{0.6}\text{Sr}_{0.4}\text{CoO}_{3-\delta}$  nanopowder. *J Power Sources* 2008;185:609–14.
- [220] Kim SJ, Choi GM. Stability of air electrode in solid oxide electrolysis cell. *ECS Trans* 2013;58(2):139–45.
- [221] Zheng Y, Li Q, Chen T, Wu W, Xu C, Wang WG. Comparison of performance and degradation of large-scale solid oxide electrolysis cells in stack with different composite air electrodes. *Int J Hydrogen Energy* 2015;40:2460–72.

- [222] Wei B, Chen K, Zhao L, Lu Z, Jiang SP. Chromium deposition and poisoning at  $\text{La}_{0.6}\text{Sr}_{0.2}\text{Fe}_{0.8}\text{O}_{3-\delta}$  oxygen electrodes of solid oxide electrolysis cells. *Phys Chem Chem Phys* 2015;17:1601–9.
- [223] Lay-Grindler E, Laurencin J, Villanova J, Kieffer I, Usseglio-Viretta F, Le Bihan T, et al. Degradation study of the  $\text{La}_{0.6}\text{Sr}_{0.4}\text{Co}_{0.2}\text{Fe}_{0.8}\text{O}_3$  solid oxide electrolysis cell (SOEC) anode after high temperature electrolysis operation. *ECS Trans* 2013;57:3177–87.
- [224] Yang Z, Jin C, Yang C, Han M, Chen F.  $\text{Ba}_{0.9}\text{Co}_{0.5}\text{Fe}_{0.4}\text{Nb}_{0.1}\text{O}_{3-\delta}$  as novel oxygen electrode for solid oxide electrolysis cells. *Int J Hydrogen Energy* 2011;36:11572–7.
- [225] Kim-Lohsoontorn P, Brett DJL, Laosiripojana N, Kim YM, Bae JM. Performance of solid oxide electrolysis cells based on composite  $\text{La}_{0.8}\text{Sr}_{0.2}\text{MnO}_{3-\delta}$ -yttria stabilized zirconia and  $\text{Ba}_{0.5}\text{Sr}_{0.5}\text{Co}_{0.8}\text{Fe}_{0.2}\text{O}_{3-\delta}$  oxygen electrodes. *Int J Hydrogen Energy* 2010;35:3958–66.
- [226] Wei B, Chen K, Zhao L, Ai N, Lu Z, Jiang SP.  $\text{SmBaCo}_2\text{O}_{5+\delta}$  as high efficient oxygen electrode of solid oxide electrolysis cells. *ECS Trans* 2013;57:3189–96.
- [227] Li J, Zhong C, Meng X, Wu H, Nie H, Zhan Z, et al.  $\text{Sr}_2\text{Fe}_{1.5}\text{Mo}_{0.5}\text{O}_{6-\delta} - \text{Zr}_{0.84}\text{Y}_{0.16}\text{O}_{2-\delta}$  materials as oxygen electrodes for solid oxide electrolysis cells. *Fuel Cells* 2014;14:1046–9.
- [228] Jiang W, Lu Z, Wei B, Wang ZH, Zhu XB, Tian YT, et al.  $\text{Sm}_{0.5}\text{Sr}_{0.5}\text{CoO}_3 - \text{Sm}_{0.2}\text{Ce}_{0.8}\text{O}_{1.9}$  composite oxygen electrodes for solid oxide electrolysis cells. *Fuel Cells* 2014;14:76–82.
- [229] Jiang W, Wei B, Lv Z, Wang ZH, Zhu L, Li YQ. Performance and stability of co-synthesized  $\text{Sm}_{0.5}\text{Sr}_{0.5}\text{CoO}_3 - \text{Ce}_{0.8}\text{Sm}_{0.2}\text{O}_{1.9}$  composite oxygen electrode for solid oxide electrolysis cells. *Int J Hydrogen Energy* 2015;40:561–7.
- [230] Laguna-Bercero MA, Kinadjan N, Sayers R, El Shinawi H, Creaves C, Skinner SJ. Performance of  $\text{La}_{2-x}\text{Sr}_x\text{Co}_{0.5}\text{Ni}_{0.5}\text{O}_{4+\delta}$  as an oxygen electrode for solid oxide reversible cells. *Fuel Cells* 2011;11:102–7.
- [231] Chauveau F, Mougin J, Mauvy F, Bassat JM, Grenier JC. Development and operation of alternative oxygen electrode materials for hydrogen production by high temperature steam electrolysis. *Int J Hydrogen Energy* 2011;36:7785–90.
- [232] Kobayashi T, Abe K, Ukyo Y, Matsumoto H. Study on current efficiency of steam electrolysis using a partial protonic conductor  $\text{SrZr}_{0.9}\text{Yb}_{0.1}\text{O}_{3-\delta}$ . *Solid State Ionics* 2001;138:243–51.
- [233] Iwahara H, Esaka T, Uchida H, Maeda N. Proton conduction in sintered oxide and its application to steam electrolysis for hydrogen production. *Solid State Ionics* 1981;3–4:359–63.
- [234] Iwahara H, Matsumoto H, Takeuchi K. Electrochemical dehumidification using proton conducting ceramics. *Solid State Ionics* 2000;136–137:133–8.
- [235] Matsumoto H, Sakai T, Okuyama Y. Proton-conducting oxide and its applications to hydrogen energy devices. *Pure Appl Chem* 2013;85:427–35.
- [236] Azimova MA, McIntosh S. On the reversibility of anode supported proton conducting solid oxide cells. *Solid State Ionics* 2011;203:57–61.
- [237] Gan Y, Zhang J, Li YX, Li S, Xie K, Irvine JTS. Composite oxygen electrode based on LSCM for steam electrolysis in a proton conducting solid oxide electrolyzer. *J Electrochim Soc* 2012;159:F763–7.
- [238] He F, Song D, Peng RR, Meng GY, Yang SF. Electrode performance and analysis of reversible solid oxide fuel cells with proton conducting electrolyte of  $\text{BaCe}_{0.5}\text{Zr}_{0.3}\text{Y}_{0.2}\text{O}_{3-\delta}$ . *J Power Sources* 2010;195:3359–64.
- [239] Rao YY, Zhong SH, He F, Wang ZB, Peng RR, Lu YL. Cobalt-doped  $\text{BaZrO}_3$ : a single phase air electrode material for reversible solid oxide cells. *Int J Hydrogen Energy* 2012;37:12522–7.
- [240] Fabbri E, Bi L, Pergolesi D, Traversa E. High-performance composite cathodes with tailored mixed conductivity for intermediate temperature solid oxide fuel cells using proton conducting electrolytes. *Energy Environ Sci* 2011;4:4984–93.
- [241] Li SS, Xie K. *J Electrochim Soc* 2013;160:F224–33.
- [242] Li S, Yan R, Wu G, Xie K, Cheng J. Composite oxygen electrode LSM-BCZY impregnated with  $\text{Co}_3\text{O}_4$  nanoparticles for steam electrolysis in a proton-conducting solid oxide electrolyzer. *Int J Hydrogen Energy* 2013;38:14943–51.
- [243] Koper MTM. Thermodynamic theory of multi-electron transfer reactions: implications for electrocatalysis. *J Electroanal Chem* 2011;660:254–60.
- [244] Jaksic MJ, Mojinovic MV, Krstajic NV. Kinetic analysis of hydrogen evolution at Ni-Mo alloy electrodes. *Electrochim Acta* 2000;45:4151–8.
- [245] Bockris JOM, Azzam AM. The kinetics of the hydrogen evolution reaction at high current densities. *Trans Faraday Soc* 1952;48:145–60.
- [246] Pentland N, Bockris JOM, Sheldon E. Hydrogen evolution reaction on copper, gold, molybdenum, palladium, rhodium and iron: mechanism and measurement technique under high purity conditions. *J Electrochim Soc* 1957;104:182–94.
- [247] Conway BE, Bockris JOM. The d-band character of metals and the rate and mechanism of the electrolytic hydrogen evolution reaction. *Nature* 1956;178:488–9.
- [248] Gerischer H. Über den Zusammenhang zwischen dem Mechanismus der electrolytischen Wasserstoffabscheidung und der Adsorptionsenergie des atomaren Wasserstoffs an verschiedenen Metallen. *Z Phys Chem (N F)* 1956;8:137–53.
- [249] Parsons R. The rate of electrolytic hydrogen evolution and the heat of adsorption of hydrogen. *Trans Faraday Soc* 1958;54:1053–63.
- [250] Krishtalik L. Kinetics of electrochemical reactions at metal-solution interfaces. In: Horsman P, Conway BE, Yeager E, editors. *Comprehensive treatise of electrochemistry*. New York: Plenum Press; 1983. p. 87–172.
- [251] Trasatti S. Work function, electronegativity and electrochemical behavior of metals: III. Electrolytic hydrogen evolution in acid solutions. *J Electroanal Chem Interfacial Electrochim* 1972;39:163–84.
- [252] Trasatti S. Electrocatalysis of hydrogen evolution: progress in cathode activation. In: Gerischer H, Tobias CW, editors. *Advances in electrochemical science and electrochemical engineering*, vol. 3. Weinheim: VCH Verlagsgesellschaft mbH; 1994. p. 1–86.
- [253] Zheng Y, Jiao Y, Jaroniec M, Qiao SZ. Advancing the electrochemistry of the hydrogen-evolution reaction through combining experiment and theory. *Angew Chem Int Ed Engl* 2015;54:52–65.
- [254] Nørskov JK, Bligaard T, Logadottir A, Kitchin JR, Chen JG, Pandelov S, et al. Trends in the exchange current for hydrogen evolution. *J Electrochim Soc* 2005;152:J23–6.
- [255] Skulason E, Tripkovic V, Bjorketun ME, Guðmundsdóttir S, Karlberg G, Rossmeisl J, et al. Modeling the electrochemical hydrogen oxidation and evolution reactions on the basis of density functional theory calculations. *J Phys Chem C* 2010;114:18182–97.
- [256] Safizadeh F, Ghali E, Houlachi G. Electrocatalysis developments for hydrogen evolution reaction in alkaline solutions – a review. *Int J Hydrogen Energy* 2015;40:256–74.
- [257] Jaccaud M, Leroux F, Millet JC. New chlor-alkali activated cathodes. *Mater Chem Phys* 1989;22:105–19.
- [258] Hall DS, Bock C, MacDougall BR. The electrochemistry of metallic nickel: oxides, hydroxides, hydrides and alkaline hydrogen evolution. *J Electrochim Soc* 2013;160:F235–43.
- [259] Danilovic N, Subbaraman R, Strmcnik D, Chang KC, Paulikas AP, Stamenkovic VR, et al. Enhancing the alkaline hydrogen evolution reaction activity through the bifunctionality of  $\text{Ni(OH)}_2$ /metal catalysts. *Angew Chem Int Ed Engl* 2012;51:12495–8.
- [260] Subbaraman R, Tripkovic D, Chang KC, Strmcnik D, Paulikas AP, Hirunsit P, et al. Trends in activity for the water electrolyser reactions on 3d M (Ni, Co, Fe, Mn) hydr(ox)oxide catalysts. *Nat Mater* 2012;11:550–7.
- [261] Strmcnik D, Uchimura M, Wang C, Subbaraman R, Danilovic N, van der Vliet D, et al. Improving the hydrogen oxidation reaction rate by promotion of hydroxyl adsorption. *Nat Chem* 2013;5:300–6.
- [262] Lohrberg K, Kohl P. Preparation and use of Raney-Ni activated cathodes for large scale hydrogen production. *Electrochim Acta* 1984;29:1557–61.
- [263] Divisek J, Malinowski P, Margel J, Schmitz H. Improved components for advanced alkaline water electrolysis. *Int J Hydrogen Energy* 1988;13:141–50.
- [264] Marceta-Kaniski MP, Nikolic VM, Tasic GS, Rakocevic ZL. Electrocatalytic activation of Ni electrode for hydrogen production by electrodeposition of Co and V species. *Int J Hydrogen Energy* 2009;34:703–9.
- [265] Tanaka SI, Hirose N, Tanaki T, Ogata YH. Effect of Ni-Al precursor alloy on the catalytic activity for a Raney-Ni cathode. *J Electrochim Soc* 2000;147:2242–5.
- [266] Wu L, He YH, Lei T, Nam B, Xu NP, Zou J. Characterization of porous  $\text{Ni}_3\text{Al}$  electrode for hydrogen evolution in strong alkali solution. *Mater Chem Phys* 2013;141:553–61.
- [267] Wu L, He Y, Lei T, Nam B, Xu N, Zou J, et al. The stability of hydrogen evolution activity and corrosion behavior of porous  $\text{Ni}_3\text{Al}$ -Mo electrode in alkaline solution during long-term electrolysis. *Energy* 2014;67:19–26.
- [268] Ullal Y, Hedge AC. Electrodeposition and electro-catalytic study of nanocrystalline Ni-Fe alloy. *Int J Hydrogen Energy* 2014;39:10485–92.
- [269] Solmaz R, Doner A, Kardas G. The stability of hydrogen evolution activity and corrosion behavior of NiCu coatings with long-term electrolysis in alkaline solution. *Int J Hydrogen Energy* 2009;34:2089–94.
- [270] Kellenberger A, Vasilić N, Brandl W, Duteanu N. Kinetics of hydrogen evolution reaction on skeleton nickel and nickel-titanium electrodes obtained by thermal arc spraying technique. *Int J Hydrogen Energy* 2007;32:3258–65.
- [271] Lacnjevac UC, Jovic BM, Radmilovic VR, Krstajic NV. Kinetics of the hydrogen evolution reaction on Ni-(Ebonex supported Ru) composite coatings in alkaline solution. *Int J Hydrogen Energy* 2013;38:10178–90.
- [272] Tang X, Xiao L, Yang C, Lu J, Zhuang L. Noble fabrication of Ni-Mo cathode for alkaline water electrolysis and alkaline polymer electrolyte water electrolysis. *Int J Hydrogen Energy* 2014;39:3055–60.
- [273] Marini S, Salvi P, Nelli P, Pesenti R, Villa M, Kiros Y. Stable and inexpensive electrodes for the hydrogen evolution reaction. *Int J Hydrogen Energy* 2013;38:11484–95.
- [274] Wang M, Wang Z, Guo Z, Li Z. The enhanced electrocatalytic activity and stability of NiW films electrodeposited under super gravity field for hydrogen evolution reaction. *Int J Hydrogen Energy* 2011;36:3305–12.
- [275] Pérez-Alonso FJ, Adán C, Rojas S, Peña MA, Fierro JLG. Ni-Co electrodes prepared by electroless-plating deposition. A study of their electrocatalytic activity for the hydrogen and oxygen evolution reactions. *Int J Hydrogen Energy* 2015;40:51–61.
- [276] Popczyk M, Łosiiewicz B, Łagiewka E, Budniok A. Electrochemical characterization of nickel-phosphorus based coatings containing cobalt. In: Łosiiewicz B, editor. *Solid state phenomena*, vol. 228. *Electrocatalysts for hydrogen energy*. TransTech Publications; 2015. p. 299–304.
- [277] Jović BM, Lacnjevac UC, Krstajić NV, Jović VD. Ni-Sn coatings as cathodes for hydrogen evolution in alkaline solutions. *Electrochim Acta* 2013;114:813–18.
- [278] Vázquez-Gómez L, Cattarin S, Guirriero P, Musioani M. Influence of deposition current density on the composition and properties of electrodeposited  $\text{Ni} + \text{RuO}_2$  and  $\text{Ni} + \text{IrO}_2$  composites. *J Electroanal Chem* 2009;634:42–8.
- [279] Krstajic NV, Lačnjevac U, Jović BM, Mora S, Jović VD. Non-noble metal composite cathodes for hydrogen evolution. Part II: the  $\text{Ni}-\text{MoO}_2$  coatings electrodeposited from nickel chloride-ammonium chloride bath containing  $\text{MoO}_2$  powder particles. *Int J Hydrogen Energy* 2011;36:6450–61.
- [280] Zheng Z, Li N.  $\text{Mn}-\text{CeO}_2$  composite cathode material for hydrogen evolution reaction in alkaline electrolyte. *Int J Hydrogen Energy* 2012;37:13921–32.

- [281] Ahn SH, Park HY, Choi I, Yoo SJ, Hwang SJ, Kim HJ, et al. Electrochemically fabricated NiCu alloy catalysts for hydrogen production in alkaline water electrolysis. *Int J Hydrogen Energy* 2013;38:13493–501.
- [282] Ngamlerdpokin K, Tantavichet N. Electrodeposition of nickel-copper alloys to use as a cathode for hydrogen evolution in an alkaline media. *Int J Hydrogen Energy* 2014;39:2505–15.
- [283] Jaksic MM. Electrocatalysis of hydrogen evolution in the light of the Brewster-Engel theory for bonding in metals and intermetallic phases. *Electrochim Acta* 1984;29:1539–50.
- [284] Santos DMF, Amaral L, Šljukić B, Macciò D, Saccone A, Sequeira CAC. Electrocatalytic activity of nickel-cerium alloys for hydrogen evolution in alkaline water electrolysis. *J Electrochem Soc* 2014;161:F386–90.
- [285] Rosalbino F, Borzone G, Angelini E, Raggio R. Hydrogen evolution reaction on Ni RE (RE = rare earth) crystalline alloys. *Electrochim Acta* 2003;48:3939–44.
- [286] Cardoso DSP, Amaral L, Santos DMF, Šljukić B, Sequeira CAC, Macciò D, et al. Enhancement of hydrogen evolution in alkaline water electrolysis by using nickel-rare earth alloys. *Int J Hydrogen Energy* 2015;40:4295–302.
- [287] Rosalbino F, Delsante S, Borzone G, Angelini E. Electrocatalytic behaviour of Co-Ni-R (R = rare earth metal) crystalline alloys as electrode materials for hydrogen evolution reaction in alkaline medium. *Int J Hydrogen Energy* 2008;33:6696–703.
- [288] Arul Raj I. Nickel-based, binary composite electrocatalysts for the cathodes in the energy-efficient industrial production of hydrogen from alkaline-water electrolytic cells. *J Mater Sci* 1993;28:4375–82.
- [289] Arul Raj I, Vasu KI. Transition metal-based cathodes for hydrogen evolution in alkaline solution: electrocatalysis on nickel-based ternary electrolytic codeposits. *J Appl Electrochem* 1992;22:471–7.
- [290] Birry L, Lasia A. Studies of the hydrogen evolution reaction on Raney nickel-molybdenum electrodes. *J Appl Electrochem* 2004;34:735–49.
- [291] McKone JR, Sadtler BF, Werlang CA, Lewis NS, Gray HB. Ni-Mo nanopowders for efficient electrochemical hydrogen evolution. *ACS Catal* 2012;3:166–9.
- [292] Bates MK, Jia Q, Ramaswamy N, Allen RJ, Mukerjee S. Composite Ni/NiO-Cr<sub>2</sub>O<sub>3</sub> catalyst for alkaline hydrogen evolution reaction. *J Phys Chem C* 2015;119:5467–77.
- [293] Hong SH, Ahn SH, Choi I, Pyo SG, Kim HJ, Jang JH, et al. Fabrication and evaluation of nickel cobalt alloy electrocatalysts for alkaline water splitting. *Appl Surf Sci* 2014;307:146–52.
- [294] Lupi C, Dell'Era A, Pasquali M. In situ activation with Mo of Ni-Co alloys for hydrogen evolution reaction. *Int J Hydrogen Energy* 2014;39:1932–40.
- [295] Meguro S, Sasaki T, Katagiri H, Habazaki H, Kawashima A, Sakaki T, et al. Electrodeposited Ni-Fe-C cathodes for hydrogen evolution. *J Electrochem Soc* 2000;147:3003–9.
- [296] Jiang N, Meng HM, Song J, Yu HY. Study on Ni-Fe-C cathode for hydrogen evolution from seawater electrolysis. *Int J Hydrogen Energy* 2010;35:8056–62.
- [297] Song LJ, Meng HM. Effect of carbon content on Ni-Fe-C electrodes for hydrogen evolution reaction in seawater. *Int J Hydrogen Energy* 2010;35:10060–6.
- [298] Flis-Kabulská I, Flis J, Zakroczymski T. Hydrogen evolution on plasma carburized nickel and effect of iron deposition from the electrolyte in alkaline water electrolysis. *Electrochim Acta* 2015;167:61–8.
- [299] Chanda D, Hnájt J, Paidar M, Schauer J, Bouzek K. Synthesis and characterization of NiFe<sub>2</sub>O<sub>4</sub> electrocatalyst for the hydrogen evolution reaction in alkaline water electrolysis using different polymer binders. *J Power Sources* 2015;285:217–26.
- [300] Herraiz-Cardona I, Ortega E, Pérez-Herranz V. Impedance study of hydrogen evolution on Ni/Zn and Ni-Co/Zn stainless steel based electrodeposits. *Electrochim Acta* 2011;56:1308–15.
- [301] Döner A, Solmaz R, Kardaş G. Enhancement of hydrogen evolution at cobalt-zinc deposited graphite electrode in alkaline solution. *Int J Hydrogen Energy* 2011;36:7391–7.
- [302] Döner A, Taşkesen E, Kardaş G. Hydrogen evolution stability of platinum modified graphite electrode. *Int J Hydrogen Energy* 2014;39:11355–9.
- [303] Rosalbino F, Macciò D, Saccone A, Scavino G. Study of Co-W crystalline alloys as hydrogen electrodes in alkaline water electrolysis. *Int J Hydrogen Energy* 2014;39:12448–56.
- [304] Tasić GS, Laćnjevac U, Tasić MM, Kaninski MM, Nikolić VM, Žugić DL, et al. Influence of electrodeposition parameters of Ni-W on Ni cathode for alkaline water electrolyser. *Int J Hydrogen Energy* 2013;38:4291–7.
- [305] Donten M, Cesiulis H, Stojek Z. Electrodeposition of amorphous/nanocrystalline and polycrystalline Ni-Mo alloys from pyrophosphate baths. *Electrochim Acta* 2005;50:1405–12.
- [306] Müller CI, Rauscher T, Schmidt A, Schubert T, Weissgärber T, Kieback B, et al. Electrochemical investigations on amorphous Fe-base alloys for alkaline water electrolysis. *Int J Hydrogen Energy* 2014;39:8926–37.
- [307] Povrozník VS, Shein AB, Mikova IN. Effect of anodic surface treatment of cobalt silicides on the hydrogen evolution reaction. *Prot Met* 2008;44:557–60.
- [308] Popczyk M. The influence of molybdenum and silicon on activity of Ni+W composite coatings in the hydrogen evolution reaction. *Surf Interface Anal* 2008;40:246–9.
- [309] Kichigin VI, Shein AB. Kinetics and mechanism of hydrogen evolution reaction on cobalt silicides in alkaline solutions. *Electrochim Acta* 2015;164:260–6.
- [310] Shalom M, Ressniq D, Yang X, Clavel G, Fellinger TP, Antonietti M. Nickel nitride as an efficient electrocatalyst for water splitting. *J Mater Chem A Mater Energy Sustain* 2015;3:8171–7.
- [311] Pierozynski B, Mikolajczyk T, Kowalski IM. Hydrogen evolution at catalytically-modified nickel foam in alkaline solution. *J Power Sources* 2014;271:231–8.
- [312] Shibli SMA, Harikrishnan GJ, Anupama VR, Chinchu KS, Meena BN. Development of nano NiO incorporated nickel-phosphorus coatings for electrocatalytic applications. *Surf Coat Technol* 2015;262:48–55.
- [313] McArthur MA, Jorge L, Coulombe S, Omanovic S. Synthesis and characterization of 3D Ni nanoparticle/carbon nanotube cathodes for hydrogen evolution in alkaline electrolyte. *J Power Sources* 2014;266:365–73.
- [314] Zhang L, Xiong K, Chen S, Li L, Deng Z, Wei Z. In situ growth of ruthenium oxide-nickel oxide nanorod arrays on nickel foam as a binder-free integrated cathode for hydrogen evolution. *J Power Sources* 2015;274:114–20.
- [315] Millet P, Mbemba N, Grigoriev SA, Fateev VN, Aukauloo A, Etiévant C. Electrochemical performances of PEM water electrolysis cells and perspectives. *Int J Hydrogen Energy* 2011;36:4134–42.
- [316] Marini S, Salvi P, Nelli P, Pesenti R, Villa M, Berrettoni M, et al. Advanced alkaline water electrolysis. *Electrochim Acta* 2012;82:384–91.
- [317] Rozain C, Millet P. Electrochemical characterization of polymer electrolyte membrane water electrolysis cells. *Electrochim Acta* 2014;131:160–7.
- [318] Siracusano S, Baglio V, Lufrano F, Staiti P, Aricò AS. Electrochemical characterization of a PEM water electrolyzer based on a sulfonated polysulfone membrane. *J Membr Sci* 2013;448:209–14.
- [319] Grigoriev SA, Mamat MS, Dzhusim KA, Walker GS, Millet P. Platinum and palladium nano-particles supported by graphitic nano-fibers as catalysts for PEM water electrolysis. *Int J Hydrogen Energy* 2011;36:4143–7.
- [320] Corrales-Sánchez T, Ampurdanés J, Urakawa A. Mo<sub>2</sub>-based materials as alternative cathode catalyst for PEM electrolysis. *Int J Hydrogen Energy* 2014;39:20837–43.
- [321] Yan Y, Xia B, Xu Z, Wang X. Recent development of molybdenum sulfides as advanced electrocatalysts for hydrogen evolution reaction. *ACS Catal* 2014;4:1693–705.
- [322] Benck JD, Hellstern TR, Kibsgaard J, Chakthaonant P, Jaramillo TF. Catalyzing the hydrogen evolution reaction (HER) with molybdenum sulfide nanomaterials. *ACS Catal* 2014;4:4395–71.
- [323] Bonde J, Moses PG, Jaramillo TF, Nørskov JK, Chorkendorff I. Hydrogen evolution on nano-particulate metal sulfides. *Faraday Discuss* 2009;140:219–31.
- [324] Hinnemann B, Moses PG, Bonde J, Jørgensen KP, Nielsen JH, Horch S, et al. Biomimetic hydrogen evolution: Mo<sub>2</sub> nanoparticles as catalyst for hydrogen evolution. *J Am Chem Soc* 2005;127:5308–9.
- [325] Tsai C, Abild-Pedersen F, Nørskov JK. Tuning the Mo<sub>2</sub> edge-site activity for hydrogen evolution via support interactions. *Nano Lett* 2014;14:1381–7.
- [326] Xie J, Zhang H, Li S, Wang R, Sun X, Zhou M, et al. Defect-rich Mo<sub>2</sub> ultrathin nanosheets with additional active edge sites for enhanced electrocatalytic hydrogen evolution. *Adv Mater* 2013;25:5807–13.
- [327] Murugesan S, Akkineni A, Chou BP, Glaz MS, Vanden-Bout DA, Stevenson KJ. Room temperature electrodeposition of molybdenum sulfide for catalytic and photoluminescence applications. *ACS Nano* 2013;7:8199–205.
- [328] Voiry D, Salehi M, Silva R, Fujita T, Chen M, Asefa T, et al. Conducting Mo<sub>2</sub> nanosheets as catalysts for hydrogen evolution reaction. *Nano Lett* 2013;13:6222–7.
- [329] Merki D, Vrubel H, Rovelli L, Fierro S, Hu X, Fe, Co and Ni ions promote the catalytic activity of amorphous molybdenum sulfide films for hydrogen evolution. *Chem Sci* 2012;3:2515–25.
- [330] Zhou W, Hou D, Sang Y, Yao S, Zhou J, Li G, et al. Mo<sub>2</sub>O<sub>5</sub> nanobelts@nitrogen self-doped Mo<sub>2</sub>S<sub>2</sub> nanosheets as effective electrocatalysts for hydrogen evolution reaction. *J Mater Chem A Mater Energy Sustain* 2014;2:11358–64.
- [331] Hou D, Zhou W, Liu X, Zhou K, Xie J, Li G, et al. Pt nanoparticle/MoS<sub>2</sub> nanosheets/carbon fibers as efficient catalyst for the hydrogen evolution reaction. *Electrochim Acta* 2015;166:26–31.
- [332] Carenco S, Portehault D, Boissière C, Mézailles N, Sanchez C. Nanoscaled metal borides and phosphides: recent developments and perspectives. *Chem Rev* 2013;113:7981–8065.
- [333] Kucernak AR, Sundaram VNN. Nickel phosphide: the effect of phosphorus content on hydrogen evolution activity and corrosion resistance in acidic medium. *J Mater Chem A Mater Energy Sustain* 2014;2:17435–45.
- [334] Pan Y, Liu Y, Zhao J, Yang K, Liang J, Liu D, et al. Monodispersed nickel phosphide nanocrystals with different phases: synthesis, characterization and electrocatalytic properties for hydrogen evolution. *J Mater Chem A Mater Energy Sustain* 2015;3:1656–65.
- [335] Pan Y, Liu Y, Liu C. Nanostructured nickel phosphide supported on carbon nanospheres: synthesis and application as an efficient electrocatalyst for hydrogen evolution. *J Power Sources* 2015;285:169–77.
- [336] Jiang P, Liu Q, Liang Y, Tian J, Asiri AM, Sun X. A cost-effective 3D hydrogen evolution cathode with high catalytic activity: FeP nanowire array as the active phase. *Angew Chem Int Ed Engl* 2015;53:12855–9.
- [337] Li Y, Wang H, Xie L, Liang Y, Hong G, Dai H. Mo<sub>2</sub>S<sub>2</sub> nanoparticles grown on graphene: an advanced catalyst for the hydrogen evolution reaction. *J Am Chem Soc* 2011;133:7296–9.
- [338] Faber MS, Dziedzic R, Lukowski MA, Kaiser NS, Ding Q, Jin S. High-performance electrocatalysis using metallic cobalt pyrite (CoS<sub>2</sub>) micro- and nanostructures. *J Am Chem Soc* 2014;136:10053–61.
- [339] Zhang Z, Hao J, Yang W, Lu B, Tang J. Modifying candle soot with FeP nanoparticles into high-performance and cost-effective catalysts for the electrocatalytic hydrogen evolution reaction. *Nanoscale* 2015;7:4400–5.
- [340] Liu Q, Tian J, Cui W, Jiang P, Cheng N, Asiri AM, et al. Carbon nanotubes decorated with CoP nanocrystals: a highly active non-noble metal nanohybrid electrocatalyst for hydrogen evolution. *Angew Chem Int Ed Engl* 2014;53:6710–14.

- [341] Tian J, Liu Q, Asiri AM, Sun X. Self-supported nanoporous cobalt phosphide nanowire arrays: an efficient 3D hydrogen-evolving cathode over the wide range pH 0–14. *J Am Chem Soc* 2014;136:7587–90.
- [342] Popczun EJ, Read CG, Roske CW, Lewis NS, Schaak RE. Highly active electrocatalysis of the hydrogen evolution reaction by cobalt phosphide nanoparticles. *Angew Chem Int Ed Engl* 2014;53:5427–30.
- [343] Kibsgaard J, Jaramillo TF. Molybdenum phosphosulfide: an active, acid-stable, earth-abundant catalyst for the hydrogen evolution reaction. *Angew Chem Int Ed Engl* 2014;53:14433–7.
- [344] Du H, Gu S, Liu R, Li CM. Tungsten diphosphide nanorods as an efficient catalyst for electrochemical hydrogen evolution. *J Power Sources* 2015;278:540–5.
- [345] Duan J, Chen S, Jaroniec M, Qiao SZ. Porous  $C_3N_4$  nanolayers@N-graphene films as catalyst electrodes for highly efficient hydrogen evolution. *ACS Nano* 2015;9:931–40.
- [346] Xiao P, Ge X, Wang H, Liu Z, Fisher A, Wang X. Novel molybdenum carbide-tungsten carbide composite nanowires and their electrochemical activation for efficient and stable hydrogen evolution. *Adv Funct Mater* 2015;25:1520–6.
- [347] Cao B, Veith GM, Neuefeind JC, Adzic RR, Khalifah PG. Mixed closed-packed cobalt molybdenum nitrides as non-noble metal electrocatalysts for the hydrogen evolution reaction. *J Am Chem Soc* 2013;135:19186–92.
- [348] Ma L, Ting LRL, Molinari V, Giordano C, Yeo BS. Efficient hydrogen evolution reaction catalyzed by molybdenum carbide and molybdenum nitride nanocatalysts synthesized via the urea glass route. *J Mater Chem A Mater Energy Sustain* 2015;3:8361–8.
- [349] Chen WF, Wang CH, Sasaki K, Marinkovic N, Xu W, Muckerman T, et al. Highly active and durable nanostructured molybdenum carbide electrocatalysts for hydrogen production. *Energy Environ Sci* 2013;6:943–51.
- [350] Nikiforov AV, Petrushina IM, Christensen E, Alexeev NV, Samokhin AV, Bjerrum NJ. WC as a non-platinum hydrogen evolution electrocatalyst for high temperature PEM electrolyzers. *Int J Hydrogen Energy* 2012;37:18591–7.
- [351] Grigoriev SA, Millet P, Fateev VN. Evaluation of carbon-supported Pt and Pd nanoparticles for the hydrogen evolution reaction in PEM electrolyzers. *J Power Sources* 2008;177:281–5.
- [352] Al-Odail FA, Anastasopoulos A, Hayden BE. Hydrogen evolution and hydrogen oxidation on palladium bismuth alloys. *Top Catal* 2011;54:77–82.
- [353] Galal A, Atta NF, Ali SM. Investigation of the catalytic activity of La $BO_3$  (B = Ni, Co, Fe or Mn) prepared by the microwave-assisted method for hydrogen evolution in acidic medium. *Electrochim Acta* 2011;56:5722–30.
- [354] Wang J, Gao D, Wang G, Miao S, Wu H, Li J, et al. Cobalt nanoparticles encapsulated in nitrogen-doped carbon as a bifunctional catalyst for water electrolysis. *J Mater Chem A Mater Energy Sustain* 2014;2:20067–74.
- [355] Xie X, Rin L, Liu RY, Jiang YF, Zhu Q, Xu AW. The synergistic effect of metallic molybdenum dioxide nanoparticle decorated graphene as an active electrocatalyst for an enhanced hydrogen evolution reaction. *J Mater Chem A Mater Energy Sustain* 2015;3:8055–61.
- [356] Wang X, Se R, Aslan H, Kibsgaard J, Wendt S, Meng L, et al. Tweaking the composition of NiMoZn alloy electrocatalyst for enhanced hydrogen evolution reaction performance. *Nano Energy* 2015;12:9–18.
- [357] Zheng Y, Li Q, Guan W, Xu C, Wu W, Wang WG. Investigation of 30-cell solid oxide electrolyzer stack modules for hydrogen production. *Ceram Int* 2014;40:5801–9.
- [358] Li Q, Zheng Y, Guan W, Lin L, Xu C, Wang WG. Achieving high-efficiency hydrogen production using planar solid-oxide electrolysis stacks. *Int J Hydrogen Energy* 2014;39:10833–42.
- [359] De Saint Jean M, Baurens P, Bouallou C, Couturier K. Economic assessment of a power-to-substitute-natural-gas process including high-temperature steam electrolysis. *Int J Hydrogen Energy* 2015;40:6487–500.
- [360] Penchini D, Cinti G, Discepoli G, Desideri U. Theoretical study and performance evaluation of hydrogen production by 200 W solid oxide electrolyzer stack. *Int J Hydrogen Energy* 2014;39:9457–66.
- [361] Accorsi R, Bergmann E. Cermet cathodes for high temperature water electrolysis with zirconia cells. *J Electrochem Soc* 1980;127:804–11.
- [362] Pihlatie MH, Kaiser A, Mogensen M, Chen M. Electrical conductivity of Ni-YSZ composites: degradation due to Ni particle growth. *Solid State Ionics* 2011;189:82–90.
- [363] Hauch A, Ebbesen SD, Jensen SH, Mogensen M. Solid oxide electrolysis cells: microstructure and degradation of the Ni/Yttria-stabilized zirconia electrode. *J Electrochem Soc* 2008;155:B1184–93.
- [364] Tietz F, Sebold D, Brisse A, Scheffold J. Degradation phenomena in a solid oxide electrolysis cell after 9000 h of operation. *J Power Sources* 2013;223:129–35.
- [365] Hauch A, Jensen SH, Bilde-Sørensen JB, Mogensen M. Silica segregation in the Ni/YSZ electrode batteries and energy storage. *J Electrochem Soc* 2007;154:A619–26.
- [366] Lay-Grindler E, Laurencin J, Villanova J, Cloetens P, Bleuet P, Mansuy A, et al. Degradation study by 3D reconstruction of a nickel-yttria stabilized zirconia cathode after high temperature steam electrolysis operation. *J Power Sources* 2014;269:927–36.
- [367] Kharton VV, editor. Solid state electrochemistry II: electrodes, interfaces and ceramic membranes. Weinheim: Wiley-VCH Verlag & Co. KGaA; 2011.
- [368] Uchida H, Osada N, Watanabe M. High-performance electrode for steam electrolysis: mixed conducting ceria-based cathode with highly-dispersed Ni electrocatalysts. *Electrochim Solid-State Lett* 2004;7:A500–2.
- [369] Yang X, Irvine JTS.  $(La_{0.75}Sr_{0.25})_{0.95}Mn_{0.5}Cr_{0.5}O_3$  as the cathode of solid oxide electrolysis cells for high temperature hydrogen production from steam. *J Mater Chem* 2008;18:2349–54.
- [370] Xu S, Chen S, Li M, Xie K, Wang Y, Wu Y. Composite cathode based on Fe-loaded LSCM in an oxide-ion-conducting solid oxide electrolyser for steam electrolysis. *J Power Sources* 2013;239:332–40.
- [371] Li Y, Gan Y, Wang Y, Xie K, Wu Y. Composite cathode based on Ni-loaded  $La_{0.75}Sr_{0.25}Co_{0.5}Mn_{0.5}O_{3-\delta}$  for direct steam electrolysis in an oxide-ion-conducting solid oxide electrolyzer. *Int J Hydrogen Energy* 2013;38:10196–207.
- [372] Xu S, Dong D, Wang Y, Doherty W, Xie K, Wu Y. Perovskite chromates cathode with resolved and anchored nickel nano-particles for direct high-temperature steam electrolysis. *J Power Sources* 2014;246:346–55.
- [373] Qin Q, Wu G, Chen S, Doherty W, Xie K, Wu Y. Perovskite titanate cathode decorated by in-situ grown iron nanocatalyst with enhanced electrocatalytic activity for high-temperature steam electrolysis. *Electrochim Acta* 2014;127:215–27.
- [374] Li Y, Wu G, Ruan C, Zhou Q, Wang Y, Doherty W, et al. Composite cathode based on doped vanadate enhanced with loaded metal nanoparticles for steam electrolysis. *J Power Sources* 2014;253:349–59.
- [375] Wang S, Zhang L, Yang Z, Zhang L, Fang S, Brinkman K, et al. Two-step co-sintering method to fabricate anode-supported  $Ba_3Ca_{1.18}Nb_{1.82}O_{9-\delta}$  proton-conducting solid oxide fuel cells. *J Power Sources* 2012;215:221–6.
- [376] Bi L, Fabbri E, Sun Z, Traversa E. A novel ionic diffusion strategy to fabricate high-performance anode-supported solid oxide fuel cells (SOFCs) with proton conducting Y-doped  $BaZrO_3$  films. *Energy Environ Sci* 2011;4:409–12.
- [377] Bi L, Fabbri E, Sun Z, Traversa E. Sinteractive anodic powders improve densification and electrochemical properties of  $BaZr_{0.8}Y_{0.2}O_{3-\delta}$  electrolyte films for anode-supported solid oxide fuel cells. *Energy Environ Sci* 2011;4:1352–7.
- [378] Bae H, Choi GM. Novel modification of anode microstructure for proton-conducting solid oxide fuel cells with  $BaZr_{0.8}Y_{0.2}O_{3-\delta}$  electrolytes. *J Power Sources* 2015;285:431–8.
- [379] Mao X, Yu T, Ma G. Performance of cobalt-free double-perovskite  $NdBaFe_2-xMn_xO_{5+d}$  cathode materials for proton-conducting IT-SOFC. *J Alloys Compd* 2015;637:286–90.
- [380] Hakim M, Yoo CY, Joo JH, Yu JH. Enhanced durability of a proton conducting oxide fuel cell with a purified yttrium-doped barium zirconate-cerate electrolyte. *J Power Sources* 2015;278:320–4.
- [381] Lim DK, Im HN, Singh S, Song SJ. Investigations on electrochemical performance of a proton-conducting ceramic-electrolyte fuel cell with  $La_{0.8}Sr_{0.2}MnO_3$  cathode. *J Electrochem Soc* 2015;162:F547–54.
- [382] Shao Q, Ge W, Lu X, Chen Y, Ding Y, Lin B, et al. A promising cathode for proton-conducting intermediate temperature solid oxide fuel cells:  $Y_{0.8}Ca_{0.2}BaCo_4O_{7-\delta}$ . *Ceram Int* 2015;41:6687–92.
- [383] Bi L, Boulfrad S, Traversa E. Reversible solid oxide fuel cells (R-SOFCs) with chemically stable proton-conducting oxides. *Solid State Ionics* 2015;275:101–5.
- [384] Becker WL, Braun RJ, Penev M, Melaina M. Production of Fischer-Tropsch liquid fuels from high temperature solid oxide co-electrolysis units. *Energy* 2012;47:99–115.
- [385] Fu Q, Mabilat C, Zahid M, Brisse A, Gautier L. Syngas production via high temperature steam/ $CO_2$  co-electrolysis: an economic assessment. *Energy Environ Sci* 2010;3:1382–97.
- [386] Chen L, Chen F, Xia C. Direct synthesis of methane from  $CO_2$ - $H_2O$  co-electrolysis in tubular solid oxide electrolysis cells. *Energy Environ Sci* 2014;7:4018–22.
- [387] Stempinski JP, Ni M, Sun Q, Chan SH. Production of sustainable methane from renewable energy and captured carbon dioxide with the use of solid oxide electrolyzer: a thermodynamic assessment. *Energy* 2015;82:714–21.
- [388] Hansen JB. Fuel processing for fuel cells and power to fuels from an industrial perspective. *J Catal* 2015;328:280–96.
- [389] Cinti J, Baldinelli A, Di Michelle A, Desideri U. Integration of solid oxide electrolyzer and Fischer-Tropsch: a sustainable pathway for synthetic fuel. *Appl Energy* 2016;162:308–20.
- [390] Graves C, Ebbesen SD, Mogensen M, Lackner KS. Sustainable hydrocarbon fuels by recycling  $CO_2$  and  $H_2O$  with renewable or nuclear energy. *Renew Sustain Energy Rev* 2011;15:1–23.
- [391] Hartvigsen J, Elangovan S, Frost L, Nickens A, Stoops C, O'Brien J, et al. Carbon dioxide recycling by high-temperature co-electrolysis and hydrocarbon synthesis. *ECS Trans* 2008;12:625–37.
- [392] Pozzo M, Lanzini A, Santarelli M. Enhanced biomass-to-liquid (BTL) conversion process through high temperature co-electrolysis in a solid oxide electrolysis cell (SOEC). *Fuel* 2015;145:39–49.
- [393] Li W, Wang H, Shi Y, Chai N. Performance and methane production characteristics of  $H_2O$ - $CO_2$  co-electrolysis in solid oxide electrolysis cells. *Int J Hydrogen Energy* 2013;38:11104–9.
- [394] Mahmood A, Bano S, Yu JH, Lee KH. Effect of operating conditions on the performance of solid electrolyte membrane reactor for steam and  $CO_2$  electrolysis. *J Membr Sci* 2015;473:8–15.
- [395] Hjalmarsson P, Sun X, Liu YL, Chen M. Influence of the oxygen electrode and inter-diffusion barrier on the degradation of solid oxide electrolysis cells. *J Power Sources* 2013;223:349–57.
- [396] Im HN, Jeon SY, Lim DK, Singh B, Choi M, Yoo YS, et al. Steam/ $CO_2$  co-electrolysis performance of reversible solid oxide cell with  $La_{0.6}Sr_{0.4}Co_{0.2}Fe_{0.8}O_{3-\delta}$ - $Gd_{0.1}Ce_{0.9}O_{2-\delta}$  oxygen electrode. *J Electrochem Soc* 2015;162:F54–9.
- [397] Sun X, Chen M, Hjalmarsson P, Ebbesen SD, Jensen SH, Mogensen M, et al. Performance and durability of solid oxide electrolysis cells for syngas production. *ECS Trans* 2012;41(33):77–85.
- [398] Sun X, Chen M, Liu YL, Hjalmarsson P, Ebbesen SD, Jensen SH, et al. Durability of solid oxide electrolysis cells for syngas production fuel cells, electrolyzers and energy conversion. *J Electrochim Soc* 2013;160:F1074–80.

- [399] Hjalmarsson P, Sun X, Chen M. Durability of high-performance Ni-yttria stabilized zirconia supported solid oxide electrolysis cells at high current density. *J Power Sources* 2014;262:316–22.
- [400] Ebbesen SD, Graves C, Mogensen M. Production of synthetic fuels by co-electrolysis of steam and carbon dioxide. *Int J Green Energy* 2009;6:646–60.
- [401] Graves C, Ebbesen SD, Mogensen M. Co-electrolysis of CO<sub>2</sub> and H<sub>2</sub>O in solid oxide cells: performance and durability. *Solid State Ionics* 2011;192:398–403.
- [402] Fu Q, Dailly J, Brisse A, Zahid M. High temperature CO<sub>2</sub> and H<sub>2</sub>O electrolysis with an electrolyte-supported solid oxide cell. *ECS Trans* 2011;35:2949–56.
- [403] Li S, Li Y, Gan Y, Xie K, Meng G. Electrolysis of H<sub>2</sub>O and CO<sub>2</sub> in an oxygen-ion conducting solid oxide electrolyzer with a La<sub>0.2</sub>Sr<sub>0.8</sub>TiO<sub>3+δ</sub> composite cathode. *J Power Sources* 2012;218:244–9.
- [404] Yue X, Irvine JTS. (La,Sr)(Cr,Mn)O<sub>3</sub>/GDC cathode for high temperature steam electrolysis and steam-carbon dioxide co-electrolysis. *Solid State Ionics* 2012;225:131–5.
- [405] Kim-Lohsoontorn P, Bae J. Electrochemical performance of solid oxide electrolysis cell electrodes under high-temperature coelectrolysis of steam and carbon dioxide. *J Power Sources* 2011;196:7161–8.
- [406] Diethelm S, van Herle J, Montinaro D, Bucheli O. Electrolysis and co-electrolysis performance of SOE short stacks. *Fuel Cells* 2013;13:631–7.
- [407] Nguyen VN, Fang Q, Packbier U, Blum L. Long-term tests of a Jülich planar short stack with reversible solid oxide cells in both fuel cell and electrolysis modes. *Int J Hydrogen Energy* 2013;38:4281–90.
- [408] Chen M, Høgh JVT, Nielsen JU, Bentzen JJ, Ebbesen SD, Hendriksen PV. High-temperature co-electrolysis of steam and CO<sub>2</sub> in a SOC stack: performance and durability. *Fuel Cells* 2013;13:638–45.
- [409] Ebbesen SD, Hogh J, Nielsen KA, Nielsen JU, Mogensen M. Durable SOC stacks for production of hydrogen and synthesis gas by high temperature electrolysis. *Int J Hydrogen Energy* 2011;36:7363–73.
- [410] Stoots C, O'Brien J, Hartvigsen J. Results of recent high temperature coelectrolysis studies at the Idaho National Laboratory. *Int J Hydrogen Energy* 2009;34:4208–15.
- [411] Alenazey F, Alyousef Y, Almisned O, Almutairi G, Ghouse M, Montinaro D, et al. Production of synthesis gas (H<sub>2</sub> and CO) by high-temperature co-electrolysis of H<sub>2</sub>O and CO<sub>2</sub>. *Int J Hydrogen Energy* 2015;40:10274–80.
- [412] Li W, Shi Y, Luo Y, Cai N. Elementary reaction modeling of solid oxide electrolysis cells: main zones for heterogeneous chemical/electrochemical reactions. *J Power Sources* 2015;273:1–13.
- [413] Tao Y, Ebbesen SD, Mogensen M. Degradation of solid oxide cells during co-electrolysis of H<sub>2</sub>O and CO<sub>2</sub>: carbon deposition under high current densities. *ECS Trans* 2013;50:139–51.
- [414] Xu J, Yang Y, Li YW. Recent development in converting coal to clean fuels in China. *Fuel* 2015;152:122–30.
- [415] <[www.syngaschem.com](http://www.syngaschem.com)>.
- [416] Hetterscheid DGH, van der Ham CJM, Diaz-Morales O, Verhoeven MWGM, Longo A, Banerjee D, et al. Early stages of catalyst aging in the iridium mediated water oxidation reaction. *Phys Chem Chem Phys* 2016;18:10931–40.
- [417] Huang J, Blakemore JD, Fazi D, Kokhan O, Schley ND, Crabtree RH, et al. Domain structure for an amorphous iridium-oxide water-oxidation catalyst characterized by X-ray pair distribution function analysis. *Phys Chem Chem Phys* 2014;16:1814–19.
- [418] McFarland EW, Metiu H. Catalysis by doped oxides. *Chem Rev* 2013;113:4391–427.